UCLouvain

École polytechnique de Louvain

Hybrid beamforming at 60GHz

Author: **Thibault BERTRAND**
Supervisor: **Jérôme LOUVEAUX**
Readers: **Steve BLANDINO, Claude OESTGES, Luc VANDENDORPE**
Academic year 2018–2019
Master [120] in Electrical Engineering

Acknowledgments

First and foremost, I would like to thank my supervisor, Jérôme Louveaux, and Steve Blandino.

For more than one year, Jérôme has been an excellent advisor and has constantly supported me in my work. Without him, I would not have met and interacted with researchers at IMEC. Jérôme has been extremely available during this year and the numerous discussions about my work progress and my writing will forever be present in my mind. I would like also to thank him for allowing me to participate to the excellent IRACON training school in Centre Tecnòlogic de Telecomunicacions de Catalunya (CTTC).

I am especially grateful to Steve who has been an incredible support for me. He has never refused to help me despite his work. I learned a lot from the countless remarks and advices that he gave to me. The different objectives of my master thesis would certainly not be fulfilled so well without him.

I would like to address a special thanks to all the people at IMEC in my work environment and particularly to Claude Desset for introducing me at IMEC and for the technical discussions we had.

The present work is the product of a strong collaboration with IMEC

Contents

Acronyms

A-BFT association beamforming training.

ACK acknowledgment.

AGC automatic gain control.

ATI announcement transmission interval.

AWV antenna weight vector.

BC beam combining.

BER bit error rate.

BF beamforming.

BFT beamforming training.

BHI beacon header interval.

BI beacon interval.

BRP beam refinement protocol.

BS base station.

BT beam tracking.

BTI beacon transmission interval.

BTP beam tracking procedure.

CBAP contention based-access period.

CDOWN countdown.

CE channel estimation.

CIR channel impulse response.

CSMA/AC carrier-sensing multiple access with collision avoidance.

DAC digital-to-analog converter.

DFT discrete Fourier transform.

DMG directional multi-gigabits.

DTI data transfer interval.

EDMG enhanced directional multi-gigabits.

ID identifier.

IS importance sampling.

ISS initiator sector sweep.

LOS line-of-sight.

MAC medium access control.

MID multiple sector ID detection.

MIMO multiple-input multiple-output.

mmWave millimeter wave.

MU-MIMO multi-user MIMO.

NLOS non line-of-sight.

OSI Open Systems Interconnection.

PF particle filter.

PHY physical.

RF radio frequency.

RSS responder sector sweep.

SISO single-input single-output.

SLS sector level sweep.

SM spatial multiplexing.

SMC sequential Monte Carlo.

SNR signal-to-noise ratio.

SP service period.

SSW sector sweep.

STA station.

STF short training field.

SU-MIMO single-user MIMO.

TDMA time division multiple access.

TRN training field.

TRN-R training field for receive beam refinement.

TRN-T training field for transmit beam refinement.

TXOP transmission opportunity.

UE user equipment.

Chapter 1

Introduction

1.1 Motivation

For more than two decades, huge efforts are done to realise networks that have a high data transfer capability (e.g. fifth generation of wireless systems (5G) will have to provide a peak data rate of 20 Gbps). To achieve this goal, the research community has identified three different ways to increase by several orders the throughput of communication[1]: large bandwidth utilisation, higher spectral efficiency and densification of the infrastructure. These three techniques are briefly discussed in the following paragraphs.

To accommodate for a large available bandwith, the millimeter wave (mmWave) spectrum with carrier frequency at 30-300GHz seems promising. For example, the IEEE802.11ad/ay amendments to the IEEE802.11 standard were defined to enable Wi-Fi communication in the unlicensed 60 GHz band where more than 12 GHz of bandwidth is available[2]. The wider is the bandwith, the higher is the channel capacity, that is the theoretical maximum data rate achievable in a communication between two or more stations (STAs) without transmission error.

Furthermore, the mmWave spectrum is very convenient for increasing the densification of the infrastructure. Obstacles and high path losses present at such frequency reduce the interferences perceived by other STAs. This allows for a better spatial reuse of the spectrum and smaller cells.

The millimeter wave spectrum is thus very convenient to enhance the data throughput of the communication thanks to large bandwidth utilisation and high density of the cellular infrastructure. Let us focus on the improvement of the spectral efficiency. For that purpose, multiple-input multiple-output (MIMO) wireless systems have been studied and related MIMO training stages are included in recent standards[3]. These systems use dozens or hundreds of antennas, which can be implemented in a small form factor thanks to the small size of the antennas at such frequencies. Two different techniques that try to exploit the full channel capacity are commonly used with MIMO systems: spatial multiplexing (SM) and beamforming (BF)[4]. This two techniques are presented here below.

Spatial multiplexing provides multiplexing gain by enabling the simultaneous transmission of multiple streams of data on the same RF channel. Those streams can either be transmitted to the same user equipment (UE) or either to multiple UEs. In the first case, the communication is said to be single-user MIMO (SU-MIMO) while on the latter case, it is said to be multi-user MIMO (MU-MIMO). SM is very efficient when the channel possesses a diversity that allows the transmission of multiple orthogonal streams. However, because the power is split among the different streams, the communication suffers from a low signal-to-noise ratio (SNR) condition and low order modulations must be used which reduces the data throughput.

In this case, BF should be used to maximise the power send over the stronger singular modes of the channel. Beamforming provides array gain by transmitting a common signal with multiple antenna elements. By adapting the relative phases between the signals emitted/received by the different antenna elements, the radiation pattern of the array may take the form of a beam in the direction of the other STA, thereby enhancing the SNR level of the link. BF allows also for a reduction of the interferences because less power is radiated toward STAs not aligned with the beam.

As explained, SM and BF are two techniques that are used by MIMO systems to maximise the spectral efficiency. Several architectures of MIMO transceivers have been proposed to extract the benefit of both techniques.

Among these architectures, fully digital ones (Figure 1.1) extract the advantages of SM and BF simultaneously. The different streams that a transmitter wants to send over the channel are first encoded before being transmitted to each antenna element. Between the encoder and the antenna elements, RF chains are inserted to convert the baseband digital signals to high frequency analog signals. They are generally composed of a digital-to-analog converter (DAC), a frequency upconverter and an amplifier.

Despite several demonstrations [5], the high power consumption, cost and complexity of an increasing number of RF chains makes currently difficult the implementation of fully digital architecture MIMO transceivers[6] and other architectures need to be explored.

Fully analog architecture relies on the use of a single RF chain for the whole antenna array. After being upconverted in RF band, the signal is divided among the different antenna elements. Before each antenna element, a phase shifter is inserted and provides beamforming capability. A fully analog single-input single-output (SISO) architecture is depicted in Figure 1.2.

Even if complexity, cost and power consumption are less problematic with them, fully analog architectures are not sufficiently optimal because they can not benefit from spatial multiplexing. Therefore, hybrid architectures containing advantages of both architectures have been designed such as the one presented in Figure 1.3.

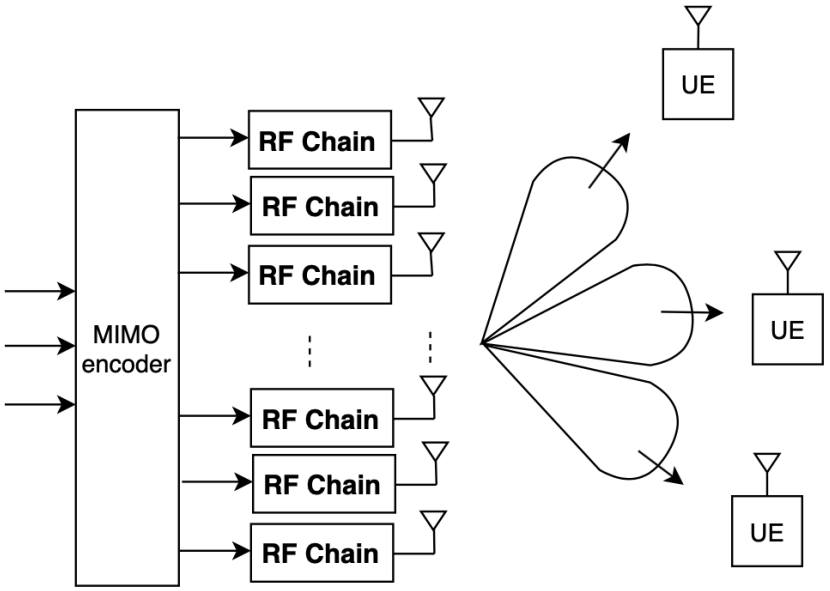

Figure 1.1: Fully digital MIMO architecture for transmitting multiple streams of data in a multi-users environment.

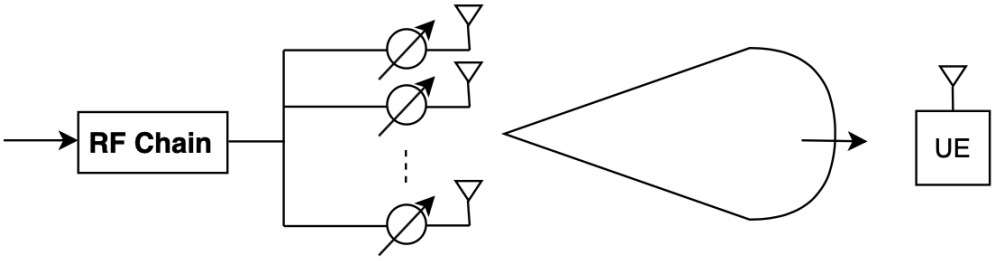

Figure 1.2: Fully analog SISO architecture for transmitting one stream of data in a single user environment.

Hybrid architectures are very convenient since they can combine SM thanks to the digital encoder with an analog BF enabled via the phase shifters.

Analog BF is however challenging. On one hand, a careful training procedure between the transmitter and the receiver must be established to allow the determination of optimal weights for the phase shifters. This procedure needs to be robust, efficient and fast. On the other hand, the weights should be adapted in the case of moving UEs in order to prevent loos of BF capacity by the STAs.

The main objective of this thesis is to design and evaluate the performance of beamforming training (BFT) algorithms compatible with the IEEE802.11ad/ay standards for Wi-Fi communication at 60GHz. More specifically, we focus on two scenarios. The first scenario considers a communication between a static base station (BS) and a static UE. The second scenario considers a communication between a stationary BS and a UE who is free to move in its environment.

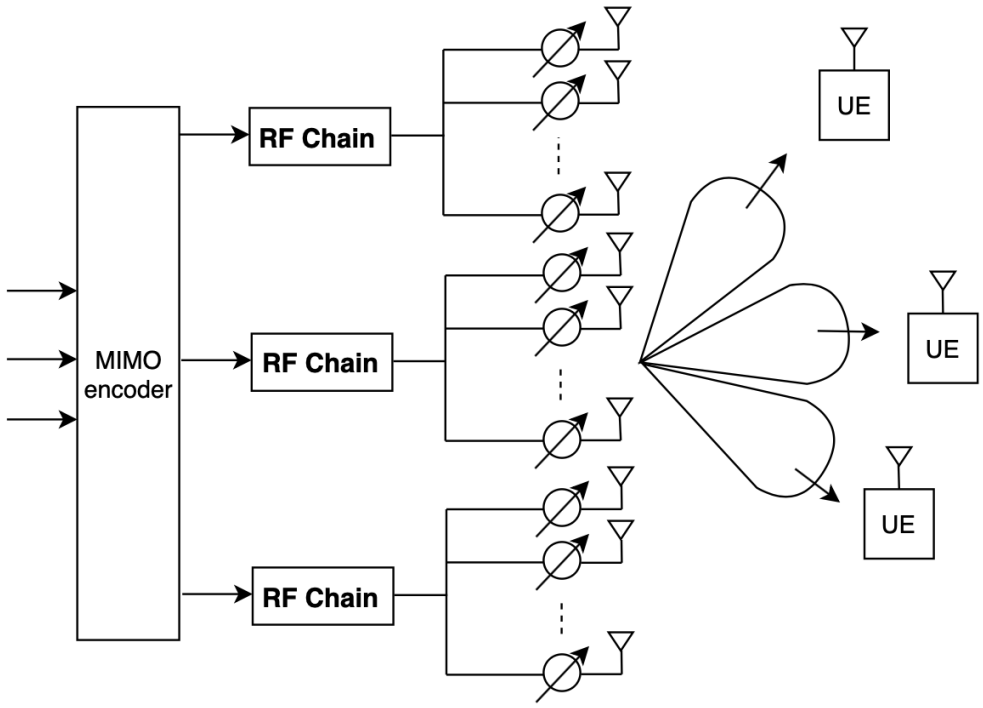

Figure 1.3: Hybrid digital/analog MIMO architecture for transmitting multiple streams of data in a multi-users environment.

1.2 Outline and contributions

Chapter 2 introduces the principle of beamforming. A theoretical study of the emission of plane waves from a linear antenna array and from a rectangular antenna array is described. This study highlights the benefits of multi-antenna systems on the link budget. For large antenna arrays, the radiation pattern of the antenna array tends to become exceedingly narrow. This leads to a high drop of the SNR level in presence of a small misalignment of the beam, ideally directed toward the other STA. To address this problem, a novel beam widening algorithm is proposed in the second part of this chapter.

Chapter 3 consists in an explanation of the different aspects of the IEEE802.11ad/ay specifications of the IEEE802.11 standard. The main contributions to the medium access control (MAC) and physical (PHY) layers of the standard will be analysed and special emphases will be given to the explanation of the different beamforming training (BFT) procedures. The *Matlab* chain used for the validations of the BFT algorithms presented in the rest of this master thesis will be described at the end of this chapter.

Chapter 4 investigates two different BFT algorithms for the communication between a BS and a stationary user. The first algorithm is based on an exhaustive beam search technique which can be considered as the conventional BFT algorithm of the IEEE802.11ad/ay amendments of the standard. The performance of this algorithm will be presented and the benefits obtained by the beam widening algorithm described

in chapter 2 will be emphasised. The second BFT algorithm tries to optimise the beamforming capability of a multi-antenna systems by estimating the channel via different SNR measurements. Two different channel estimation methods will be presented. The first one is based on [7] and proposes a procedure based on four SNR measurements for each channel coefficients. The second method has been derived from the first method and requires three SNR measurements for estimating each channel coefficient. The performance of those methods in presence of additive noise on the SNR measurements will be investigated.

In **Chapter 5**, a novel beam tracking (BT) algorithm is presented. The purpose of this algorithm is to adapt continuously the weights of the phase shifters in a scenario considering a moving user to conserve high beamforming gain. This algorithm is totally compatible with the IEEE802.11 standard and is based on stochastic prediction of the user motion thanks to the use of a particle filter (PF). Unless the author is mistaken, this technique has never been explored before and its performance will be evaluated via simulations.

Chapter 2

Beamforming

MmWave signals suffer from high penetration and path losses. These phenomenons degrade the quality of wireless communications. To understand better the impact of the path loss, let us illustrate it through a simple example. The path loss between two antennas can be estimated using the well know Friis transmission equation:

$$\frac{P_R}{P_T} = D_T D_R \Big(\frac{\lambda}{4\pi d}\Big)^2, \tag{2.1}$$

Where P_R and P_T are the received and transmitted powers, D_R and D_T are the antenna directivities, d is the distance between the transmitter and the receiver and λ is the wavelength. Since $\lambda = c/f$, where c is the travelling light speed and f is the wave frequency, the path loss is proportional to $(1/f^2)$. Therefore, the path loss for communications at 60GHz compared to the one for communications at 6 GHz is increased by 20dB.

To enhance the link quality, multi-antenna systems are interesting due to their beamforming (BF) capability. The principle is to focus the energy sent by a transmitting station (STA) toward a receiving STA and thus beneficing from array gain. Another advantage of BF is the reduction of interferences that could potential harm other wireless communications.

In this chapter, a review of the BF principle will be presented, considering the emission of a plane wave from a linear array and a rectangular array. The utilisation of the BF principle for the reception of a plane wave over linear and rectangular antenna arrays is similar.

The second part of this chapter is dedicated to the description and validation of a beam widening algorithm. The purpose of this algorithm is to design a codebook containing a set of weights, named antenna weight vector (AWV), for the different phase shifters connected to the different antenna elements (see section 1.1). This set should allow the STA to properly steered its radiation pattern toward the STA with whom it is communicating.

2.1 Emission of a plane wave by a linear antenna array

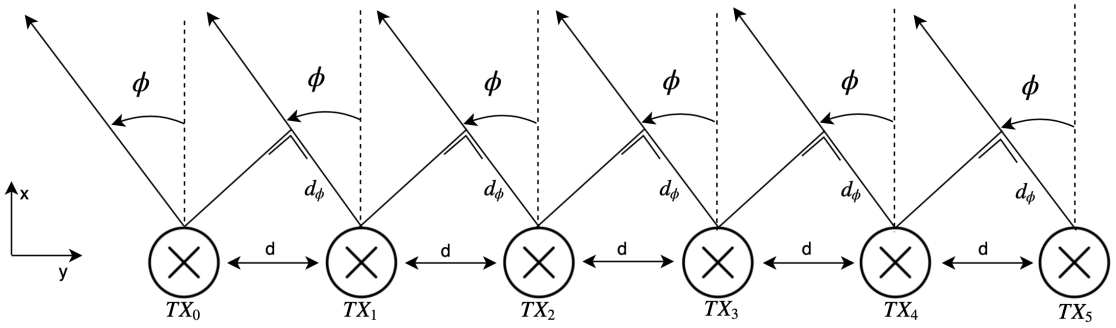

Figure 2.1: Single plane wave emitted by a linear array of $N = 6$ antennas.

Let us consider a single plane wave emitted by a linear array of N antennas each equally spaced by a distance d (see Figure 2.1). The antennas are placed along the y-direction so that the n$^{\text{th}}$ antenna is located in $\mathbf{a_n} = (0, nd)$ with $n = 0, 1, 2, ..., N-1$. The direction of departure of the wave is described by $\hat{\mathbf{u}} = (\cos\phi, \sin\phi)$. By considering that the receiver is sufficiently far away from the user, the difference of travelling distance between the wave emitted by antenna 0 and the wave emitted by antenna n is given by the projection of $\mathbf{a_n}$ over $\hat{\mathbf{u}}$:

$$d_{n,\phi} = nd_\phi = \mathbf{a_n} \cdot \hat{\mathbf{u}} = nd\sin\phi. \tag{2.2}$$

The additional travelling time τ_n between antenna 0 and antenna n can be written as:

$$\tau_n = \frac{d_{n,\phi}}{c} = \frac{nd\sin\phi}{c}, \tag{2.3}$$

where c represents the travelling speed of light. Suppose that a narrowband signal is emitted by the linear antenna array. That is a signal with a bandwidth not exceeding the channel coherence bandwidth or, in other word, for which the channel can be consider as being "flat". The signal $s_n(t)$ received from each antenna element is described by the set:

$$\mathbf{s}(t) = \begin{bmatrix} s_0(t) \\ s_1(t) \\ s_2(t) \\ \vdots \\ s_{N-1}(t) \end{bmatrix} = \begin{bmatrix} s_0(t) \\ s_0(t+\tau_1) \\ s_0(t+\tau_2) \\ \vdots \\ s_0(t+\tau_{N-1}) \end{bmatrix}. \tag{2.4}$$

Because the signal is narrowband, the system of equations here above can be rewritten

as:

$$\mathbf{s}(t) = s_0(t) \begin{bmatrix} 1 \\ e^{j\omega\tau_1} \\ e^{j\omega\tau_2} \\ \vdots \\ e^{j\omega\tau_{N-1}} \end{bmatrix} = s_0(t) \underbrace{\begin{bmatrix} 1 \\ e^{j2\pi\frac{d}{\lambda}\sin\phi} \\ e^{j2\pi\frac{2d}{\lambda}\sin\phi} \\ \vdots \\ e^{j2\pi\frac{(N-1)d}{\lambda}\sin\phi} \end{bmatrix}}_{\mathbf{R}(\phi)}, \tag{2.5}$$

where $\omega = 2\pi f$ denotes the carrier frequency of the transmitted signal and $\lambda = c/f$ the carrier wavelength. The displacement phase factor $\mathbf{R}(\phi) \in \mathbb{C}^N$ describes the phase shift between the different emitted waves perceived by a receiving STA standing in the angular direction ϕ.

Let us denote by $\boldsymbol{\alpha} = \{\alpha_0, \alpha_1, \ldots, \alpha_{N-1}\} \in \mathbb{C}^{1\times N}$ the antenna weight vector (AWV) (= weights of the phase shifters). At the reception, the signals of the different antennas will be combined according to a weighted sum:

$$\begin{aligned} \mathbf{y}(t) &= \alpha_0 s_0(t) + \alpha_1 s_1(t) + \ldots + \alpha_{N-1} s_{N-1}(t), \\ &= \alpha_0 s_0(t) + \alpha_1 e^{j2\pi\frac{d}{\lambda}\sin\phi} s_0(t) + \ldots + \alpha_{N-1} e^{j2\pi\frac{(N-1)d}{\lambda}\sin\phi} s_0(t), \\ &= \boldsymbol{\alpha}\mathbf{R}(\phi) s_0(t), \\ &= A(\phi) s_0(t), \end{aligned} \tag{2.6}$$

With $A(\phi)$ being a complex scalar. The term $|A(\phi)|^2$ describes the power gain of the antenna array (= array gain) in the direction ϕ.

Figure 2.2 presents some power gain for linear arrays with equal weights and isotropic antennas. The effect of the number of antennas is an increasing gain of the main lobe and the apparition of secondary lobes in the radiation pattern with a reduced gain. The inter-antenna distance d has also an impact. The smaller is d compared to the wavelength, the larger and fewer are the lobes. For $d > \lambda/2$, there is an apparition of lobes steered in $\phi = \pm 90°$, named grating lobes. Those lobes are generally unwanted since the array is emitting power toward these directions which can potentially increase the interference level perceived by other STAs. For the rest of this thesis, half wavelength inter-antenna distance will be assumed since it combines a good array gain with a low emission of potential interferences.

Multi-antenna transceivers are thus able to focus their radiation pattern into a beam. However, the beam should be oriented in the direction of the receiver so that it can really benefit on an enhanced quality link. This is possible by adapting the AWV of the transmitter. If $\mathbf{R}(\phi)$ is known, $\boldsymbol{\alpha}$ should be chosen to maximise the received power. This optimisation problem is equivalent to maximise the array gain $A(\phi)$ and can be written as in (2.7).

$$\boldsymbol{\alpha}^{star} = \arg\max_{\boldsymbol{\alpha}} |\boldsymbol{\alpha}\mathbf{R}(\phi)|^2 \quad \text{such that} \quad ||\boldsymbol{\alpha}|| = 1. \tag{2.7}$$

In (2.7), the normalisation constraint imposes that the total emitted power should not be modified with $\boldsymbol{\alpha}$. One can show that the solution of this optimization problem

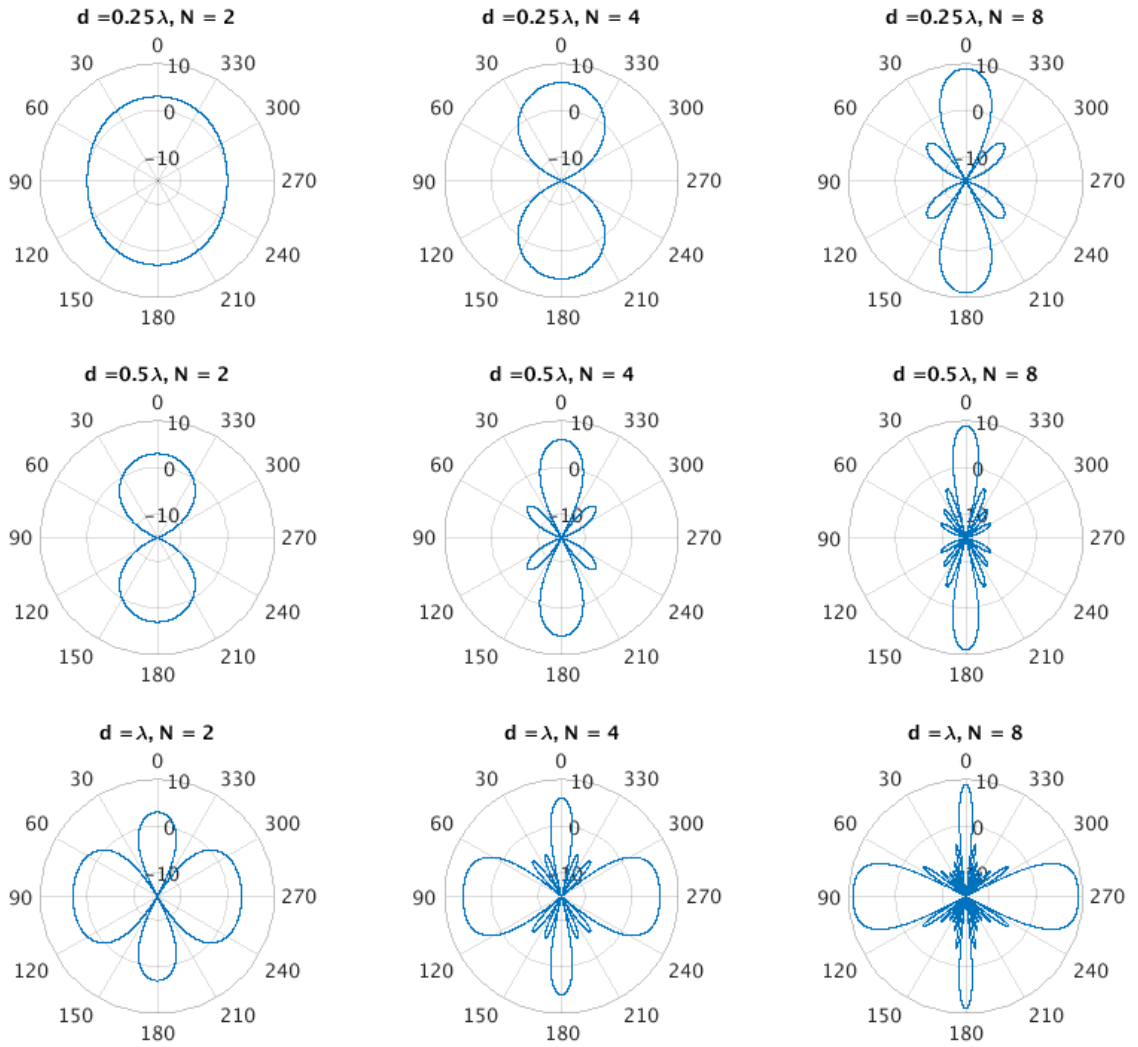

Figure 2.2: Array gain $|A(\phi)|^2$ with $\boldsymbol{\alpha} = 1^N/||1^N||$ for $N = \{2, 4, 8\}$ and $d = \{0.25\lambda, 0.5\lambda, \lambda\}$. Array gains are expressed in dB.

is:

$$\boldsymbol{\alpha}^{star} = \frac{\mathbf{R}^H(\phi)}{||\mathbf{R}(\phi)||}, \tag{2.8}$$

And the array gain for this AWV is given by:

$$|A(\phi)|^2 = |\boldsymbol{\alpha}^{star}\mathbf{R}(\phi)|^2 = ||\mathbf{R}(\phi)||^2 = N. \tag{2.9}$$

Equation (2.9) implies that the optimal array gain of a multi-antenna transceiver is N and increases thus linearly with the size of the array. This is the beamforming effect. In practice, $\mathbf{R}(\phi)$ is not always known and the emitter and the receiver must estimate it.

As explained, the effect of $\boldsymbol{\alpha}$ is to steer the beam toward a particular reference direction, noted ϕ_0. Figure 2.3 depicts the radiation pattern for different directions ϕ_0. One can observe that the width of the main lobe increases as the beam is steered

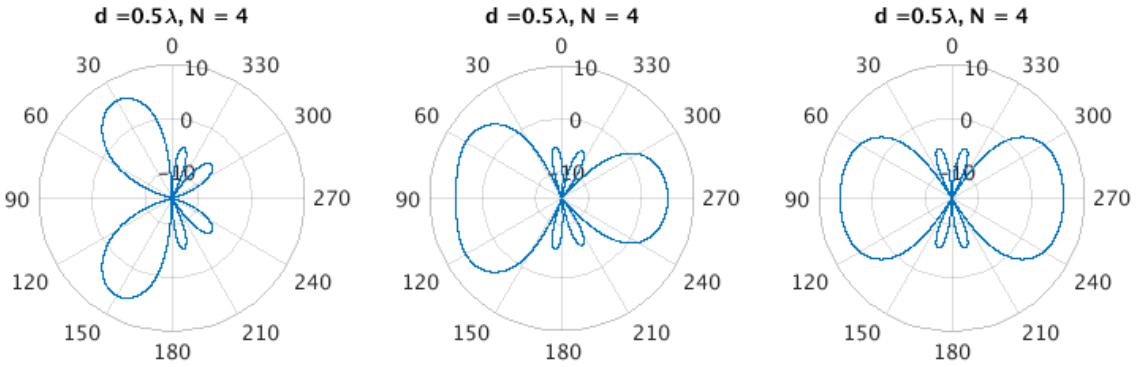

Figure 2.3: Array gain $|A(\phi)|^2 = |\boldsymbol{\alpha}\mathbf{R}(\phi)|^2$ for $\boldsymbol{\alpha} = \mathbf{R}^H(\phi_0)/||\mathbf{R}(\phi_0)||$ with $\phi_0 = \{30°, 60°, 90°\}$.

more and more toward 90°. This means that the directivity of the radiation pattern is reduced when emitting into these directions.

The directivity of the radiation pattern of an antenna array can be measured via the half-power beamwidth. This parameter is a measure of the angle of the half-power angle in the main lobe and is defined as the angle ϕ at which:

$$|A(\phi)|^2 = \frac{|A(\phi_0)|^2}{2}. \tag{2.10}$$

Considering (2.5), $|A(\phi)|^2$ can be simplified as follow:

$$\begin{aligned} |A(\phi)|^2 &= \frac{1}{||\mathbf{R}(\phi_0)||^2} \left|\mathbf{R}(\phi_0)^H \mathbf{R}(\phi)\right|^2 \\ &= \frac{1}{N} \left| \begin{bmatrix} 1 & e^{-j2\pi \frac{d}{\lambda} \sin\phi_0} & \dots & e^{-j2\pi \frac{(N-1)d}{\lambda} \sin\phi_0} \end{bmatrix} \begin{bmatrix} 1 \\ e^{j2\pi \frac{d}{\lambda} \sin\phi} \\ e^{j2\pi \frac{2d}{\lambda} \sin\phi} \\ \vdots \\ e^{j2\pi \frac{(N-1)d}{\lambda} \sin\phi} \end{bmatrix} \right|^2 \\ &= \frac{1}{N} \left| \sum_{n=0}^{N-1} e^{-j2\pi n \frac{d}{\lambda}(\sin\phi_0 - \sin\phi)} \right|^2. \end{aligned} \tag{2.11}$$

Remembering that $\sum_{n=0}^{N-1} a^n = \frac{1-a^N}{1-a}$ if $a \neq 1$. Equation (2.11) leads to:

$$\begin{aligned} |A(\phi)|^2 &= \frac{1}{N} \left| \frac{1 - e^{-j2\pi N \frac{d}{\lambda}(\sin\phi_0 - \sin\phi)}}{1 - e^{-j2\pi \frac{d}{\lambda}(\sin\phi_0 - \sin\phi)}} \right|^2 \\ &= \frac{1}{N} \left| \frac{\sin\left(\frac{1}{2} N 2\pi \frac{d}{\lambda}(\sin\phi_0 - \sin\phi)\right)}{\sin\left(\frac{1}{2} 2\pi \frac{d}{\lambda}(\sin\phi_0 - \sin\phi)\right)} e^{-j2\pi \frac{N-1}{2} \frac{d}{\lambda}(\sin\phi_0 - \sin\phi)} \right|^2 \\ &= \frac{1}{N} \left(\frac{\sin\left(N\pi \frac{d}{\lambda}(\sin\phi_0 - \sin\phi)\right)}{\sin\left(\pi \frac{d}{\lambda}(\sin\phi_0 - \sin\phi)\right)} \right)^2. \end{aligned} \tag{2.12}$$

At $\phi = \phi_0$, the optimal array gain $|A(\phi_0)|^2 = N$ is obtained. So, we are looking for the value of ϕ such that $|A(\phi)|^2 = N/2$.

Figure 2.4 represents the evolution of the beamwidth with ϕ_0 and N. The beamwidth is minimal in $\phi_0 = 0°$. However, the influence of ϕ_0 is relatively small compared to the influence of the number of antennas. When N increases, the beamwidth rapidly decreases. As it will be discussed in section 2.3, a too narrow radiation pattern might be problematic and AWVs with larger beamwidth are generally preferred at the price of a smaller array gain.

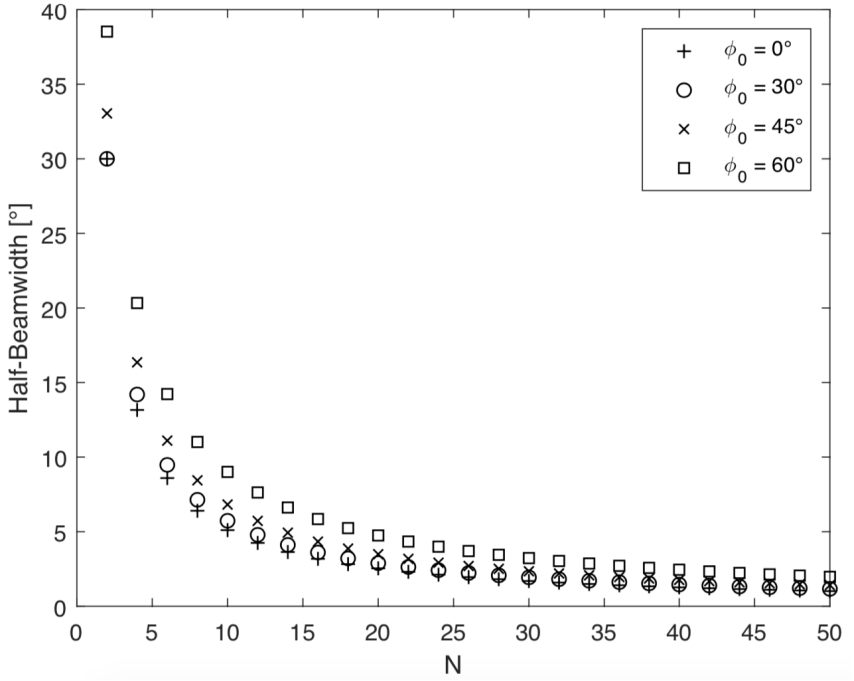

Figure 2.4: Half-beamwidth angle with respect to N with $d = \lambda/2$.

2.2 Emission of a plane wave from a rectangular array

Let us consider a rectangular array with N antennas in the horizontal direction (y-direction) and M antennas in the vertical direction (z-direction). The total number of antennas is thus $N \times M$. The vector describing the position of the n^{th} antenna in the y-direction and m^{th} antenna in z-direction is $\mathbf{a_{n,m}} = (0, nd_y, md_z)$ where d_y and d_z are describing the distance between adjacent antennas along y- and z-directions. The azimuth angle of the plane wave emitted from the antenna array is denoted by ϕ while the elevation angle is denoted by θ (Figure 2.5).

The planar wave is emitted by the rectangular antenna array with a direction given by $\hat{\mathbf{u}} = (\sin\theta\cos\phi, \sin\theta\sin\phi, \cos\theta)$. Once again, the additional travelling distance

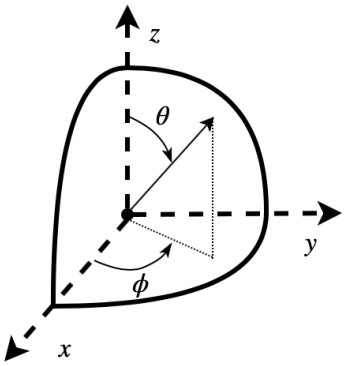

Figure 2.5: Spherical coordinates - convention

for the wave emitted by an antenna at localization (n,m) on the antenna array is given by the projection of the direction of departure $\hat{\mathbf{u}}$ over $\mathbf{a_{n,m}}$:

$$d_{n,m,\phi,\theta} = \hat{\mathbf{u}} \cdot \mathbf{a_{n,m}} = nd_y \sin\theta \sin\phi + md_z \cos\theta. \tag{2.13}$$

The additional travelling time of the wave is

$$\tau_{n,m} = \frac{d_{n,m,\phi,\theta}}{c} = \frac{nd_y \sin\theta \sin\phi + md_z \cos\theta}{c}. \tag{2.14}$$

Similarly as for the linear antenna array, the displacement phase factor $\mathbf{R}(\phi,\theta) \in \mathbb{C}^{NM\times 1}$ is of the form:

$$\mathbf{R}(\phi,\theta) = \begin{bmatrix} 1 \\ e^{j\omega\tau_{1,0}} \\ \vdots \\ e^{j\omega\tau_{N-1,0}} \\ e^{j\omega\tau_{0,1}} \\ e^{j\omega\tau_{1,1}} \\ \vdots \\ e^{j\omega\tau_{N-1,1}} \\ \vdots \\ e^{j\omega\tau_{0,M-1}} \\ e^{j\omega\tau_{1,M-1}} \\ \vdots \\ e^{j\omega\tau_{N-1,M-1}} \end{bmatrix} = \begin{bmatrix} 1 \\ e^{j2\pi\frac{d_y \sin\theta\sin\phi}{\lambda}} \\ \vdots \\ e^{j2\pi\frac{(N-1)d_y \sin\theta\sin\phi}{\lambda}} \\ e^{j2\pi\frac{d_z\cos\theta}{\lambda}} \\ e^{j2\pi\frac{d_y \sin\theta\sin\phi + d_z\cos\theta}{\lambda}} \\ \vdots \\ e^{j2\pi\frac{(N-1)d_y \sin\theta\sin\phi + d_z\cos\theta}{\lambda}} \\ \vdots \\ e^{j2\pi\frac{(M-1)d_z\cos\theta}{\lambda}} \\ e^{j2\pi\frac{d_y \sin\theta\sin\phi + (M-1)d_z\cos\theta}{\lambda}} \\ \vdots \\ e^{j2\pi\frac{(N-1)d_y \sin\theta\sin\phi + (M-1)d_z\cos\theta}{\lambda}} \end{bmatrix}.$$

The displacement phase factor represents the phase shift between the signals emitted by the different antennas and that are perceived by a receiving STA localised in the direction ϕ. The AWV that maximises the received power must verify the following expression:

$$\boldsymbol{\alpha}^{star} = \arg\max_{\boldsymbol{\alpha}} |\boldsymbol{\alpha}\mathbf{R}(\phi,\theta)|^2 \quad \text{such that} \quad ||\boldsymbol{\alpha}|| = 1, \tag{2.15}$$

And the solution of this problem is:

$$\boldsymbol{\alpha}^{star} = \frac{\mathbf{R}^H(\phi,\theta)}{||\mathbf{R}(\phi,\theta)||}. \tag{2.16}$$

This leads to an array gain given by:

$$|A(\phi,\theta)|^2 = |\boldsymbol{\alpha}^{star}\mathbf{R}(\phi,\theta)|^2 = ||\mathbf{R}(\phi,\theta)||^2 = NM. \tag{2.17}$$

Similarly as for the linear array, the array gain increases linearly with the total number of antennas. Examples of radiation pattern are depicted in Figure 2.6. The advantage of a rectangular array compared to a linear array is to steer the beam in both azimuth and elevation directions. More complex geometries of antenna array can be used in practice that modify the vector $\mathbf{a_{n,m}}$. In this report, we consider only the geometry of rectangular arrays with $d_y = d_z = \lambda/2$.

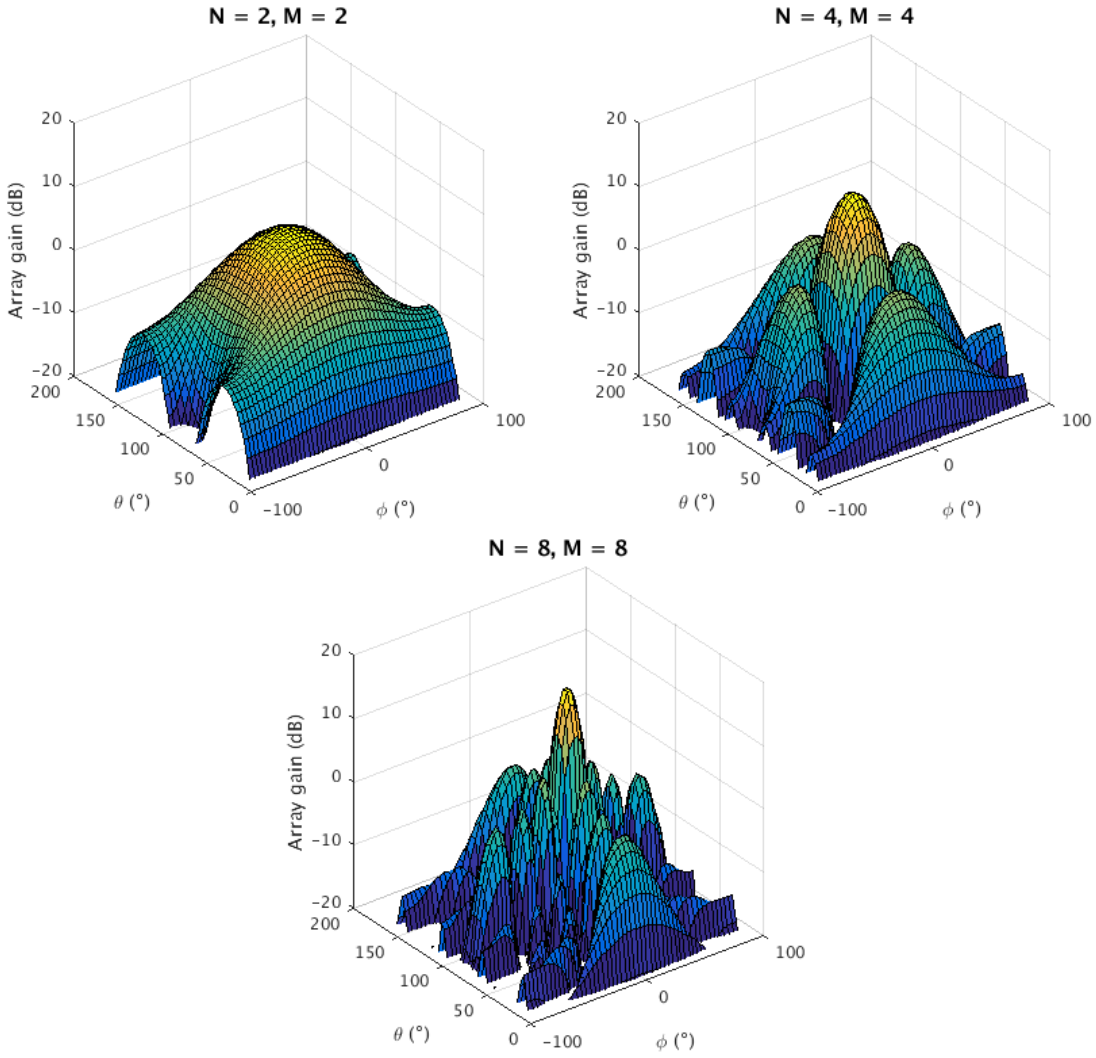

Figure 2.6: Radiation pattern of rectangular arrays steered at $(\phi,\theta) = (0°, 90°)$ and $d_y = d_z = \lambda/2$.

2.3 Codebook design

In sections 2.1 and 2.2, the benefit of the BF technique on the array gain has been demonstrated. From the displacement phase factor $\mathbf{R}(\phi, \theta)$, the weights $\boldsymbol{\alpha}^\star$ that maximise the received power can be dertermined from (2.16).

However, $\mathbf{R}(\phi, \theta)$ is rarely known in practice so the optimal steering vector $\boldsymbol{\alpha}^\star$ can not be easily computed. To overcome this issue, one could directly estimate $\mathbf{R}(\phi, \theta)$ or one could estimate the directions ϕ and θ to compute $\mathbf{R}(\phi, \theta)$. This second method is less complex since only two coefficients must be estimated.

The estimation of ϕ and θ is performed during a training stage, named beamforming training (BFT). During this stage, different AWVs should be tested. Because the transceivers must be able to quickly switch between the different AWVs, predefined AWVs are generally stored in a codebook. This reduces the computation complexity and the power consumption[8].

But working with a high number of antennas raises a new problem when designing those codebooks. As depicted in Figure 2.4, the beamwidth goes down with an increasing number of antennas. This means that, for a high number of antennas, a small mismatch between the estimation and the true value of the angle directions ϕ and θ will cause an important reduction of the array gain. The codebook should therefore comprises AWVs with larger beams.

To overcome this issue, author in [9] proposed a beam widening algorithm based on the division of the array into subarrays. Each subarray steers a beam in a direction slightly different than the other so that the total beam appears wider. In [10], beam broadening is performed through the use of window coefficients (e.g. rectangular or Hamming windows). In this section, a new algorithm for beam widening will be presented. The algorithm considers a linear array but can easily be extended for a rectangular array.

Let us consider the case of a linear array that would like to steer a wide beam in $\phi = 0°$. We note by ϕ_{wd} the beamwidth. The expected performance is a large and constant array gain in the angular range $\phi \in \Phi = [-\phi_{wd}/2, \phi_{wd}/2]$. To express numerically the performance of any steering vector $\boldsymbol{\alpha}$, a fitness function $\mathbb{F}(\boldsymbol{\alpha})$ has been defined. From the minimisation of this fitness function, one would like to extract an AWV with the desired radiation pattern.

Let us investigate the choice of $\mathbb{F}(\boldsymbol{\alpha})$ and its minimisation. We note by $\bar{\Phi} = [-90°, -\phi_{wd}/2] \cup [\phi_{wd}/2, 90°]$, the range of azimuth directions for which the array gain should be minimised. The chosen fitness function is defined as in (2.18):

$$\mathbb{F}(\boldsymbol{\alpha}) = \underbrace{\frac{1}{\phi_{wd}} \int_{\phi \in \Phi} (A_m - |A(\phi)|)^2 d\phi}_{\mathbb{F}_1(\boldsymbol{\alpha})} + \beta \underbrace{\frac{1}{180 - \phi_{wd}} \int_{\phi \in \bar{\Phi}} |A(\phi)|^2 d\phi}_{\mathbb{F}_2(\boldsymbol{\alpha})}, \tag{2.18}$$

Where A_m is the mean of $|A(\phi)|$ in the directions for $\phi \in \Phi$ and β is an arbitrary real scalar. As a reminder, from (2.6) we have $A(\phi) = \boldsymbol{\alpha}\mathbf{R}(\phi)$. In (2.18), the fitness function has been chosen to trade off the minimisation of array gain in $\bar{\Phi}$ $(= \mathbb{F}_2(\boldsymbol{\alpha}))$ and the minimisation of the level of ripple of $|A(\phi)|$ in Φ $(= \mathbb{F}_1(\boldsymbol{\alpha}))$.

To compute $\boldsymbol{\alpha}$ that minimises the fitness function, a simplified version of a greedy algorithm has been used. The algorithm starts with an initial population of AWVs for which the coefficients have all the same amplitude but a random phase. At each iteration, the best individual (in the sense of the minimisation of $\mathbb{F}(\boldsymbol{\alpha})$) is selected and a new population is created from the perturbation of this individual (see Algorithm 1).

Algorithm 1 Beam widening

Input: N, N_{pop} ▷ N = #antennas, N_{pop} = population size
1: $Pop = e^{2\pi i \cdot rand(N, N_{pop})}$ ▷ Generate initial population
2: $\eta = 1$ ▷ Perturbation amplitude
3: **while** $\eta > 10^{-6}$ **do**
4: $\quad Pop^\star = \{Pop(i) | \mathbb{F}(Pop(i)) \leq \mathbb{F}(Pop(j)) \ \forall j\}$ ▷ Selection of best individual
5: $\quad \eta = update(\eta)$
6: $\quad Pop = [Pop^\star, Replicate(Pop^\star, N_{pop} - 1) \odot e^{i \cdot rand(N, N_{pop}-1) \cdot \eta}]$ ▷ Perturbation
7: **end while**
8: **return** $Pop^\star / ||Pop^\star||$

In Algorithm 1, the Hadamard product is represented by the symbol $\odot$. The perturbation amplitude η is a coefficient used to speed up the convergence of the algorithm. For our algorithm, η was divided by two each time 200 loop iterations have been done without any improvement on the minimisation of the fitness function. Note that during the replication operation, one copy of the best individual should be kept unperturbed.

The result of the beam widening algorithm for $N = 64$ antennas, $N_{pop} = 100$ and different beamwidth is depicted in Figure 2.7. We observe that the array gain is at least 10dB higher for $\phi \in \Phi$ than for $\phi \notin \Phi$. Compared to optimal steering the loss of array gain in $\phi = 0°$ is of the order of 5dB for $\phi_{wd} = 10°$ and increases progressively with the beamwidth.

The performance of the steering vector can be adapted by the modification of β in the expression of $\mathbb{F}(\boldsymbol{\alpha})$ in (2.18). This is illustrated in Figure 2.8. For a large value of β, the array gain in $\phi \in \bar{\Phi}$ becomes less important meaning that interferences management is facilitated. However, the level of ripple of array gain in $\phi \in \Phi$ is in this case more pronounced.

From the algorithm presented here above, one can design a codebook of predefined AWVs with different beamwidths. The steering direction of the beams should also be investigated because the receiving STA is not necessarily standing in $\phi \in [-\phi_{wd}/2, \phi_{wd}]$. To steer the beams in angular direction $\phi \neq 0°$, two different methods

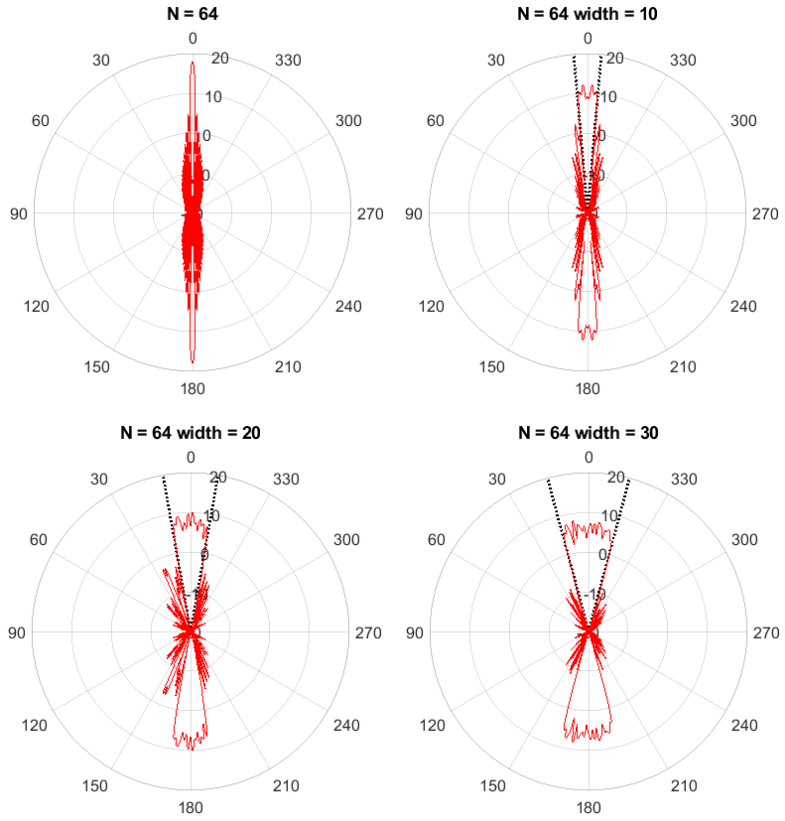

Figure 2.7: Array gain $|A(\phi)|^2 = |\boldsymbol{\alpha}\mathbf{R}(\phi)|^2$ for optimal beam (top left) and for wide beams with $\phi_{wd} = \{10°, 20°, 30°\}$ and $\beta = 10$. The black dot lines are located in $\phi = \pm\phi_{wd}/2$. Array gains are expressed in dB.

are considered:

- **Steering vector adaptation:** modification of the steering vector $\boldsymbol{\alpha}$ [10].
- **Angular range adaptation:** modification of the angular range Φ and $\bar{\Phi}$.

Let us focus on the first method. The steering vector adaptation applies a phase shift on each coefficient of $\boldsymbol{\alpha}$ in order to orient the beam in the desired direction ϕ_{des}. It can be shown that this adaption is performed through the following operation:

$$\boldsymbol{\alpha} = \boldsymbol{\alpha}_0 \odot \mathbf{R}^H(\phi_{des}), \tag{2.19}$$

Where $\odot$ is the Hadamard product, $\boldsymbol{\alpha}_0$ is the steering vector obtained via Algorithm 1 and $\mathbf{R}(\phi)$ was defined in (2.5). The result of this operation is depicted in Figure 2.9.

Even if the steering direction is well oriented, the performance of this method is relatively disappointed. When the steering direction is getting closer to $\phi = 90°$, the beamwidth is importantly increased. However, for sufficiently small steering directions (e.g. 30°), the performance of the AWV is almost similar to the one steered at $\phi = 0°$. The main advantage of the steering vector adaptation method is that from only one AWV, other steering vectors with different steering directions can

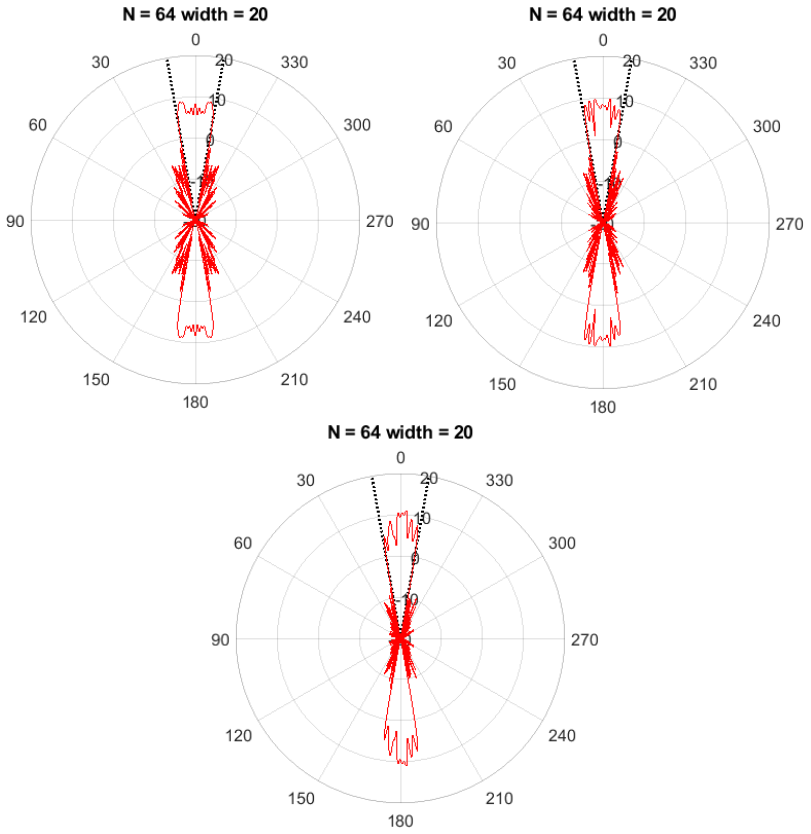

Figure 2.8: Array gain $|A(\phi)|^2$ obtained with $\phi_{wd} = 10°$ and $\beta = \{2, 10, 50\}$ (left to right). The black dot lines are located in $\phi = \pm\phi_{wd}/2$. Array gains are expressed in dB.

be easily computed. The size of the codebook is thus kept constant as well as the required memory size to store the codebook.

If the memory management is not critical, one can also adapt Algorithm 1 to generate a codebook with a higher number of steering vectors $\boldsymbol{\alpha}$, each pointing their radiation pattern in different directions. This is the principle of the second method, angular range adaptation. To do so, it is only required to redefine Φ and $\bar{\Phi}$. A natural choice is simply to impose $\Phi = [\phi_{des} - \phi_{wd}/2, \phi_{des} + \phi_{wd}/2]$ and $\bar{\Phi} = [-90°, \phi_{des} - \phi_{wd}/2] \cup [\phi_{des} + \phi_{wd}/2, 90°]$.

The result of this adaptation is depicted in Figure 2.10. Compared to the steering vector adaptation, angular range adaptation conserves better the beamwidth when steering toward $\pm 90°$.

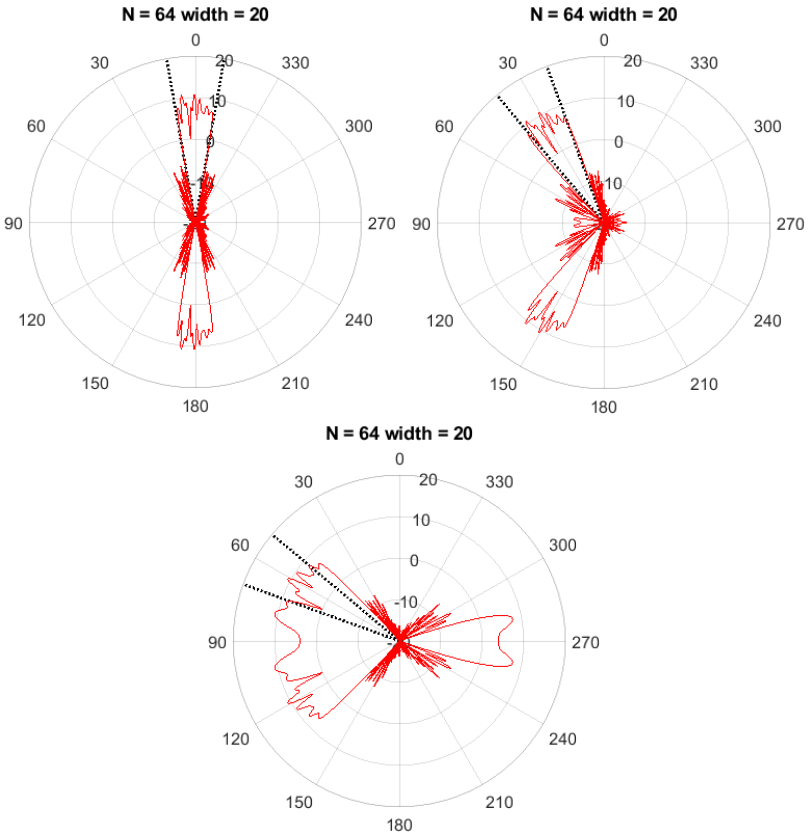

Figure 2.9: Array gain $|A(\phi)|^2$ obtained with the steering vector adaptation method with $\phi_{des} = \{0°, 30°, 60°\}$ ($\beta = 10$). The black dot lines are located in $\phi = \phi_{des} \pm \phi_{wd}/2$. Array gains are expressed in dB.

2.4 Conclusion

The physical aspects of beamforming technique exploitable by a multi-antenna transceiver have been investigated in this chapter. Thanks to the phase shifters, the radiation pattern of the antenna array can be steered in a desired direction. This steering allows an increase of the quality link and a reduction of the interferences perceived by other STAs.

The narrowness of the beam formed in the radiation pattern is however critical if the position of the other STA is not sufficiently well estimated. To remedy this, a beam widening algorithm has been proposed showing a good trade-off between low level of ripple of array gain in the angular passband and large reduction of array gain in the angular stopband.

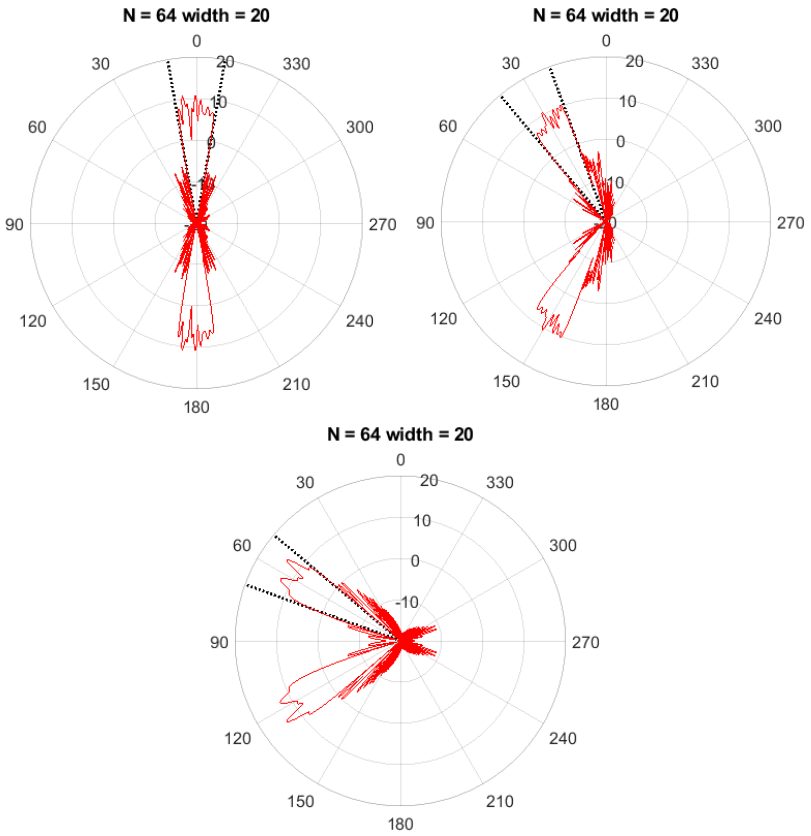

Figure 2.10: Array gain $|A(\phi)|^2$ obtained with the angular range adaptation method for $\phi_{des} = \{0°, 30°, 60°\}$ ($\beta = 10$). The black dot lines are located in $\phi = \phi_{des} \pm \phi_{wd}/2$. Array gains are expressed in dB.

Chapter 3

IEEE 802.11ad/ay standards

Since 1997, the IEEE802.11 standard (= Wi-Fi standard) has emerged as the most widely used wireless networking standard around the world[11]. It includes frequency bands at 2.4 and 5GHz. In December 2012, the IEEE802.11ad specification of the standard was released to enable Wi-Fi communications over the 60GHz band with data throughput up to 6.75Gbps[12, 13]. This amendment is taking advantage of the large unlicensed bandwidth available at that frequency. Furthermore, IEEE802.11ad redefined the IEEE802.11 medium access control (MAC) and physical (PHY) layers in order to cope with the necessary beamforming training (BFT) that improves the budget link quality.

IEEE802.11ad was mainly designed for applications requiring high data throughput such as HDMI cable replacement (e.g. wireless displays), instant wireless synchronisation and high speed media file exchange[14]. With new emerging technologies such as augmented reality and virtual reality, the need for Wi-Fi allowing higher throughput is still necessary[2]. To address this problem, the IEEE802.11ay specification was designed on top of IEEE802.11ad. This enhancement of the standard is still under development and should provide Wi-Fi communication of up to 20-40Gbps.

The first part of this chapter aims at describing the implementation of the different BFT procedures in the IEEE802.11ad/ay specifications of the IEEE802.11 standard. The main differences between these two specifications will be shortly presented. The rest of the chapter describes the *Matlab* chain used during the simulations of chapters 4 and 5.

3.1 IEEE802.11ad/ay amendments description

The development of the IEEE802.11ad/ay amendments of the IEEE802.11 standard has been motivated by the need for Wi-Fi communication allowing very high data throughput. As explained in section 1.1, the research community has identified the mmWave spectrum as being interesting for high speed communication thanks to three different techniques: large bandwidth utilisation, higher spectral efficiency and densification of the cellular infrastructure.

Let us focus on the large bandwidth available in the mmWave spectrum. The IEEE802.11ad/ay specifications are designed for the utilisation of the 60GHz band where a large unlicensed band has been made available (see Figure 3.1). This 60GHz band is further divided in several 2.16GHz subchannels in which the stations (STAs) (BS or UE) are allowed to communicate. In the IEEE802.11ad specification, only one of those subchannels can be used by a STA at a time. We will refer a STA working under the IEEE802.11ad as directional multi-gigabits (DMG) STA.

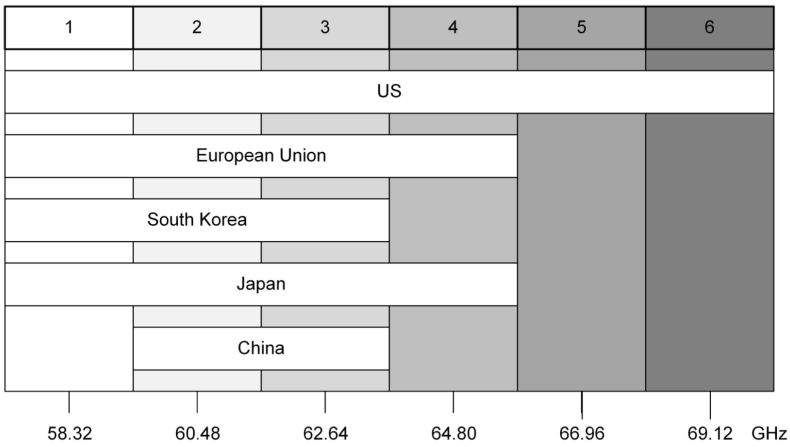

Figure 3.1: Available 802.11ad/ay 2.16GHz subchannels in the 60 GHz band[15].

In IEEE802.11ay, two important evolutions have been introduced in the medium access control (MAC) and physical (PHY) layers of the standard to increase the bandwidth utilisation and the spectral efficiency. They will be presented in the following paragraphs and we will refer a STA supporting both IEEE802.11ad and IEEE802.11ay specifications as enhanced directional multi-gigabits (EDMG) STA.

To allow for a larger bandwidth utilisation, EDMG STAs are allowed to use up to four contiguous 2.16GHz subchannels (=channel bonding) or non-contiguous 2.16GHz subchannels (= channel aggregation) instead of one for DMG STAs. The maximal bandwidth utilisation is therefore equivalent to 8.64GHz. An announcement mechanism of scheduling and transmission opportunity (TXOP) has been established [2] to support channel bonding and channel aggregation. In scheduling, the total channel bandwidth is specified during the network announcement (i.e. in the BHI, see section 3.1.1). In TXOP, the STAs extend their bandwidth when secondaries channels are idle.

The second evolution brings to the IEEE802.11ay specifications is the introduction of the spatial multiplexing (SM) technique that increases the spectral efficiency of the communication. While DMG STAs are authorised to transmit one data stream at a time, EDMG STAs are allowed to transmit up to eight data streams simultaneously to one (=SU-MIMO) or several (=MU-MIMO) STAs. Because every communication link related to a data stream should be trained, the BFT procedure as been modified

for EDMG STAs.

In this section is proposed an explanation of the MAC layer of the IEEE802.11 standard. A particular emphasis will be bring to the channel access which is necessary to better understand how the DMG and EDMG BFTs have been inserted in the standard.

3.1.1 (E)DMG channel access

This operation is managed by the Data Link Layer which is the second of the seven-layers Open Systems Interconnection (OSI) model. This layer serves to: [16]

- Convert the bits streams coming from the network into frames that will be transmitted through the channel.
- Perform flow control between STAs.

The lower sublayer of the Data Link Layer is the MAC sublayer. In the MAC sublayer, a protocol is implemented (= MAC protocol) and determines who can transmit on a broadcast channel. For IEEE 802.11ad/ay, time division multiple access (TDMA) is mainly used and carrier-sensing multiple access with collision avoidance (CSMA/AC) can be used to handle bursty traffic [17].

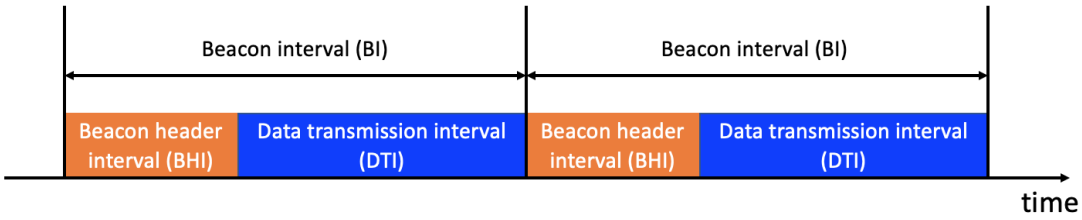

Figure 3.2: MAC sublayer: beacon interval (BI).

Each time a STA wants to send frames to one or more other STAs, it must be performed within a beacon interval (BI). Any BI is composed of two periods of time (see Figure 3.2): a beacon header interval (BHI) following by a data transfer interval (DTI).

The BHI determines which STAs will be the next ones to transfer data frames during the DTI. This protocol aims at avoiding collision between data packets coming from several STAs. The BHI comprises three different intervals: beacon transmission interval (BTI), association beamforming training (A-BFT) and announcement transmission interval (ATI) (see Figure 3.3), each having its own function. More information can be found in [18].

The DTI includes one or more service periods (SPs) and contention based-access periods (CBAPs). A SP is a scheduled timing period during which STAs can communicate in a TDMA scheme. A CBAP is a timing period during which all

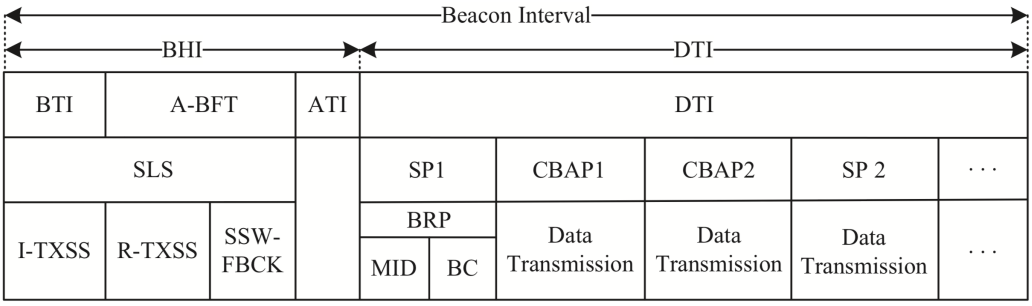

Figure 3.3: Example of access period within a beacon interval [18].

STAs can access the channel by listening to it and transmitting data when it is idle. This period combines TDMA and CSMA/AC techniques. More information can be found in [17].

3.1.2 DMG beamforming training

As explained in chapter 2, beamforming (BF) is a technique used by multi-antenna transceivers. With BF, a STA is able to increase its array gain in the direction of another STA for which it wants to enhance the communication link budget. The determination of this direction requires dedicated beamforming training (BFT) stages.

The IEEE802.11ad specification defines three different BFT procedures (see Figure 3.3):

1. Sector level sweep (SLS): transmit BFT performed during the BHI .
2. Beam refinement protocol (BRP): receive BFT and refinement performed during the first SP of the DTI (optional).
3. Beam tracking (BT): transmit and/or receive BFT training performed during the DTI to manage STA mobility (optional).

The SLS and the BRP phases are performed either when the communication link is not established or broken or either periodically. When at least one of the STAs is moving, the steering direction of the radiation pattern should be updated regularly. Because the SLS and the BRP phases are expensive in terms of timing and training overhead, the BT phase should be used to adjust the AWV of the transceivers.

Those three BFT procedures consist in bidirectional exchanges of training frames between the STAs. The training frames contain pilot sequences and are not the same for the three procedures. Figure 3.4 presents an overview of the SLS and the BRP phases.

The STA initiating the beamforming training procedure is called the initiator while the other is named responder. Let us described the different BFT procedures in the following paragraphs.

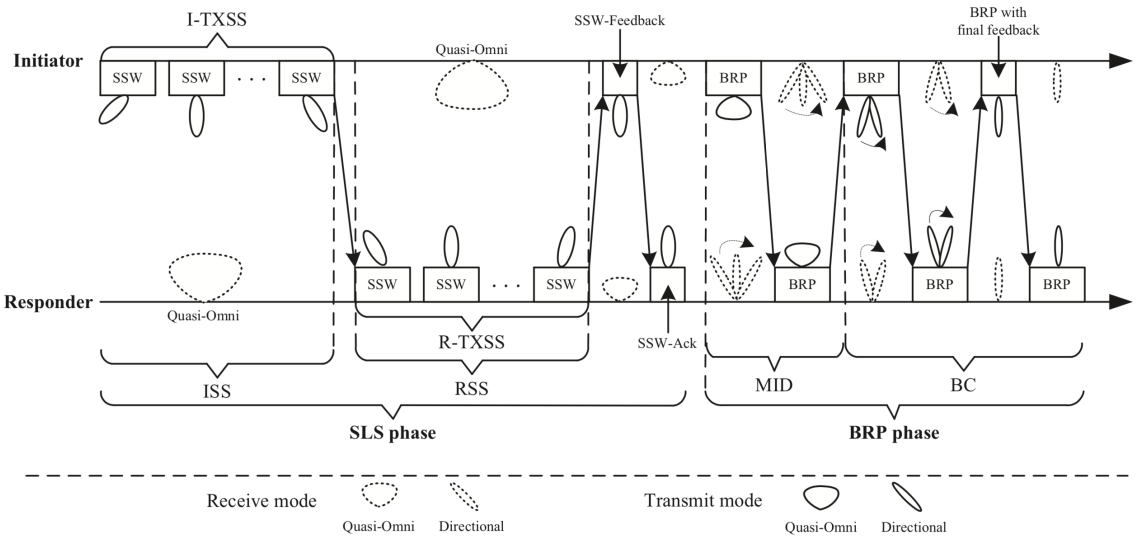

Figure 3.4: SLS and BRP phases: illustration of the principle [18]

3.1.2.1 Sector level sweep phase

In the SLS phase, the initiator and responder are exchanging training frames in order to train their transmit antenna weight vector (AWV). An explanation of the role of the AWV has been given in chapter 2. The general principle of the SLS phase is depicted in Figure 3.5.

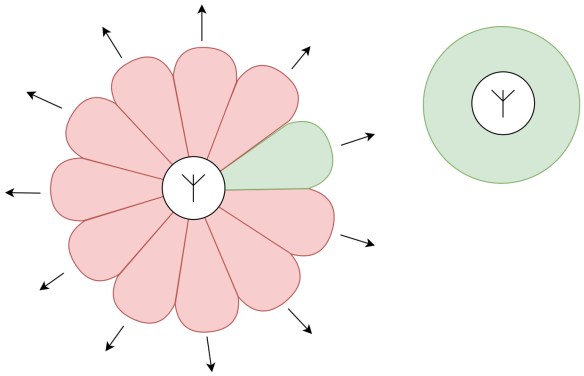

Figure 3.5: Illustration of the SLS phase. The transmitting STA trains its transmit AWV by sending successively sector sweep (SSW) frames toward different directions or sectors. The receiving STA measured the different SNR level for each sector and communicates to the trained STA the sector for which the measured SNR level was the highest.

The SSW frames contain two mandatory fields. The first one is the countdown (CDOWN) field and is used to indicate how many SSW frames still have to be sent/received. The second one is the Sector ID that uniquely identifies the tested sector. All SSW frames containing the same Sector ID are sent using a common AWV. The maximal number of SSW frames is 512 and the maximal number of

different Sector IDs is 64. Let us investigate in practice how this training stage is performed. The SLS phase is composed of four subphases:

- The initiator sector sweep (ISS) to train the initiator.
- The responder sector sweep (RSS) to train the responder.
- The SSW feedback.
- The sector sweep acknowledgment (SSW-ACK).

In Figure 3.6 is shown an example of a SLS procedure. The initiator first sends SSW frames using different AWVs. The same amount of power is emitted during the transmission of all SSW frames. The responder receives the packets using a quasi omnidirectional AWV (i.e. quasi isotropic radiation pattern) and evaluates the SNR level of the different packets.

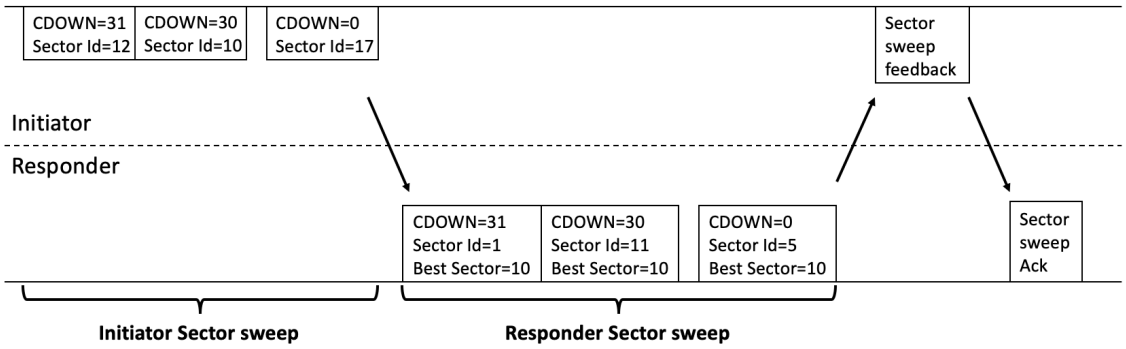

Figure 3.6: Example of SLS phase

Once the responder gets the last SSW frame (CDOWN = 0), the ISS subphase is completed and the RSS subphase starts. The RSS subphase is identical to the ISS subphase with inverse role between initiator and responder. In this subphase, a third field is included in the SSW frames to indicate to the initiator which sector reached the highest level of SNR in the ISS subphase.

During the SSW feedback subphase, the initiator transmits to the responder the Sector ID and the measured SNR level of the best sector during the RSS subphase. The initiator may also indicate if it wants to perform the BRP training.

Finally, the responder sends a SSW-ACK frame to acknowledge the SLS termination. Again, the responder may announce if it wants to perform the BRP training.

3.1.2.2 Beam refinement protocol phase

The beam refinement protocol (BRP) aims at training the receive antenna configuration and at refining the AWVs at the transmitter and receiver sides. It can be skipped if not requested during the SLS phase. The training frames exchanged during

this procedure consist in training fields (TRNs) that are appended at the end of the data packets.

A data packet is made of different fields as depicted in Figure 3.7. The short training field (STF) and first channel estimation (CE) field are part of the preamble and are used for synchronisation. The header field contains some setting parameters such as the packet type or the number of TRN-Units contained in the TRN field. The automatic gain control (AGC) field is used at the reception to train the signal amplifier in order to maintain a suitable signal amplitude at its output. Finally, the optional TRN field is appended at the end of the packet.

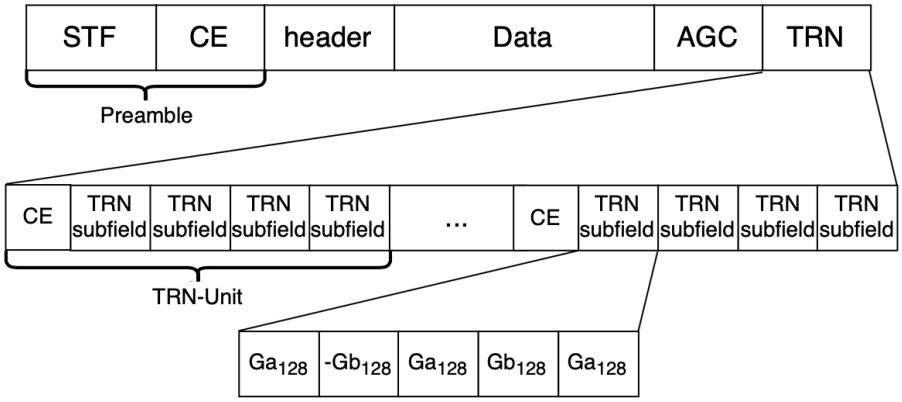

Figure 3.7: Data packet structure.

The TRN field is composed of different TRN-Units that are generated by the concatenation of a CE field and four TRN subfields. Each TRN subfields consists in five Golay sequences of 128bits. Because the receiving STA knows those sequences, it can precisely measure the SNR level of the link.

Two different TRN fields can be used by DMG STAs: TRN-R and TRN-T fields. During the transmission of a TRN-R field, the same transmit AWV must be used for the transmission of all TRN subfields so that the receiver can train its receive AWV. Inversely, during the reception of a TRN-T field, the same receive AWV must be used so that the transmitter can train its transmit AWV.

Let us come back to the description of the BRP phase. The BRP phase is divided into two subphases: multiple sector ID detection (MID) and beam combining (BC). The principle of these two subphases is depicted in Figure 3.8 and Figure 3.9.

In the MID subphase, the initiator uses a quasi omnidirectional AWV for transmitting the TRN-R field and the responder trains its receive AWV. Then roles are inverted between the initiator and the responder.

During the BC subphase, the initiator and responder select a set of potentially good transmit and receive AWVs and all combinations are tested by exchanging TRN-T

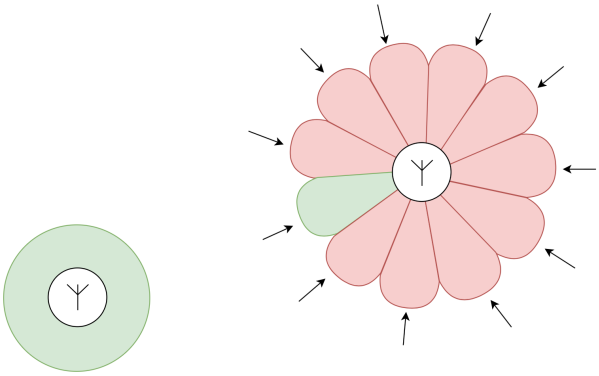

Figure 3.8: Illustration of the MID subphase. The transmitting STA is sending training frames using a quasi omnidirectional AWV. The receiving STA trains its receive AWV by testing successively different AWVs and measuring the resulting SNR level.

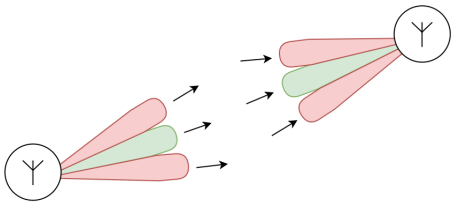

Figure 3.9: Illustration of the BC subphase. Different transmit and receive AWVs are tested successively. The receiver measures the SNR level of every pair of tested AWVs and then informs the transmitter of the best combination.

and TRN-R fields. The pair of AWVs leading to the highest SNR level is then used for the transmission of the next data packets.

3.1.2.3 Beam tracking

Since the UE mobility, the SNR of the transmission link usually decreases over time. When the SNR becomes too low (generally below a threshold), it becomes necessary to find a more suitable AWV. Instead of performing once again the SLS and BRP phases, a procedure named beam tracking (BT) has been included in the IEEE802.11ad specification and allows a fast beam refinement.

The principle is illustrated in Figure 3.10. This BFT procedure is a request/response procedure. Similarly as for the BRP phase, TRN-T and TRN-R fields are appended at the end of data packets so that the STAs can train their transmit and receive AWVs.

3.1.3 EDMG beamforming training

To support multiple independent data streams, the IEEE802.11ay specification introduces two new BF procedures[2]: single-user MIMO (SU-MIMO) BF training and multi-user MIMO (MU-MIMO) BF training. SU-MIMO allows two EDMG STAs to

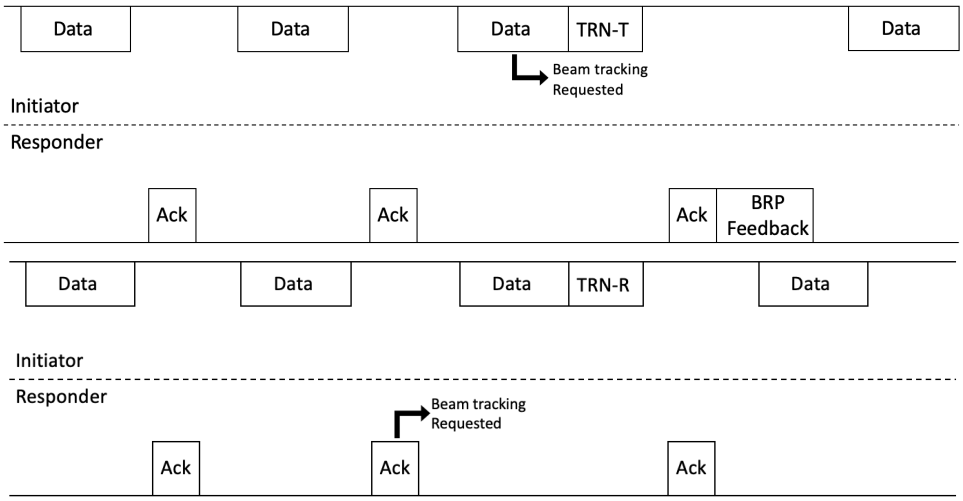

Figure 3.10: Examples of beam tracking for transmit (up) and receive (down) AWV training. In the case of transmit AWV training, the receiving STA must transmit a BRP feedback frame to the trained STA which indicates the Sector ID of the best sector (=AWV) tested.

exchange multiple streams of data while MU-MIMO allows multiple EDMG STAs to exchange frames with a single EDMG STA (= AP/PCP or BS) in downlink.

These two procedures are performed in the DTI. The data packets have been redesigned and new training frame (short SSW) and training fields (EDMG TRN fields) have been introduced in this release of the standard in order to increase the training efficiency. More information can be found in [2]. Similarly as for DMG training frames/fields, EDMG training frames/fields allow EDMG STAs to test different transmit and receive AWVs and select the optimal one based on the best measured SNR level.

In section 3.1.3.1 is developed the procedure of SU-MIMO BFT. Section 3.1.3.2 investigates the MU-MIMO BFT procedure.

3.1.3.1 SU-MIMO beamforming training

The principle of the SU-MIMO BF training is depicted in Figure 3.11. The IEEE802.11 standard considers that the antenna array of an EDMG STA is divided in several DMG antennas. Those DMG antennas are configurable to cover overlapping or non-overlapping spatial sectors and each DMG STA is able to transmit/receive only one data stream in its sector.

The different data streams coming from different DMG antennas should follow different paths so that they do not interfere with each other. The SU-MIMO BF training aims at determining those different paths. This MIMO BF training is divided into two consecutive phases: a SISO phase and a MIMO phase (see Figure 3.12).

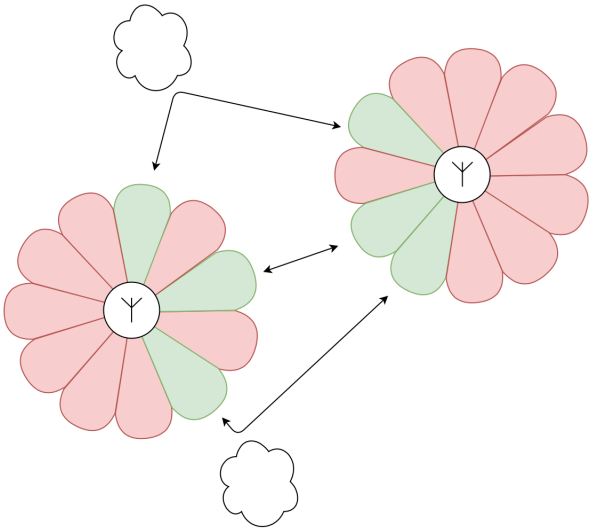

Figure 3.11: SU-MIMO beamforming training illustration. For each DMG antenna, the transmit and receive STAs train their transmit/receive AWVs using sector sweep.

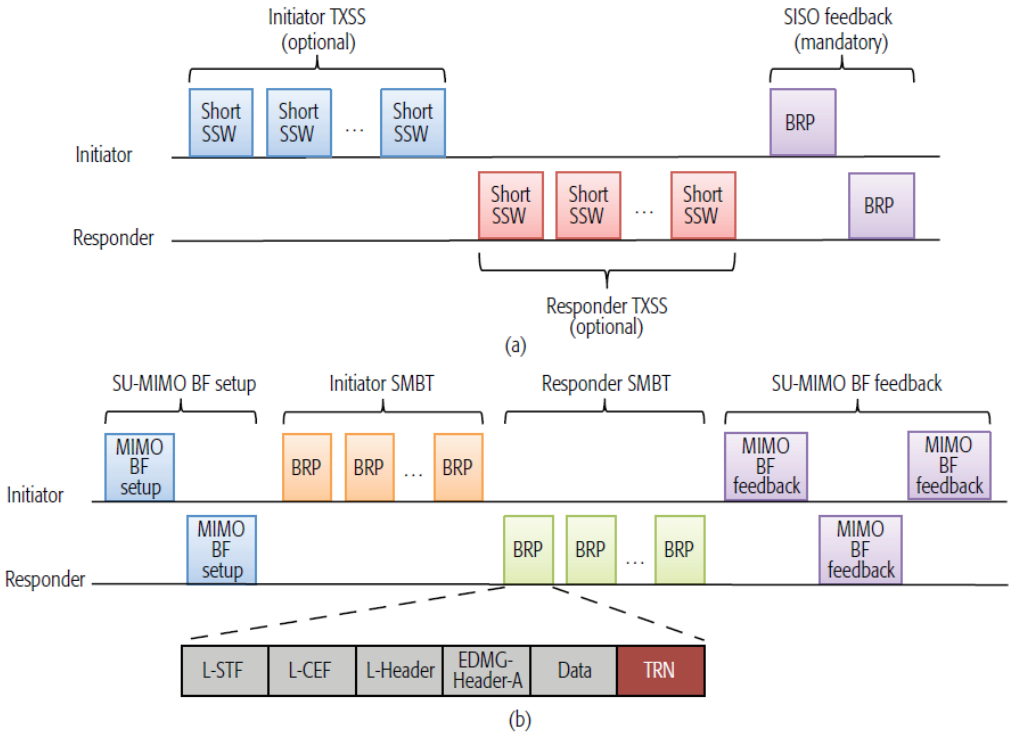

Figure 3.12: Single-user MIMO (SU-MIMO) beamforming training. (a) SISO phase and (b) MIMO phase. [2]

During SISO phase, the initiator sends short SSW packets to enable the training of its transmit AWV. Then the responder trains its transmit AWV using the same technique. These two operations can be skipped if the STAs decide to determine the quality of each tested sectors based on a previous sector sweep stage (e.g. during SLS).

In the mandatory SISO feedback subphase, the initiator and responder transmits the list of Sector IDs of all the tested AWVs and the measured SNR levels.

During the MIMO phase, the initiator and responder first announce for each DMG antenna the number of sectors that they want to train. This is performed in the SU-MIMO BF setup subphase. Then, transmit and receive AWV trainings are performed by appending EDMG TRN fields at the end of data packets. Finally, in the SU-MIMO BF feedback subphase, the initiator and responder communicate the final transmit/receive AWVs for each DMG antenna and the measured SNR level.

3.1.3.2 MU-MIMO beamforming training

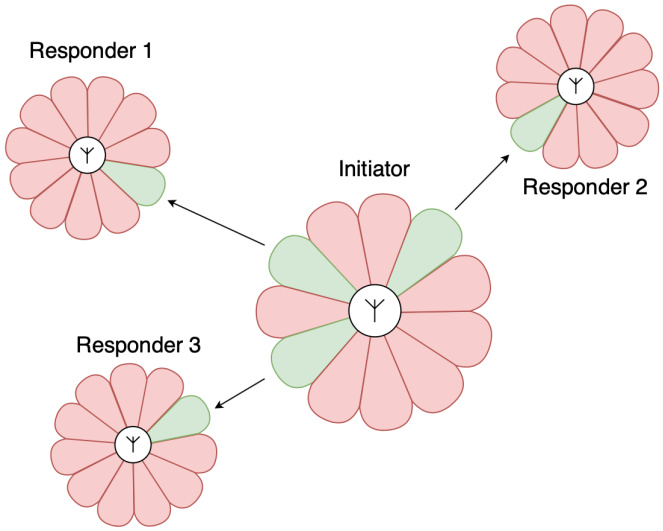

Figure 3.13: MU-MIMO beamforming training illustration. The initiator first transmits training frames in each sector. The responders send back the list of Sector IDs and the measured SNR level. The initiator selects the best sector for each responder and transmit/receive AWV trainings are then performed.

The principle is illustrated in Figure 3.13. The multi-user MIMO (MU-MIMO) is also divided into the two same phases: SISO and MIMO (see Figure 3.14). Because the IEEE802.11ay specification allows MU-MIMO only in downlink, the initiator is the AP/PCP (BS) and initiates the BFT procedure.

In the SISO phase, the initiator sends short SSW packets so that responders can estimate the level of SNR for each tested sectors. Again, this phase can be skipped if the STAs would rather reuse the results obtained in a previous training stage (e.g. SLS phase). All responders send then a feedback frame containing the list of Sector IDs and measured SNR levels for each DMG antenna.

In the MIMO phase, the initiator selects the STAs with whom it wants to communicate, specifies the order of training and announces the number of sectors tested

for each DMG antenna. Then transmit/receive AWV trainings are performed for each responder and the initiator polls each responder to get its BF feedback frame containing the measured SNR for each sector. Finally, the initiator selects and transmits the antenna configuration chosen for each responder in the MU-MIMO BF selection subphase.

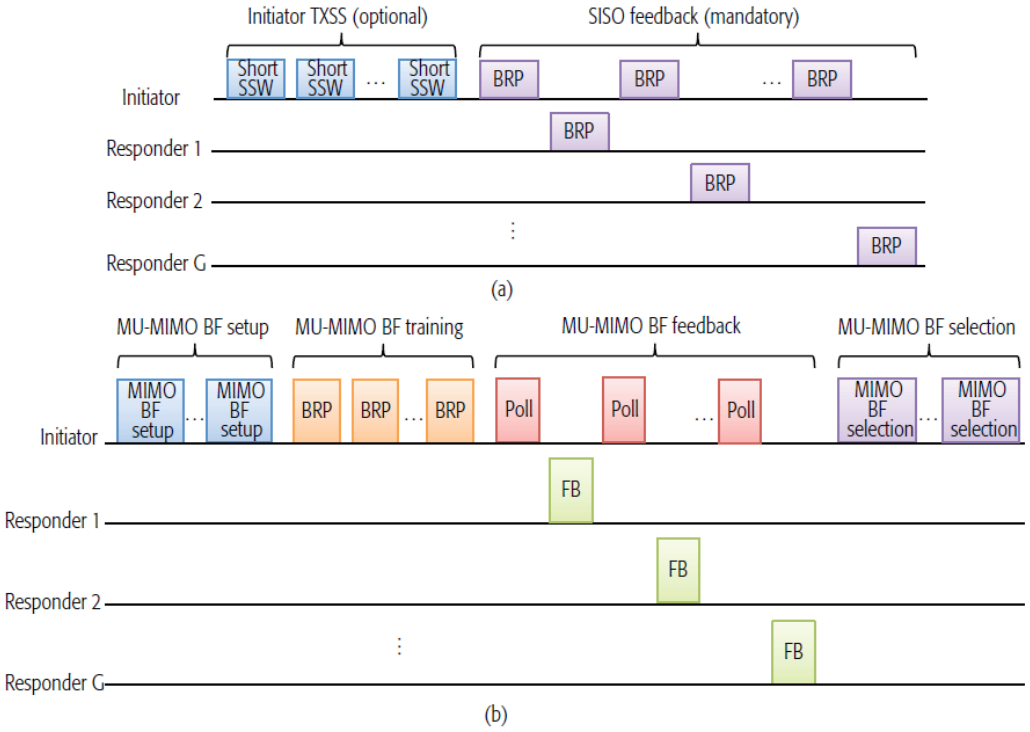

Figure 3.14: multi-user MIMO (MU-MIMO) beamforming training. (a) SISO phase and (b) MIMO phase. [2]

3.1.4 Overview of the different BFT procedures

In Table 3.1 is resumed the goal and compatibility of the different BFT procedures that have been proposed in this section.

BFT	Compatibility	Interval	Goal
SLS	(E)DMG	BHI	Transmit AWV training
BRP	(E)DMG	First SP	Receive AWV training and refinement
BT	(E)DMG	DTI	Transmit/Receive AWV trainings for managing UE mobility
SU-MIMO	EDMG	DTI	Transmit/Receive AWV trainings for single user MIMO
MU-MIMO	EDMG	DTI	Transmit/Receive AWV trainings for multi user MIMO (downlink)

Table 3.1: Overview fo the different beamforming training (BFT) procedures in the IEEE802.11ad/ay specifications of the IEEE802.11 standard.

3.2 Matlab Chain

The next chapters of this report will investigate the implementation and simulation of different BFT algorithms. In this section is proposed a presentation of the *Matlab* chain used for the different validations of the BFT algorithms. The *Matlab* chain is depicted in Figure 3.15.

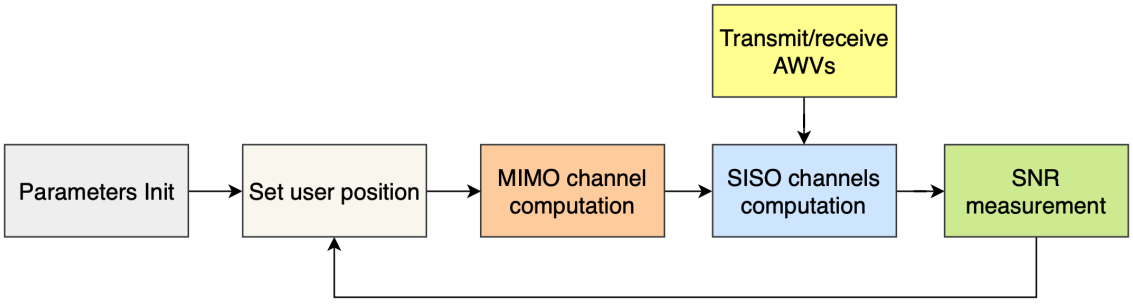

Figure 3.15: *Matlab* chain

Parameters init: Set up the different simulation parameters. For example, the number of antennas, the transmit power, the thermal and figure noise levels, ...

Set user position: Define the user position in the environnement depicted in Figure 3.16. In chapter 4, a fixed user scenario will be considered during the BFT procedure and the user will be standing at $(x, y, z) = (2.4, -1, 1.5)$. In chapter 5, a moving user scenario will be considered in which the user is allowed to move freely in the xy plane at z = 1.5m.

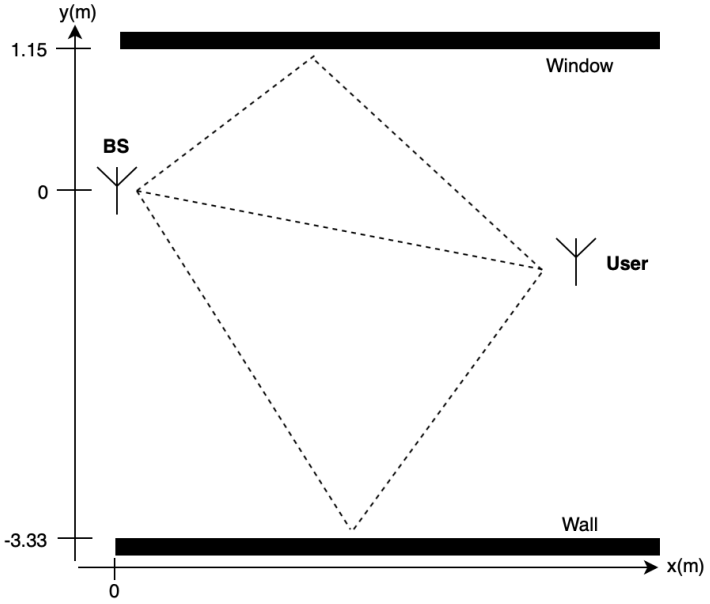

Figure 3.16: User and base station (BS) environnement. The user and the BS are standing in z = 1.5m. Reflection on the ground (z = 0m) and ceiling (z = 2.5m) are not shown.

MIMO channel computation: Compute the channel between the N_{BS} antennas of the BS and the N_{UE} antennas of the user. The computation is performed according to the following operations:

1. **Power and angular delay profile estimation:** For the line-of-sight (LOS) ray, the travelling distance and angles of arrival/departure of the wave is computed. From the travelling distance, the delay is estimated via the light speed and the wave attenuation is computed from the Friis formula (see (2.1)).

   For the non line-of-sight (NLOS) rays (window, ceiling, ground and wall reflections), the positions of the reflection points are first computed. Only first reflections are taken into account. Then the travelling distance and angles of arrival/departure are derived for each rays. From the travelling distance and the light speed, one can derived the delay profile. The wave attenuation is computed from the Friis formula and a supplementary attenuation factor (related to the dielectric constant and roughness of the surface of reflection) is added.

2. **Quasi-determinist channel generation:** From the obtained power delay profile, additional lower power random rays (R-rays) are added to it in order to consider reflections on random objects or far walls. Figure 3.17 represents an example of power delay profile obtained after this operation. The first ray is the LOS ray and contains most of the received power. From the LOS ray, different R-rays are generated according to a Poisson distribution. The angles of arrival/departure of the R-rays are chosen randomly according to a uniform

distribution.

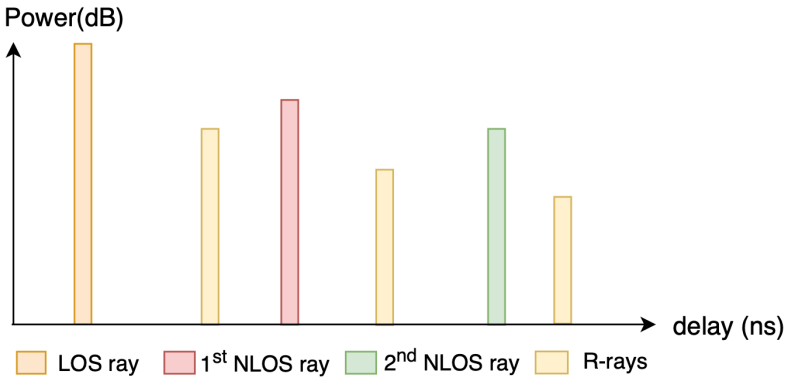

Figure 3.17: Example of quasi-determinist power delay profile with one LOS and two NLOS rays.

3. **Quasi-determinist channel generation (2):** The roughness of the reflection surfaces creates a scattering phenomenon in which multiple copies of the same signal arrive with short differences of delay (see Figure 3.18). In the power delay profile, scattering is represented by the addition of supplementary rays according to a Poisson distribution (see Figure 3.19).

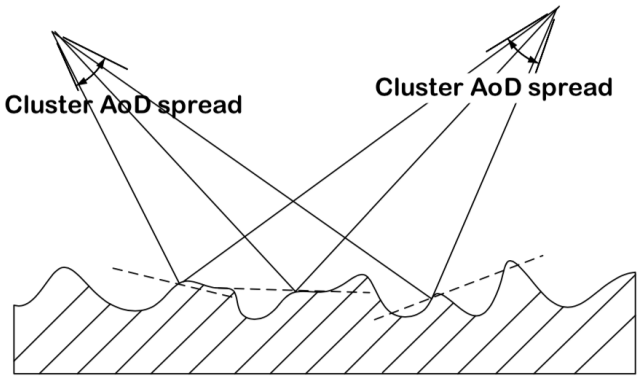

Figure 3.18: Reflection scattering mechanism[19]

4. **MIMO channel impulse response:** From the power delay profile and the angular delay profile of each pair of transmit/receive antennas, a channel impulse response is generated. The channel impulse responses are then resampled according to the symbol rate.

SISO channel computation The SISO impulse channel response is constructed by applying a complex weight (specified in the AWVs) to each of those channel impulse responses and then by adding them. At then end of this procedure, a single channel impulse response is derived representing the whole filtering effect of the propagation chain, from the input of the antenna array of the BS to the output of the antenna array of the user.

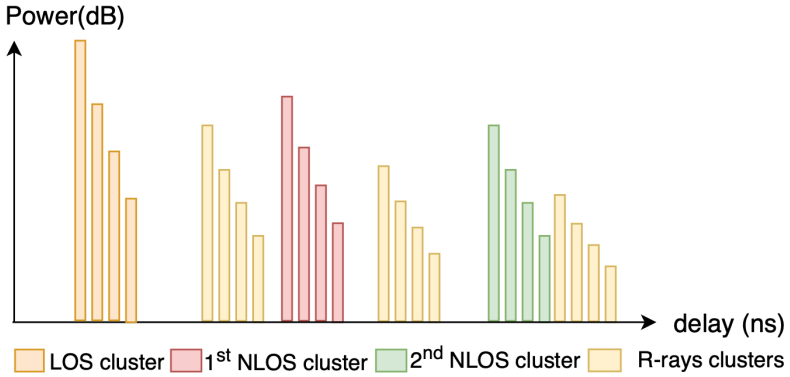

Figure 3.19: Example of quasi-determinist power delay profile with one LOS and two NLOS rays.

SNR measurement: This operation consists in measuring the SNR level of the link. The principle is depicted in Figure 3.20. A pilot sequence x with a given power is transmitted through the SISO channel and an additive noise is then added to represent the thermal and figure noises. The pilot sequence contains Golay sequences and allows the user to estimate the channel. More information can be found in Appendix A. The level of SNR is estimated at the reception by comparing the noisy received signal y with the signal obtained after convolving the pilot sequence x with the estimated channel.

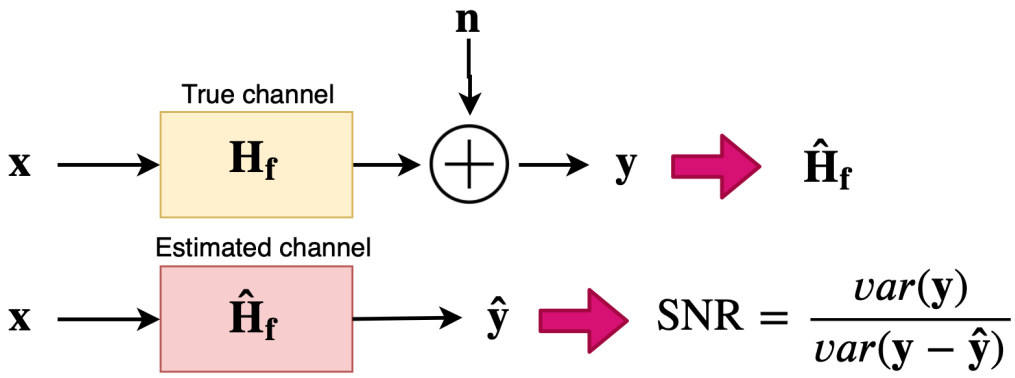

Figure 3.20: SNR measurement principle.

Chapter 4

Stationary user beamforming training

As explained in chapter 3, the IEEE802.11 standard comprises different training procedures enabling multi-antenna stations (STAs) to exploit their beamforming (BF) and spatial multiplexing (SM) capabilities. All these trainings rely on the principle of exchanging pilot sequences with different transmit and/or receive antenna weight vectors (AWVs). From these transmit pilot sequences, the receiver is able to estimate the SNR level of the link and informs the transmitter via the transmission of an ACK of the best tested antenna configuration and its SNR level.

If the training procedures are specified in the standard, training algorithms are implementation free. In this chapter, two different beamforming training (BFT) algorithms will be presented. These two algorithms consider downlink training in which a base station (BS) located in $(x, y, z) = (0, 0, 0)$ is communicating with a stationary user situated in position $(x, y, z) = (2.4, -1, 1.5)$ (see Figure 3.16).

In section 4.1, the first BFT algorithm is proposed and is based on an exhaustive beam search. This algorithm tries to determine the angular direction in which the user is standing. The second BFT algorithm is proposed in section 4.2 and selects the optimal transmit AWV based on the evaluation of the one-tap SISO channel. This evaluation is done through SNR level measurements and two different channel estimation methods are presented.

4.1 Exhaustive beam search BFT

In Figure 4.1 is depicted the principle of the exhaustive beam search BFT algorithm. This algorithm should be performed when the communication is not established, i.e. in the BHI during the SLS phase (see section 3.1.2 for more details).

The exhaustive beam search algorithm requires to steer the radiation pattern inside different sectors. In section 2.3 was presented a beam widening algorithm allowing the design of AWVs steering the radiation pattern into a desired direction. The

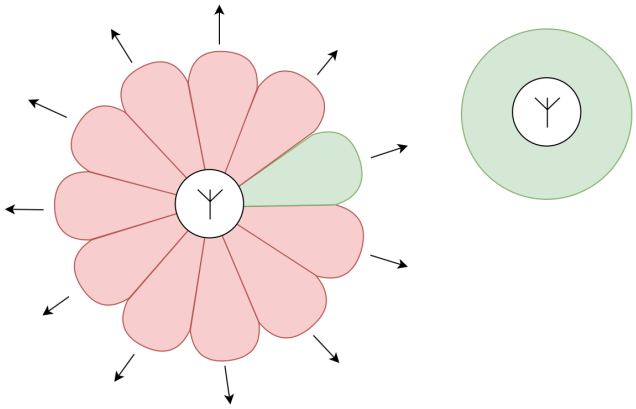

Figure 4.1: Illustration of the exhaustive beam search BFT algorithm. The BS divides the space into virtual sectors of equal dimensions and steers its radiation pattern toward each of these sectors successively. The receiver measures the SNR level and communicates the Sector ID of the tested sector with the highest SNR level.

radiation pattern takes the form of a beam and it was shown how the beamwidth can be controlled.

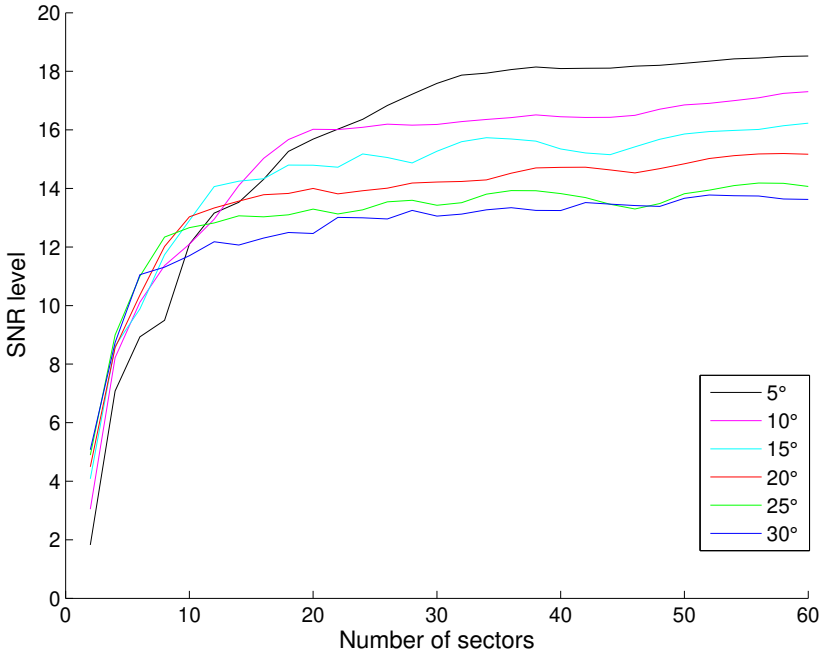

Figure 4.2: Mean SNR level obtained at the end of the exhaustive beam search algorithm for $\phi_{wd} = \{5°, 10°, 15°, 20°, 25°, 30°\}$. The BS is a linear array of $N_{bs} = 64$ antennas while the receiver is a single antenna element. Mean SNR operation was made over 1000 different divisions into sectors of the azimuth space.

The performance of this algorithm should be evaluated according to the number

of virtual sectors tested and the beamwidth ϕ_{wd}. Figure 4.2 presents the expected SNR level of the best tested sectors obtained with this algorithm. As one can see, the evolution of the mean SNR level is dependent on ϕ_{wd}. When low number of tested sectors is considered, the probability to have at least one beam steered directly toward the user is higher for larger beams. Therefore, the expected SNR level becomes higher with increasing ϕ_{wd}. On the contrary, the array gain inside the beam increases with lower ϕ_{wd}. This explained the good performance of narrow beams at high number of tested sectors.

One can also note that the SNR level starts to saturate when the number of sectors is equivalent to $180°/\phi_{wd}$ meaning that the whole space is covered by the beams. Above this number of sectors, the small increase of the expected SNR level can be explained by the ripple of array gain present inside the beam (see section 2.3).

4.2 Channel estimation from SNR measurements

This section presents a second BFT algorithm based on the evaluation of the one-tap SISO channel via SNR measurements. The one-tap channel is the wave attenuation and phase shift resulting from the propagation of a signal between the antennas of the BS and the antennas of the user via the dominant path (=line-of-sight (LOS) path in our case).

Let us denote this channel $\mathbf{H_{MIMO}} \in \mathbb{C}^{N_{UE} \times N_{BS}}$ and suppose that a symbol $\mathbf{x}$ is transmitted. The received signal $\mathbf{y}$ is expressed as in (4.1):

$$\mathbf{y} = \mathbf{Fa_{UE}}^H \mathbf{H_{MIMO}} \mathbf{Fa_{BS}} \mathbf{x} + \mathbf{Fa_{UE}}^H \mathbf{n}, \tag{4.1}$$

Where $\mathbf{Fa_{BS}} \in \mathbb{C}^{N_{BS}}$ and $\mathbf{Fa_{UE}} \in \mathbb{C}^{N_{BS}}$ represent the transmit and receive antenna weight vectors (AWVs) respectively and $\mathbf{n} \in \mathbb{C}^{N_{UE}}$ is an additive white gaussian noise. Let us denote $\mathbf{h_{RX}} = \mathbf{Fa_{UE}}^H \mathbf{H_{MIMO}} \in \mathbb{C}^{1 \times N_{BS}}$ the receiving channel. The received signal can be rewritten as:

$$\mathbf{y} = \mathbf{h_{RX}} \mathbf{Fa_{BS}} \mathbf{x} + \mathbf{Fa_{UE}}^H \mathbf{n}. \tag{4.2}$$

In this section, the BFT algorithm consists in estimating $\mathbf{h_{RX}}$. The $\mathbf{Fa_{BS}}$ that maximises the SNR can then be computed using maximal ratio combing:

$$\mathbf{Fa_{BS}}^\star = \frac{\mathbf{h_{RX}}^H}{||\mathbf{h_{RX}}||}. \tag{4.3}$$

Two different channel estimation methods will be presented and are based on the measurement of the SNR level obtained with different transmit AWVs. Let us define what is represented by each measurement of SNR. The expression of the SNR (in linear scale) is the following one:

$$SNR = \frac{|\mathbf{h_{RX}} \mathbf{Fa_{BS}}|^2 \sigma_x^2}{||\mathbf{Fa_{UE}}||^2 \sigma_n^2}, \tag{4.4}$$

With σ_x^2 representing the signal power and σ_n^2 the noise power. During the channel estimation procedure, modifications of the SNR value will be done through perturbations of the transmit steering vector $\mathbf{Fa_{BS}}$. The ratio $\sigma_x^2/(||\mathbf{Fa_{UE}}||^2\sigma_n^2)$ is independent of $\mathbf{Fa_{BS}}$ and is assumed to be equal to one by definition.

This simplification implies that the estimated channel is no longer $\mathbf{h_{RX}}$ but $\mathbf{h_{RX}}\sigma_x/(||\mathbf{Fa_{UE}}||\sigma_n)$. This has in practice no influence on the choice of $\mathbf{Fa_{BS}}^\star$ because of the normalisation operation performed in (4.3). This leads to a simplified expression of the SNR as in (4.5).

$$SNR = |\mathbf{h_{RX}}\mathbf{Fa_{BS}}|^2. \tag{4.5}$$

From the formula above, one can observe how a modification of $\mathbf{Fa_{BS}}$ impacts the measured SNR.

4.2.1 Method based on four SNR measurements

The first channel estimation method is based on four SNR measurements for each coefficient of $\mathbf{h_{RX}}$. In [7], Palacios and al. present a novel method for estimating the channel through SNR measurements. Its principle is depicted in Figure 4.3.

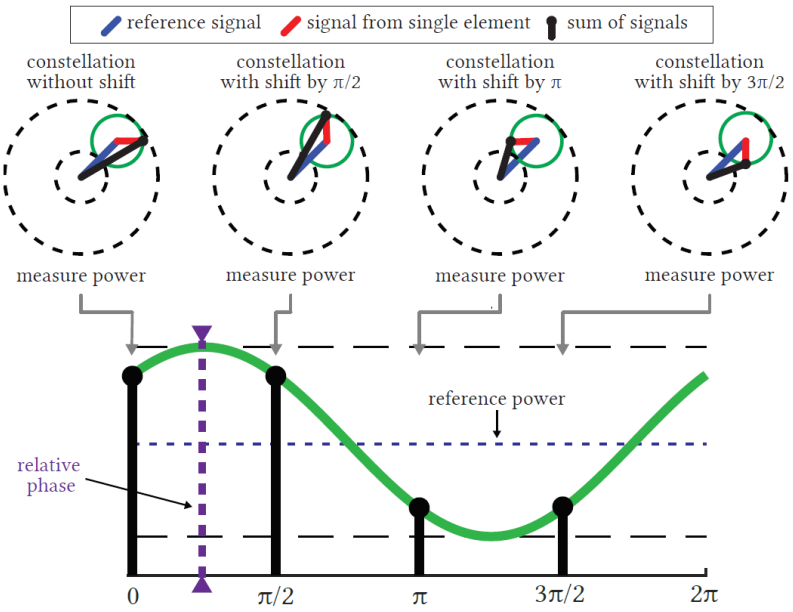

Figure 4.3: Illustration of channel the estimation method using four SNR measurements. The upper graph shows the signal constellations with the four phase shifts. The lower graph represents the evolution of the measured SNR with the phase shift and how the relative phase of the channel can be found[7].

The channel coefficients are computed successively. We define the index k as being the index of the antenna for which we want to estimate the channel coefficient. In Figure 4.3, the signal received by antenna k is represented by the red line in the constellations. This signal is added to the reference signal generated by the other

antennas (blue line). At antenna k, we impose four different antenna weights. This leads to four different SNR level measured (black line amplitude). From those SNR measurements, it will be shown how the BS is able to recover the kth coefficient of $\mathbf{h_{RX}}$, denoted by $[\mathbf{h_{RX}}]_k$. Only the relative phase and amplitude with respect to a reference will be estimated.

Two different techniques based on the discrete Fourier transform (DFT) operation are explored by the authors and will be described here below. The omnidirectional technique considers that the reference signal is coming from a unique reference antenna. The directional technique considers a reference signal generated from the whole antenna array meaning that the BS benefit from antenna gain during the whole procedure. This second technique is possible if the BS has already established a connection with the UE and that a non-optimal AWV has been extracted from a previous BFT stage.

4.2.1.1 Omnidirectional channel estimation method based on four SNR measurements

The reference signal is coming from one antenna, being the reference antenna. We denote with an index $\bar{k}$ the index of the reference antenna. The principle is based on two steps. The first step computes the relative amplitude of the channel coefficient with respect to the reference channel coefficient. The second step computes the relative phase between the channel coefficients. Because the differences of amplitude between all the channel coefficients are generally small, the amplitude step is optional.

1. **Amplitude measurement:** Only the k^{th} antenna is activated while the others are turned off:
$$[\mathbf{Fa_{BS}}]_{k'} = \begin{cases} 1 & \text{if } k' = k \\ 0 & \text{if } k' \neq k \end{cases} \tag{4.6}$$
Combining (4.5) and (4.6), the amplitude of the k^{th} channel coefficient is therefore directly known:
$$|[\mathbf{h_{RX}}]_k|^2 = SNR. \tag{4.7}$$
From this, we define the reference index as being the one for which the channel amplitude is the highest. If this first step is skipped, the reference antenna can be taken arbitrary and $|[\mathbf{h_{RX}}]_k|$ is set to unity for all k.

2. **Phase measurement:** Now, we need to measure the phase of each channel coefficient except for the reference for which the phase is null by definition. Non-normalised AWV will be denoted with a prime symbol ($\mathbf{Fa^m_{BS}} = \mathbf{Fa^m_{BS}}'/||\mathbf{Fa^m_{BS}}'||$). The principle is to activate both antennas k and $\bar{k}$ with four

different weights on antenna k

$$[\mathbf{Fa}_{\mathbf{BS}}^{\mathbf{m}\,\prime}]_{k'} = \begin{cases} \{1, i, -1, -i\} & \text{if } k' = k \\ 1 & \text{if } k' = \bar{k} \\ 0 & \text{if } k' \neq k \end{cases} \tag{4.8}$$

and we group the four measurements of $|\mathbf{h_{RX}}\mathbf{Fa}_{\mathbf{BS}}^{\mathbf{m}}|^2 = SNR$ in a vector $\mathbf{a} \in \mathbb{R}^{4\times 1}$. The index $\mathbf{m} \in \{0, 1, 2, 3\}$ indicates which antenna weight (resp. 1, i, -1, -i) was used at antenna k. Each element of $\mathbf{a}$ can be expressed as:

$$\begin{aligned} [\mathbf{a}]_m &= |\mathbf{h_{RX}}\mathbf{Fa}_{\mathbf{BS}}^{\mathbf{m}}|^2, \\ &= |\frac{1}{\sqrt{2}}([\mathbf{h_{RX}}]_{\bar{k}} + [\mathbf{h_{RX}}]_k e^{m\frac{\pi}{2}i})|^2, \\ &= \frac{1}{2}(|[\mathbf{h_{RX}}]_{\bar{k}}|^2 + |[\mathbf{h_{RX}}]_k|^2 + 2\mathbb{R}\{[\mathbf{h_{RX}}]_{\bar{k}}^* [\mathbf{h_{RX}}]_k e^{m\frac{\pi}{2}i}\}). \end{aligned} \tag{4.9}$$

Since by definition $\arg([\mathbf{h_{RX}}]_{\bar{k}}) = 0$, the equation can be rewritten under the following form:

$$\begin{aligned} [\mathbf{a}]_m &= \frac{[\mathbf{h_{RX}}]_{\bar{k}}^2 + |[\mathbf{h_{RX}}]_k|^2}{2} + [\mathbf{h_{RX}}]_{\bar{k}} |[\mathbf{h_{RX}}]_k| \cos(\arg([\mathbf{h_{RX}}]_k) + m\frac{\pi}{2}), \\ &= \Gamma + \Delta e^{(\arg([\mathbf{h_{RX}}]_k) + m\frac{\pi}{2})i} + \Delta e^{-(\arg([\mathbf{h_{RX}}]_k) + m\frac{\pi}{2})i}, \end{aligned} \tag{4.10}$$

Where $\Gamma = \frac{[\mathbf{h_{RX}}]_{\bar{k}}^2 + |[\mathbf{h_{RX}}]_k|^2}{2}$ and $\Delta = \frac{[\mathbf{h_{RX}}]_{\bar{k}} |[\mathbf{h_{RX}}]_k|}{2}$. Let us now apply a Fourier transform on $\mathbf{a}$. We note the result $\mathbf{f} \in \mathbb{R}^{4\times 1}$. For each element of $\mathbf{f}$, we have

$$[\mathbf{f}]_n = \sum_{m=0}^{3} \frac{[\mathbf{a}]_m}{4} e^{-nm\frac{\pi}{2}i}, \tag{4.11}$$

With $n \in \{0, 1, 2, 3\}$. One has ($\rho_k = \arg([\mathbf{h_{RX}}]_k)$):

$$\begin{aligned} \mathbf{f} &= \frac{1}{4} \underbrace{\begin{bmatrix} \Gamma & \Delta & \Delta \end{bmatrix} \begin{bmatrix} 1 & 1 & 1 & 1 \\ e^{\rho_k i} & ie^{\rho_k i} & -e^{\rho_k i} & -ie^{\rho_k i} \\ e^{-\rho_k i} & -ie^{-\rho_k i} & -e^{-\rho_k i} & ie^{-\rho_k i} \end{bmatrix}}_{=\mathbf{a}^T} \begin{bmatrix} 1 & 1 & 1 & 1 \\ 1 & -i & -1 & i \\ 1 & -1 & 1 & -1 \\ 1 & i & -1 & -i \end{bmatrix}, \\ &= \frac{1}{4} \begin{bmatrix} \Gamma & \Delta & \Delta \end{bmatrix} \begin{bmatrix} 4 & 0 & 0 & 0 \\ 0 & 4e^{\rho_k i} & 0 & 0 \\ 0 & 0 & 0 & 4e^{-\rho_k i} \end{bmatrix}, \\ &= \begin{bmatrix} \Gamma & \Delta e^{\rho_k i} & 0 & \Delta e^{-\rho_k i} \end{bmatrix}. \end{aligned}$$

This leads to the following result

$$\mathbf{f} = (\Gamma, \Delta e^{\arg([\mathbf{h_{RX}}]_k)i}, 0, \Delta e^{-\arg([\mathbf{h_{RX}}]_k)i}). \tag{4.12}$$

The phase of the channel coefficient, $\arg[\mathbf{h_{RX}}]_k$, can directly be extracted by computing the phase of $[\mathbf{f}]_2$. This method requires a total of $N_{BS} + 4(N_{BS} - 1)$ SNR measurements ($4(N_{BS} - 1)$ if the amplitude step is skipped).

4.2.1.2 Directional channel estimation method based on four SNR measurements

During the omnidirectional channel estimation procedure described in section 4.2.1.1, different AWVs are tested and activated only two antennas at a time. Because the signals coming from those two antennas can sometimes interact destructively at the receiver side, the SNR level can be very low during the procedure. In some cases, it is necessary to guarantee a minimal level of SNR at the reception in order to synchronise and accurately estimate the SNR level. To remedy this, the authors in [7] proposed to reuse a non-optimal AWV ($\mathbf{Fa_{BS,P}}$) found in a previous training stage. Then directional method for channel estimation can be performed in one step by imposing at four different time instant the following AWVs:

$$[\mathbf{Fa_{BS}^{m}}']_{k'} = \begin{cases} \{1, i, -1, -i\} & \text{if } k' = k \\ [\mathbf{Fa_{BS,P}}']_{k'} & \text{if } k' \neq k \end{cases} \tag{4.13}$$

Now the reference phase is such that $\arg(\mathbf{h_{RX}Fa_{BS}}) = 0$. The element in $\mathbf{a}$ can then be expressed as:

$$\begin{aligned} [\mathbf{a}]_m &= |\mathbf{h_{RX}Fa_{BS}^{m}}|^2, \\ &= \frac{1}{||\mathbf{Fa_{BS,P}}'||} |\mathbf{h_{RX}Fa_{BS,P}}' + [\mathbf{h_{RX}}]_k[\mathbf{Fa_{BS}}]'_k - [\mathbf{h_{RX}}]_k[\mathbf{Fa_{BS,P}}']_k|^2. \end{aligned} \tag{4.14}$$

The analytical result is more protracted than with the omnidirectional technique. The final result is [7]:

$$|[\mathbf{h_{RX}}]_k| = \frac{||\mathbf{Fa_{BS,P}}'||}{2} \sqrt{[\mathbf{f}]_0 + 2|[\mathbf{f}]_1|} - \sqrt{[\mathbf{f}]_0 - 2|[\mathbf{f}]_1|}, \tag{4.15}$$

$$\arg([\mathbf{h_{RX}}]_k) = \arg([\mathbf{f}]_1) - \arg\left(\gamma + |[\mathbf{h_{RX}}]_k|[\mathbf{Fa_{BS,P}}']_k e^{\arg([\mathbf{f}]_1)}\right). \tag{4.16}$$

Where γ is present in order to compensate for the phase contribution of the k^{th} antenna on $\mathbf{Fa_{BS,P}}$:

$$\gamma = \frac{||\mathbf{Fa_{BS,P}}'||}{2} \sqrt{[\mathbf{f}]_0 + 2[\mathbf{f}]_1} + \sqrt{[\mathbf{f}]_0 - 2[\mathbf{f}]_1}. \tag{4.17}$$

Again, $\mathbf{f}$ represents the discrete Fourier transform of $\mathbf{a}$. For N_{BS} antennas at the the transmitter side, $4N_{BS}$ SNR measurements are needed.

4.2.2 Method based on three SNR measurements

In this section, a channel estimation method based on three SNR measurements for each channel coefficient will be presented. This method is largely inspired from the channel estimation method presented in section 4.2.1. Again, two techniques will be investigated. The first technique considers that the signal of reference is emitted from a single antenna (omnidirectional scenario) and the second technique considers that the reference signal is emitted from the whole antenna array (directional scenario).

4.2.2.1 Omnidirectional channel estimation method based on three SNR measurements

The reference signal is coming from a single antenna, called the reference antenna. The reference antenna is identified with the index $\bar{k}$. During the preliminary step, the reference antenna is activated alone. The AWV associated is:

$$[\mathbf{Fa_{BS}}]_{k'} = \begin{cases} 1 & \text{if } k' = \bar{k} \\ 0 & \text{if } k' \neq \bar{k} \end{cases} \tag{4.18}$$

And the measured SNR is given by:

$$SNR_0 = |[\mathbf{h_{RX}}]_{\bar{k}}|^2 = [\mathbf{h_{RX}}]_{\bar{k}}^2, \tag{4.19}$$

Since by definition $\arg([\mathbf{h_{RX}}]_{\bar{k}}) = 0$. Now that SNR_0 is known, we can estimate the channel coefficients of the other antennas. This technique is based on three steps for each antenna k.

1. **First measurement:** For the first measurement, only the k^{th} antenna is activated while the other are turned off:

$$[\mathbf{Fa_{BS}}]_{k'} = \begin{cases} 1 & \text{if } k' = k \\ 0 & \text{if } k' \neq k \end{cases} \tag{4.20}$$

   The measured SNR is therefore given by

$$SNR_{1,k} = |[\mathbf{h_{RX}}]_k|^2, \tag{4.21}$$

   And the amplitude of the k^{th} channel coefficient can be estimated by $\sqrt{SNR_{1,k}}$. We define $\Gamma = \frac{[\mathbf{h_{RX}}]_{\bar{k}}^2 + |[\mathbf{h_{RX}}]_k|^2}{2} = \frac{SNR_0 + SNR_{1,k}}{2}$ and $\Delta = \frac{[\mathbf{h_{RX}}]_{\bar{k}} |[\mathbf{h_{RX}}]_k|}{2} = \frac{\sqrt{SNR_0}\sqrt{SNR_{1,k}}}{2}$.

2. **Second measurement:** The AWV associated with the second measurement is given by (4.22).

$$[\mathbf{Fa_{BS}^{m\,\prime}}]_{k'} = \begin{cases} 1 & \text{if } k' = k \\ 1 & \text{if } k' = \bar{k} \\ 0 & \text{if } k' \neq k \end{cases} \tag{4.22}$$

   For this antenna weight, the receiver measures an SNR given by the expression in (4.23).

$$SNR_{2,k} = \Gamma + 2\Delta \cos\Big(\arg([\mathbf{h_{RX}}]_k\Big). \tag{4.23}$$

3. **Third measurement:** For the last SNR measurement, the used AWV is the following one:

$$[\mathbf{Fa_{BS}^{m\,\prime}}]_{k'} = \begin{cases} i & \text{if } k' = k \\ 1 & \text{if } k' = \bar{k} \\ 0 & \text{if } k' \neq k \end{cases} \tag{4.24}$$

   And the measured SNR is given by:

$$SNR_{3,k} = \Gamma + 2\Delta \cos\Big(\arg([\mathbf{h_{RX}}]_k) + \frac{\pi}{2}\Big) = \Gamma + 2\Delta \sin\Big(\arg([\mathbf{h_{RX}}]_k\Big). \tag{4.25}$$

From these SNR measurements, one can recover the amplitude and the phase of $[\mathbf{h_{RX}}]_k$ using the formula (4.26) and (4.27) with $l = 0$ if $SNR_{2,k} > \Gamma$ and $l = 1$ otherwise.

$$|[\mathbf{h_{RX}}]_k| = \sqrt{SNR_{1,k}}. \tag{4.26}$$

$$\arg([\mathbf{h_{RX}}]_k) = \arctan\Big(\frac{SNR_{3,k} - \Gamma}{SNR_{2,k} - \Gamma}\Big) + l\pi. \tag{4.27}$$

This technique requires a total of $1 + 3(N_{BS} - 1)$ SNR measurements to estimate the whole channel.

4.2.2.2 Directional channel estimation method based on three SNR measurements

The idea is to reuse a good beam pattern in order to benefit from transmit antenna gain while performing the measurements. Let us denote again by $\mathbf{Fa_{BS,P}}$ the reused AWV taken from a previous training stage. The level of SNR using this AWV is given by:

$$SNR_0 = (\mathbf{h_{RX}}\mathbf{Fa_{BS,P}})^2, \tag{4.28}$$

Where we define our reference phase such that $\arg(\mathbf{h_{RX}}\mathbf{Fa_{BS,P}}) = 0$. Now, let us consider the three following perturbations for antenna k and see how channel coefficient $[\mathbf{h_{RX}}]_k$ can be extracted from the measured SNR levels.

1. **First perturbation**: We impose the perturbation as in (4.29) with ϵ being a real value. Its magnitude will be discussed later on.

$$[\mathbf{Fa_{BS}}]_{k'} = \begin{cases} [\mathbf{Fa_{BS,P}}]_{k'} + \epsilon & \text{if } k' = k \\ [\mathbf{Fa_{BS,P}}]_{k'} & \text{if } k' \neq k \end{cases} \tag{4.29}$$

   The level of SNR can then be computed as being

$$\begin{aligned} SNR_{1,k} &= |\mathbf{h_{RX}}\mathbf{Fa_{BS}}|^2, \\ &= |\mathbf{h_{RX}}\mathbf{Fa_{BS,P}} + \epsilon[\mathbf{h_{RX}}]_k|^2, \\ &= (\mathbf{h_{RX}}\mathbf{Fa_{BS,P}})^2 + \epsilon^2|[\mathbf{h_{RX}}]_k|^2 + 2\epsilon\mathbf{h_{RX}}\mathbf{Fa_{BS,P}}\Re\{[\mathbf{h_{RX}}]_k\}, \\ &= (\mathbf{h_{RX}}\mathbf{Fa_{BS,P}})^2 + \epsilon^2|[\mathbf{h_{RX}}]_k|^2 + 2\epsilon\mathbf{h_{RX}}\mathbf{Fa_{BS,P}}|[\mathbf{h_{RX}}]_k|\cos(\arg([\mathbf{h_{RX}}]_k)). \end{aligned} \tag{4.30}$$

2. **Second perturbation**: For this measurement, we impose that the perturbation is done on the imaginary part of $[\mathbf{Fa_{BS}}]_k$. This gives

$$[\mathbf{Fa_{BS}}]_{k'} = \begin{cases} [\mathbf{Fa_{BS,P}}]_{k'} + j\epsilon & \text{if } k' = k \\ [\mathbf{Fa_{BS,P}}]_{k'} & \text{if } k' \neq k \end{cases} \tag{4.31}$$

Leading to a second measured SNR given by:

$$\begin{aligned} SNR_{2,k} &= |\mathbf{h_{RX}}\mathbf{Fa_{BS}}|^2, \\ &= |\mathbf{h_{RX}}\mathbf{Fa_{BS,P}} + j\epsilon[\mathbf{h_{RX}}]_k|^2, \\ &= (\mathbf{h_{RX}}\mathbf{Fa_{BS,P}})^2 + \epsilon^2|[\mathbf{h_{RX}}]_k|^2 + 2\epsilon\mathbf{h_{RX}}\mathbf{Fa_{BS,P}}\Im\{[\mathbf{h_{RX}}]_k\}, \\ &= (\mathbf{h_{RX}}\mathbf{Fa_{BS,P}})^2 + \epsilon^2|[\mathbf{h_{RX}}]_k|^2 + 2\epsilon\mathbf{h_{RX}}\mathbf{Fa_{BS,P}}|[\mathbf{h_{RX}}]_k|\sin(\arg([\mathbf{h_{RX}}]_k)). \end{aligned} \tag{4.32}$$

3. **Third perturbation**: We impose our third perturbation on the k^{th} component of $\mathbf{Fa_{BS}}$ as shown in (4.33).

$$[\mathbf{Fa_{BS}}]_{k'} = \begin{cases} [\mathbf{Fa_{BS,P}}]_{k'} - \epsilon & \text{if } k' = k \\ [\mathbf{Fa_{BS,P}}]_{k'} & \text{if } k' \neq k \end{cases} \tag{4.33}$$

The SNR is given by

$$\begin{aligned} SNR_{3,k} &= |\mathbf{h_{RX}}\mathbf{Fa_{BS}}|^2, \\ &= |\mathbf{h_{RX}}\mathbf{Fa_{BS,P}} - \epsilon[\mathbf{h_{RX}}]_k|^2, \\ &= (\mathbf{h_{RX}}\mathbf{Fa_{BS,P}})^2 + \epsilon^2|[\mathbf{h_{RX}}]_k|^2 - 2\epsilon\mathbf{h_{RX}}\mathbf{Fa_{BS,P}}\Re\{[\mathbf{h_{RX}}]_k\}, \\ &= (\mathbf{h_{RX}}\mathbf{Fa_{BS,P}})^2 + \epsilon^2|[\mathbf{h_{RX}}]_k|^2 - 2\epsilon\mathbf{h_{RX}}\mathbf{Fa_{BS,P}}|[\mathbf{h_{RX}}]_k|\cos(\arg([\mathbf{h_{RX}}]_k)). \end{aligned} \tag{4.34}$$

One has at the end of the procedure the following expressions:

$$\begin{aligned} SNR_0 &= (\mathbf{h_{RX}}\mathbf{Fa_{BS,P}})^2, \\ SNR_{1,k} &= (\mathbf{h_{RX}}\mathbf{Fa_{BS,P}})^2 + \epsilon^2|[\mathbf{h_{RX}}]_k|^2 + 2\epsilon\mathbf{h_{RX}}\mathbf{Fa_{BS,P}}|[\mathbf{h_{RX}}]_k|\cos(\arg([\mathbf{h_{RX}}]_k)), \\ SNR_{2,k} &= (\mathbf{h_{RX}}\mathbf{Fa_{BS,P}})^2 + \epsilon^2|[\mathbf{h_{RX}}]_k|^2 + 2\epsilon\mathbf{h_{RX}}\mathbf{Fa_{BS,P}}|[\mathbf{h_{RX}}]_k|\sin(\arg([\mathbf{h_{RX}}]_k)), \\ SNR_{3,k} &= (\mathbf{h_{RX}}\mathbf{Fa_{BS,P}})^2 + \epsilon^2|[\mathbf{h_{RX}}]_k|^2 - 2\epsilon\mathbf{h_{RX}}\mathbf{Fa_{BS,P}}|[\mathbf{h_{RX}}]_k|\cos(\arg([\mathbf{h_{RX}}]_k)). \end{aligned} \tag{4.35}$$

By combining SNR_0, $SNR_{1,k}$, $SNR_{2,k}$ and $SNR_{3,k}$, one can easily obtain the value of $[\mathbf{h_{RX}}]_k$:

$$|[\mathbf{h_{RX}}]_k|^2 = \frac{SNR_{1,k} + SNR_{3,k} - 2SNR_0}{2\epsilon^2}, \tag{4.36}$$

$$\arg([\mathbf{h_{RX}}]_k) = \begin{cases} \arctan\dfrac{SNR_{2,k} - \Gamma}{SNR_{1,k} - \Gamma} & \text{if } SNR_{1,k} > \Gamma \\ \arctan\dfrac{SNR_{2,k} - \Gamma}{SNR_{1,k} - \Gamma} + \pi & \text{if } SNR_{1,k} < \Gamma \end{cases} \tag{4.37}$$

With $\Gamma = \dfrac{SNR_{1,k} + SNR_{3,k}}{2}$. The number of measurements for this technique of channel estimation is given by $3N_{BS}$.

In (4.35), one can see the influence of ϵ over the SNR measured. Because the SNR measurements can be perturbed by an additive noise, the value of ϵ should be taken

as high as possible. However, the higher is ϵ, the higher is the power emitted by the k^{th} antenna during the procedure. In the case of a destructive interference between the signal received from antenna k and the reference signal, the SNR level can be drastically reduced.

If one wants to ensure that the level of SNR stays always above αSNR_0 with $0 < \alpha < 1$, ϵ should be limited. Let us determine the maximal value of ϵ that met this constraint. By inspection of the set of equations in (4.35), the condition is met for all $\arg([\mathbf{h_{RX}}]_k)$ if and only if:

$$(\mathbf{h_{RX}}\mathbf{Fa_{BS,P}})^2 + \epsilon^2|[\mathbf{h_{RX}}]_k|^2 - 2\epsilon\mathbf{h_{RX}}\mathbf{Fa_{BS,P}}|[\mathbf{h_{RX}}]_k| > \alpha SNR_0, \tag{4.38}$$

Which, using (4.28), is equivalent to (4.39).

$$\epsilon^2|[\mathbf{h_{RX}}]_k|^2 - 2\epsilon\sqrt{SNR_0}|[\mathbf{h_{RX}}]_k| + (1-\alpha)SNR_0 > 0. \tag{4.39}$$

This equation is a second order polynomial with two real roots given by

$$\epsilon_1 = \frac{\sqrt{SNR_0}}{|[\mathbf{h_{RX}}]_k|}(1-\sqrt{\alpha}) \quad \text{and} \quad \epsilon_2 = \frac{\sqrt{SNR_0}}{|[\mathbf{h_{RX}}]_k|}(1+\sqrt{\alpha}) \tag{4.40}$$

Figure 4.4 represents the evolution of the polynomial in (4.39). This inequation is respected for $\epsilon < \epsilon_1$ or $\epsilon > \epsilon_2$. The value of ϵ should be taken as high as possible. However, taking $\epsilon > \epsilon_2$ increases significantly the power emitted by the k^{th} antenna. This can in general not be accepted and it was decided to set the ϵ equivalent to ϵ_1.

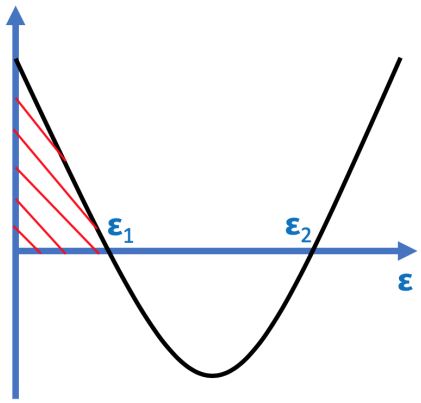

Figure 4.4: Evolution of the second order polynomial given in (4.39). The red hatched area represents the authorized value for ϵ. For $\epsilon_1 < \epsilon < \epsilon_2$, the SNR of the measurement is not guarantee to be higher than αSNR_0. For $\epsilon > \epsilon_2$, the power imposed on antenna k is considered as being too important.

The problem is that $|[\mathbf{h_{RX}}]_k|$ is only known at the end of the procedure and so ϵ_1 is not known. To cope with this problem, the BS should first perform the measurement with a small ϵ. Once $|[\mathbf{h_{RX}}]_k|$ has been estimated, the BS can decide to perform a second time the procedure with a more optimal ϵ if the channel estimation is not satisfactory.

4.2.3 Comparison of performance

In practice, the channel estimation methods should be robust to scenario where the measured SNR is not perfectly deterministic. This effect can be due to non-ideal antenna components, small channel variation or even because the SNR is quantified in a finite number of bits in the ACKs transmitted to the BS.

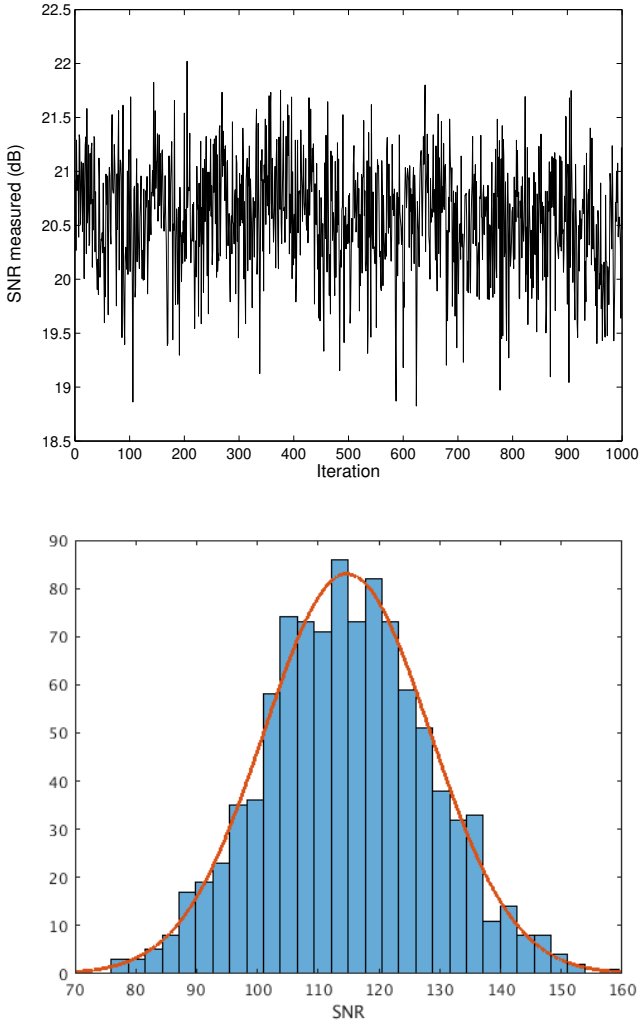

Figure 4.5: Up: Measured SNR level. Down: resulting distribution (SNR in linear scale). The orange curve corresponds to a gaussian distribution of mean of 114.75 and a standard deviation of 13.63.

Figure 4.5 shows the distribution of the SNR level measured in the lab of IMEC facility. PHARA4 TX/RX antennas developed by IMEC manufacturer and operating at 60GHz were used for the setup and all measurements were taken in a row with constant conditions (antenna setting, lab environment, ...). Clearly, the SNR distribution is gaussian meaning that an additive gaussian noise can be considered on the SNR measurements.

In this section, we will compare by simulation the robustness of the different channel estimation techniques when an additive noise is added to the measured SNR levels. The additive noise will be taken from a zero mean gaussian distribution with variance σ_s^2.

Figure 4.6 shows the performance of the two channel estimation methods presented in this report with σ_s^2. For each curve, the BS first estimates the channel via the noisy SNR measurements and then uses (4.3) to compute the transmit AWV. The final SNR depicted is the SNR level obtained when the BS used the computed AWV. For the directional methods, the SNR level obtained with $\mathbf{Fa_{BS,P}}$ was 19.29dB.

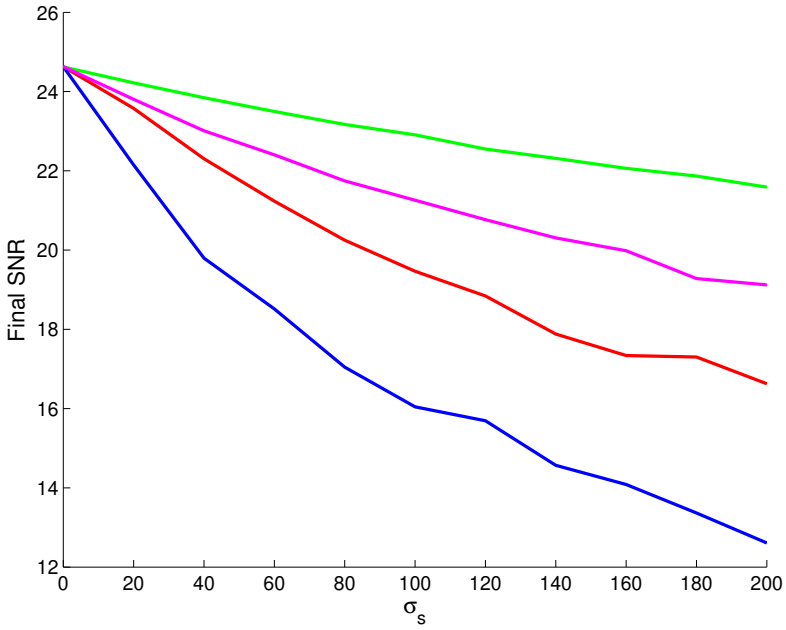

Figure 4.6: SNR obtained with channel estimation methods based on three and four SNR measurements. Red: omnidirectional with 4 measurements, green: directional with 4 measurements, blue: omnidirectional with 3 measurements, pink: directional with 3 measurements ($\alpha = 0.5$).

Clearly, omnidirectional techniques are less resistant to noise on SNR measurements. This is simply due to the fact that the SNR level is smaller for those methods because of the absence of antenna gain. Therefore, for the same noise power, the fluctuation of SNR will be proportionally more important.

The four SNR measurements methods are more robust to noise than the three SNR measurements methods. This can be explained considering that the DFT operation of the four SNR measurements method averages the noise present on the SNR measurements. The price to pay is an increasing number of SNR measurements.

Figure 4.7 shows the effect of α over the performance of the directional method based

on three SNR measurements. The performance becomes better when α decreases. This effect is due to the fact that ϵ_1 becomes more important with a smaller value of α. However, the power sent over the k^{th} antenna is becoming considerably higher than the power sent by the other antenna. That is generally not accepted by the system in practice.

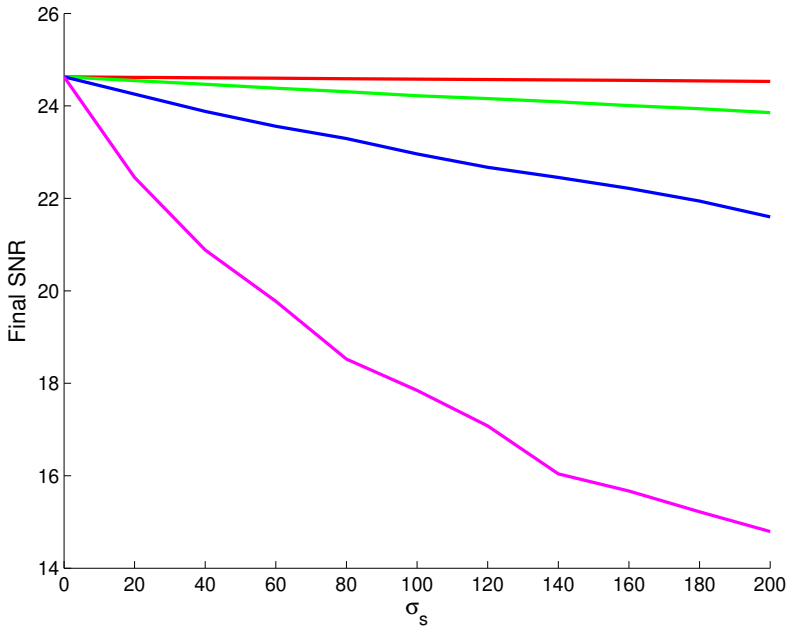

Figure 4.7: Performance of directional method for channel estimation based on three SNR measurements. In red, $\alpha = 0$. In blue, $\alpha = 0.2$. In green, $\alpha = 0.4$. In pink, $\alpha = 0.6$. These values correspond to an increase of power on antenna k by a factor of 294, 90, 40 and 15 respectively.

4.3 Conclusion

In this chapter was proposed two different BFT algorithms allowing a transmitter to determine an appropriate AWV steering the radiation pattern toward a stationary receiving STA.

The first algorithm is based on an exhaustive beam search. This algorithm is promising for its ease of implementation in the framework of the IEEE802.11ad/ay specifications. The influence of the number of tested sectors has been highlighted.

The second algorithm considers the determination of optimal AWV via the estimation of the one-tap SISO channel thanks to SNR measurements. Two channel estimation methods were presented and the robustness of these methods in presence of noise on the SNR measurements has been analysed.

Chapter 5

Beam tracking

In the case of a scenario with one or more moving STAs, the maintenance of a good beam alignment requires a continuous adaptation of the antenna weight vectors (AWVs) at both side of the communication link.

As explained in chapter 3, the IEEE802.11ad specification has defined a new training procedure for this adaptation named beam tracking (BT). In this training procedure, pilot symbols are appended at the end of data packets (see Figure 3.10) and enable the tests of different steering vectors. The quality of each AWV is then measured at the reception side via the measurement of the SNR level. Finally, the SNR level and the Sector ID of the best AWV is communicated to the trained STA through the transmission of an ACK.

Beam tracking requires therefore the transmission of pilot sequences. To reduce the training overhead, different solutions have been proposed in the literature. In [20], Palacios and al. proposed to track the channel dynamics using a probabilistic optimisation problem solved by gradient descent. To collect the channel information, authors consider the spatial multiplexing (SM) ability of hybrid MIMO architecture transceivers. In [21], a low recursive beam tracker has been designed considering analog beamforming from a linear antenna array. In [22], a technique alternating between exhaustive scans of the whole angular space and frequent fast refinement operations is proposed. In [23], authors propose an adaptative algorithm based on the prediction of the channel evolution with a Kalman filter.

All the mentioned techniques were not specifically designed considering the IEEE802.11ad/ay specifications but either are compatible with it or either require small modifications. The performance (training overhead, energy consumption, complexity) of those algorithms depends largely on the scenario simulated and new BT algorithms, such as the one proposed hereafter, will continue to draw attention.

In this chapter, we proposed a novel beam tracking method based on the stochastic estimation of the evolution of the user position through a particle filter (PF). The first part is devoted to the description of the simulated scenario (= user trajectory in the environment described in section 3.2). In the second part of this chapter is

proposed a first BT method based on classical beam sweeping of a portion of the azimuth space. Finally, the necessity and the performance of the BT method using a particle filter will be presented.

5.1 Working scenario

Let us consider an indoor scenario where a single moving user equipment (UE) is communicating with a stationary base station (BS). The antenna array of the UE is made of a single antenna element while the antenna array of the BS is a fully analog linear array of $N = 64$ antennas. Let us also consider that the UE is moving with a speed of 5 km/h (=1.39m/s) and follows the trajectory depicted in Figure 5.1.

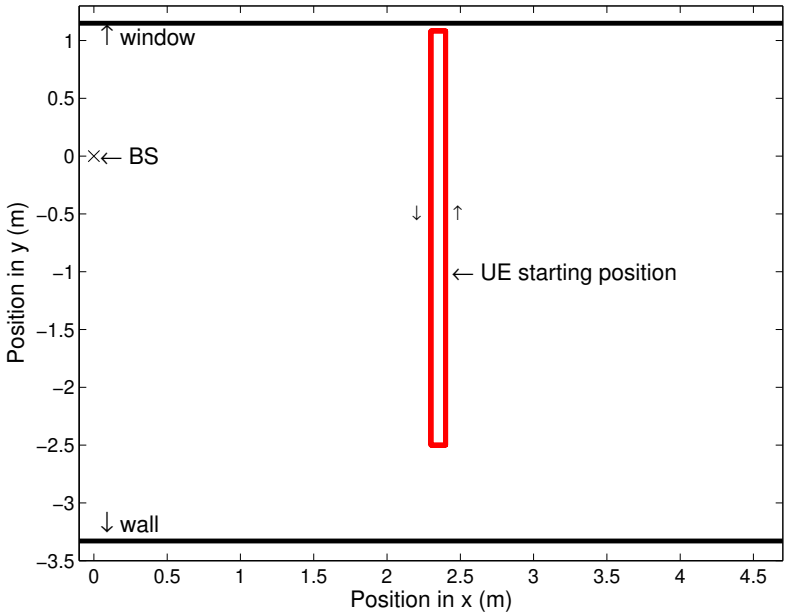

Figure 5.1: UE trajectory for the validation of the BT methods. The environment (window, wall, ceiling, ...) is identical to the one described in section 3.2. The trajectory is performed twice by the user.

The relative evolutions of the angular position and speed of the user with respect to the BS is depicted in Figure 5.2. Because of the UE motion, the steering vector (= AWV) at the BS side should be adapted regularly in order to keep the beam of the radiation pattern aligned with the user.

For the sake of simplicity, it is assumed that the BS knows perfectly the initial angular position of the user equipment (UE). This azimuth direction is noted ϕ_0. In practice, ϕ_0 should be estimated during the SLS and BRP phases. At the start of the BT, the BS is thus steering its beam directly toward the UE. Because the user is moving away from the beam, the BS has to understand thanks to a BT algorithm

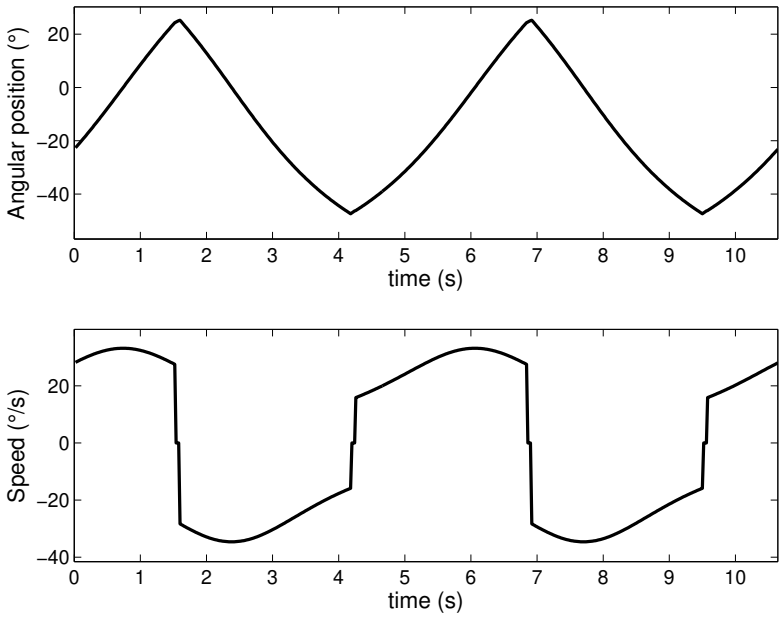

Figure 5.2: Angular position and speed evolutions of the UE.

how to adapt its AWV.

To performed the BT, we will assume that the BS is authorised to transmit BT training frames every 20 ms. Thanks to these frames, the BS can test different AWVs and the receiver communicates the ID number of the best AWV to the BS in the next ACK. This beam tracking training is totally in accordance with the IEEE802.11 standard (see section 3.1.2.3).

5.2 Beam tracking algorithm

In this section is developed the beam tracking (BT) algorithm used to track the user. A distinction between BT algorithm and the beam tracking procedure (BTP) is made. The BT algorithm designed the ensemble of operations made by the BS and UE to ensure a significant level of beamforming gain at the transmission and the reception. These operations can be SNR measurement, AWV adaptation or BTP. The BTP designed the operation during which the BS transmit different BT training frames to test different AWVs and, after getting the ACK from the user, knows how to adapt its AWV.

As explained in section 5.1, the BS has the choice to perform or not a BTP every 20ms. This choice will be based on the measured SNR of the communication link. Typically, if the SNR level goes below a reference SNR minus a threshold value (e.g. 3dB), the BTP is triggered (see Algorithm 2). We denote SNR_{ref} for the reference SNR and SNR_t for the threshold value.

Algorithm 2 Beam tracking algorithm

Input: SNR_t, ϕ_0

$SNR_{ref} = 0$
$\phi_r = \phi_0$
$Adapt\_AWV(\phi_r)$ ▷ Set steering direction to ϕ_0
while $BTIsOn()$ **do** ▷ Check if BT is activated
    $SNR = MeasureSNR()$ ▷ SNR measurement
    if $SNR < SNR_{ref} - SNR_t$ **then**
        $(\phi_r, SNR_{ref}) = BeamTracking()$ ▷ Perform BTP
        $Adapt\_AWV(\phi_r)$
    else
        $SNR_{ref} = SNR$
    end if
end while

In Algorithm 2, we will consider that the adaptation of the AWV (= $Adapt\_AWV()$) is performed as follow:

- If a BTP has been performed during the loop iteration : the AWV becomes the one that gives the best SNR level during the BTP.
- If no BTP has been performed during the loop iteration : the AWV is unchanged.

This adaptation will be modified in section 5.3. Figure 5.3 depicts the principle of the BT algorithm. The BS is steering a beam at $\phi = \phi_r$ with a beamwidth of ϕ_{wd}. Once the user has moved away from the beam of the BS, the BTP is triggered because the SNR level has dropped. The BS does not know the user motion but knows that three different situations can lead to a drop of the SNR level (ϕ_{ue} represents the angular user position):

1. $\phi_{ue} > \phi_r + \phi_{wd}/2$.
2. $\phi_{ue} \in [\phi_r - \phi_{wd}/2; \phi_r + \phi_{wd}/2]$.
3. $\phi_{ue} < \phi_r - \phi_{wd}/2$.

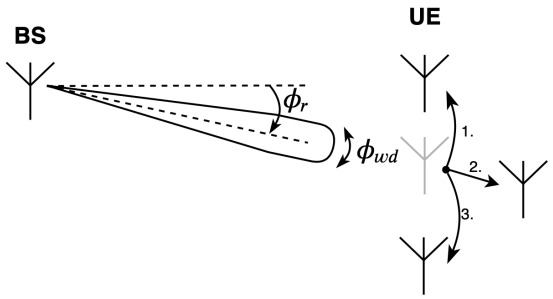

In the first and third situations, the reduction of SNR was mainly due to the fact that the user is not aligned anymore with the beam. The second situation occurs when the SNR level is reduced because the user is moving away from the BS.

The BS must decide what AWVs to test during the BTP. The three situations will be considered with equal probabilities and the choice of the steering directions tested

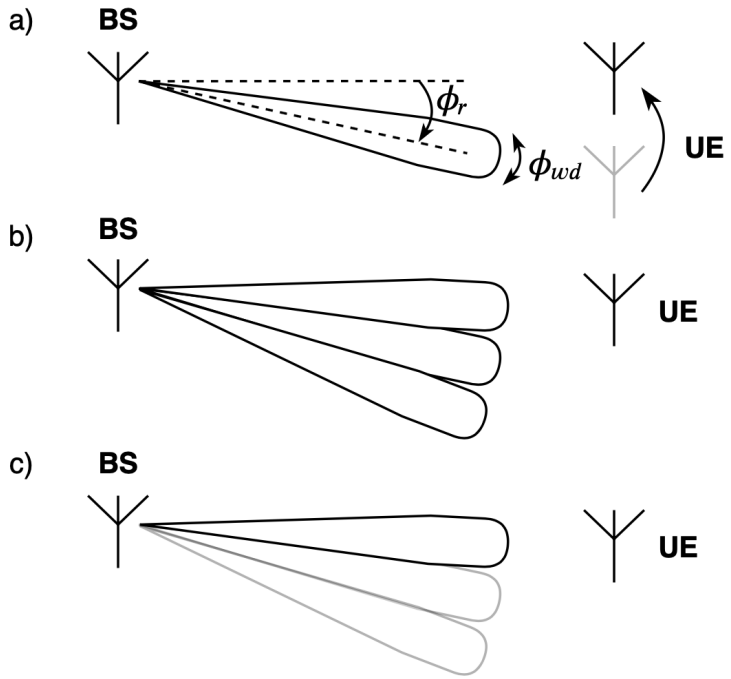

Figure 5.3: Beam tracking algorithm. a) The user has moved and the beam is therefore not aligned with him anymore. The SNR level decreases and the BTP is triggered. b) During BTP, three different AWVs are tested. c) The UE communicates the ID number of the best AWV and its SNR level.

during the BTP is dictated by the beamwidth and ϕ_r: $\phi_{BTP} = \{\phi_r - \phi_{wd}, \phi_r, \phi_r + \phi_{wd}\}$. Once the BS receives the ACK, it knows what steering vector to use for the communication and sets SNR_{ref} to the new SNR level.

The performance of the BT algorithm is depicted in Figure 5.4. To modify the direction of the beam, the steering vector adaptation method (see section 2.3) has been used. During the whole simulation, the BS was able to estimate the user position with a precision corresponding to half the beamwidth ϕ_{wd}. The algorithm is also robust to any modification of the motion direction of the UE.

Nevertheless, the BT algorithm could be improved because the BS can take advantage of the fact that most of the time, the user motion is nearly constant. By predicting the user motion, the BS could continuously adapt its beam toward the user and less BTP should then be performed. This will be investigated in section 5.3 in which a particle filter is used to estimate the user motion.

In Figure 5.5, one can see the evolution of the measured SNR level during the simulation. The misalignments of the user with the beam have led to some visible drops of SNR level. These drops can be of the order of 8dB and trigger the BTP because the measured SNR becomes lower than $SNR_{ref} - SNR_t$. After each BTP, the related drop of SNR level has been well compensated.

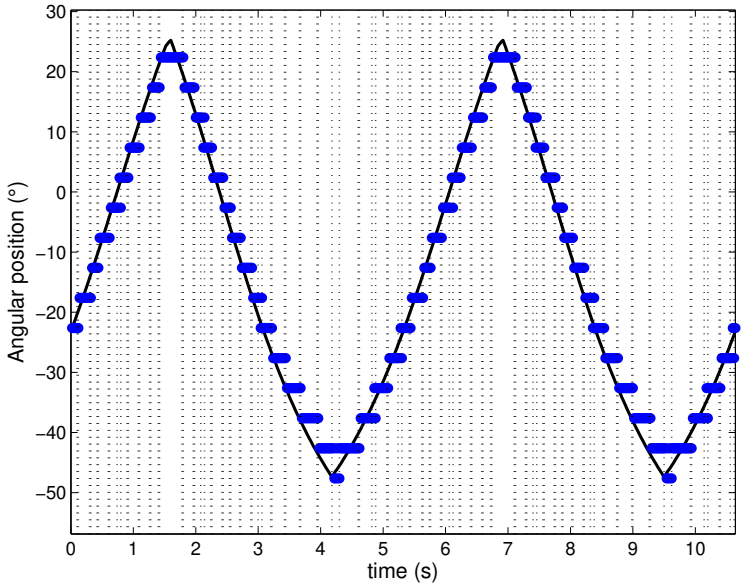

Figure 5.4: Black line: angular position evolution of the UE. Blue line: Steering direction of the AWV at the BS side. The vertical dotted lines represent the time instant for which a beam tracking algorithm was triggered. For this simulation, $\phi_{wd} = 5°$ and $SNR_t = 3$dB.

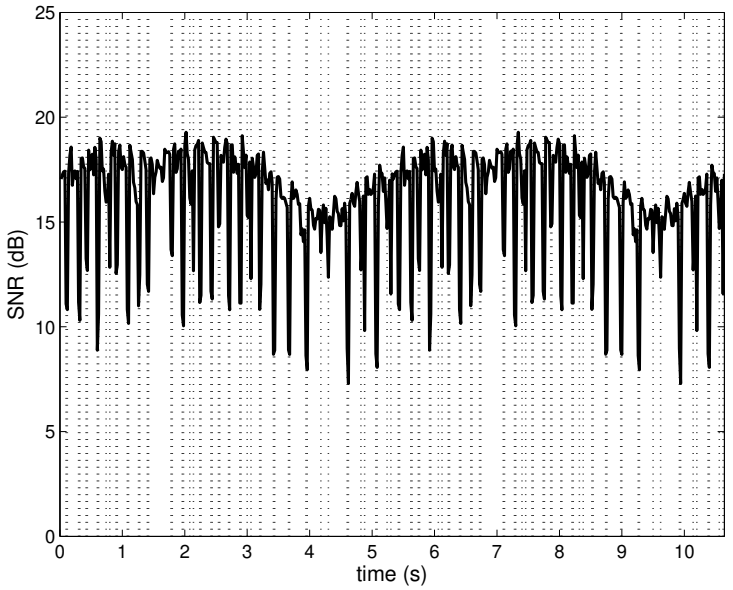

Figure 5.5: SNR evolutions.The vertical dotted lines represent the time instant for which a beam tracking algorithm was triggered. For this simulation, $\phi_{wd} = 5°$ and $SNR_t = 3$dB.

The BT algorithm has been explained and validated but two parameters should be discussed: the beamwidth of the AWVs ϕ_{wd} and the SNR threshold SNR_t. They

will be investigated in the following paragraphs.

Let us focus on the beamwidth ϕ_{wd}. In section 2.3, an algorithm for designing AWV with different ϕ_{wd} was proposed. Intuitively, if the beamwidth is increased, the number of BTPs should be reduced because the user will necessarily stay longer inside the beam. Unfortunately, the array gain tends to be reduced when using larger beams. A compromise between high array gain and low number of BTPs performed should thus be made for designing ϕ_{wd}.

The design of the beam also impacts the second parameter, SNR_t. The threshold SNR is necessary to allow the BS to detect that the user has moved away from the beam. Its value should therefore not be smaller than the maximum difference of SNR level present inside the used (less than 3 dB in our simulation). On the contrary, a too large SNR_t is not interesting. Indeed, the radiation pattern of the BS is never a perfect beam. Therefore, SNR_t should be lower than the difference between the lowest value of array gain inside the main lobe and the highest value of array gain outside the main lobe.

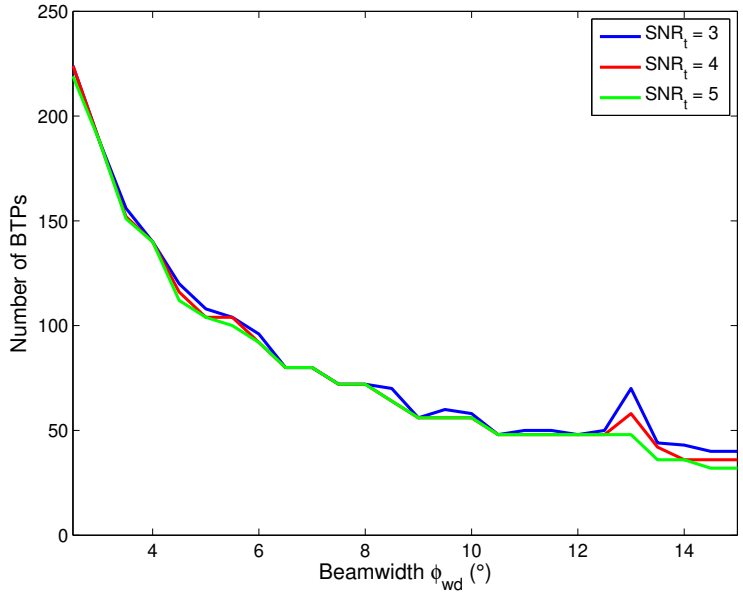

Figure 5.6: Simulated evolution of the number of BTPs with ϕ_{wd} and SNR_t.

Figure 5.6 and 5.7 show the evolution of the number of BTPs and the mean SNR level with ϕ_{wd} and SNR_t for the working scenario described in section 5.1. The results confirm our expectations. The influence of SNR_t is negligible if it is chosen in the correct range. Concerning the ϕ_{wd}, the number of BTPs is decreased by a factor of two every time the beamwidth is doubled. Furthermore, even if less SNR drops occurred with larger beams, the mean SNR decreases also with ϕ_{wd} because the array gain becomes less important.

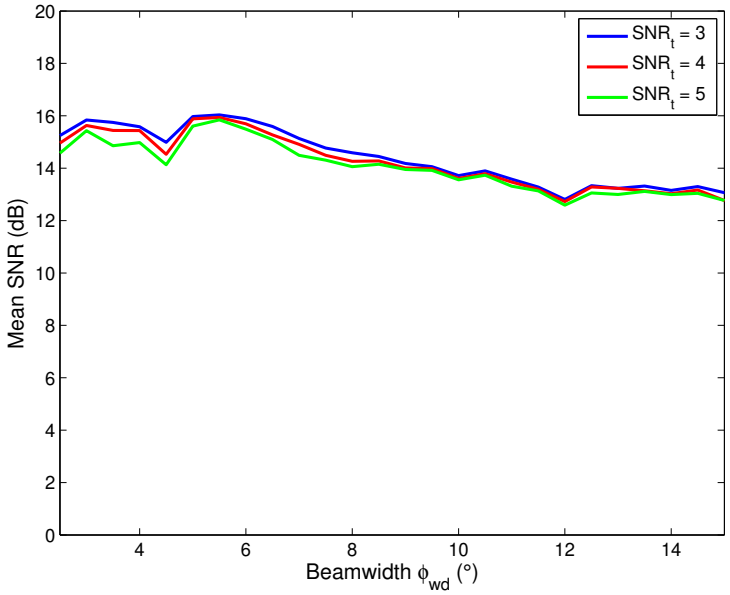

Figure 5.7: Simulated mean evolution of the number of measured SNR with ϕ_{wd} and SNR_t.

5.3 Predictive beam tracking procedure

In this section, we propose to adapt the BT algorithm proposed in the previous section. Indeed, even if the BS is able to track the user and prevent communication from breaking, performance could be enhanced if the BS is able to predict the user motion. Thanks to this prediction, the BS is then able to adapt continuously the steering direction of its radiation pattern toward the user direction. In this case, the number of BTPs should be reduced and, consequently, the BT training overhead decreases as well.

To estimate the user motion, a particle filter (PF) is used. The goal of a PF is to estimate the past, current or futur states of a process thanks to some noisy and partial observations. For the BT application, the angular user position and velocity that the BS must estimate constitute the state of the user.

The user state is not known by the BS and is said to be hidden. The first part of this section will investigate mathematically how a PF is able to estimate the hidden state of any Markov process. In the second part, an explanation on how the PF can be integrated in our BT algorithm will be presented and validated through simulation.

It is assumed that the reader has a good understanding of the fundamentals of the theory of probabilities and the bayesian theory. If not, we invite the reader to get familiar with these topics before pursuing the lecture of this thesis.

5.3.1 The particle filter principle

This section presents an explanation of the principle of the PF based on [24]. This filter is part of the sequential Monte Carlo (SMC) methods and has different names in the literature[25] such as *Sequential sampling-importance resampling* or *Bootstrap filters*.

A PF computes the posterior distribution of the states of a Markov process taking into account noisy and partial observations. Let us consider the Markov process defined in (5.1). $\mathbf{x}_t$ represents the value of the hidden state at time t. For our algorithm, the time $t \in \mathbb{N}$ is an adimensional variable expressed in term of intervals of 20ms (e.g. $\mathbf{x}_5$ represents the hidden state after $5 \cdot 20 = 100$ms). $\mathbf{y}_t$ represents the observation of the state at time t. f_t and g_t are functions describing the process evolution. ν_t and w_t are random variables.

$$\begin{aligned} \mathbf{x}_t &= f_t(\mathbf{x}_{t-1}, \nu_t) \\ \mathbf{y}_t &= g_t(\mathbf{x}_t, w_t) \end{aligned} \tag{5.1}$$

We define $\mathbf{x}_{0:t} = \{\mathbf{x}_0, \ldots, \mathbf{x}_t\}$ and $\mathbf{y}_{1:t} = \{\mathbf{y}_1, \ldots, \mathbf{y}_t\}$ the signal and observation sets up to time t. The stochastic process can be described by:

1. An initial probabilistic distribution $p(\mathbf{x}_0)$
2. A conditional probabilistic state evolution $p(\mathbf{x}_t|\mathbf{x}_{t-1}) \quad \text{for} \quad t \geq 1$
3. A conditional probabilistic state observation $p(\mathbf{y}_t|\mathbf{x}_t) \quad \text{for} \quad t \geq 1$

From the stochastic process described here above, one would like to estimate recursively the posterior distribution of the hidden state $p(\mathbf{x}_{t+1}|\mathbf{y}_{1:t})$ using a particle filter. The problem is addressed recursively in two steps[24]:

- *Prediction:* $p(\mathbf{x}_t|\mathbf{y}_{1:t-1}) = \int p(\mathbf{x}_t, \mathbf{x}_{t-1}|\mathbf{y}_{1:t-1})d\mathbf{x}_{t-1} = \int p(\mathbf{x}_t|\mathbf{x}_{t-1})p(\mathbf{x}_{t-1}|\mathbf{y}_{1:t-1})d\mathbf{x}_{t-1}$.
- *Update:* $p(\mathbf{x}_t|\mathbf{y}_{1:t}) = \dfrac{p(\mathbf{y}_t|\mathbf{x}_t)p(\mathbf{x}_t)|\mathbf{y}_{1:t-1})}{p(\mathbf{y}_t|\mathbf{y}_{1:t-1})} = \dfrac{p(\mathbf{y}_t|\mathbf{x}_t)p(\mathbf{x}_t)|\mathbf{y}_{1:t-1})}{\int p(\mathbf{y}_t|\mathbf{x}_t)p(\mathbf{x}_t|\mathbf{y}_{1:t-1})d\mathbf{x}_t}$.

On one hand, the prediction step uses the probabilistic distribution of the hidden state $p(\mathbf{x}_{t-1}|\mathbf{y}_{1:t-1})$ and, based on the conditional probabilistic state evolution $p(\mathbf{x}_t|\mathbf{x}_{t-1})$, tries to estimate the most probable state at the next time instant. On the other hand, the update step estimates the most probable state given all the observations up to time t by using the predicted distribution $p(\mathbf{x}_t|\mathbf{y}_{1:t-1})$ and the conditional probabilistic state observation $p(\mathbf{y}_t|\mathbf{x}_t)$.

But how does the PF consider those probabilistic distributions? The PF represents the probabilistic distribution of the hidden state by particles. Each particle can be seen as one possible evolution of the hidden state and the density of the particles describes the probabilistic distribution of the hidden state. In other word, a

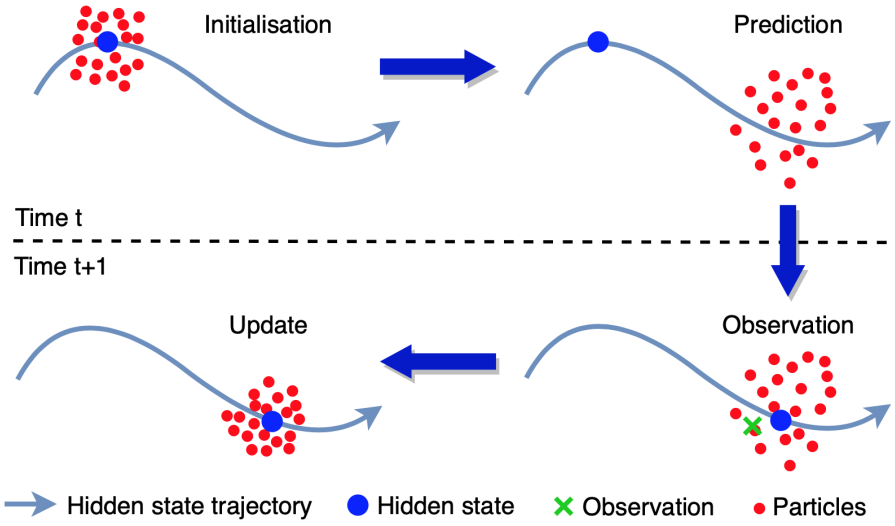

Figure 5.8: Illustration of the particle filter principle

given hidden state is more probable if lots of particles have a state similar or close to it.

The recursive principle of the particle filter is illustrated in Figure 5.8. At each iterations, the prediction and update steps are performed. Let us explain how these two steps impact the evolution of the particles:

1. Prediction: the next state of the particles is reevaluated according to $p(\mathbf{x}_t|\mathbf{x}_{t-1})$. Let us identify with an index i the different particles ($i = 1, \ldots, N_{part}$). We denote by $\mathbf{x}_t^i$ the state of the i^{th} particle. The prediction step consists in applying the function $f_t(\mathbf{x}_{t-1}^i, \nu_t)$ to each particle i.

2. Update: particles are selected according to $p(\mathbf{y}_t|\mathbf{x}_t)$ and are then resampled. The resampling operation is commonly known as importance sampling (IS) and ensures that a sufficient number of particles are describing the probabilistic distribution of the hidden state. We denote by $\tilde{\mathbf{x}}_t^i$ the state of particle i after the prediction step ($\tilde{\mathbf{x}}_t^i = f_t(\mathbf{x}_{t-1}^i, \nu_t)$. IS consists in according an importance weight w_t^i to each particles. The value of the importance weight w_t^i should follows $p(\mathbf{y}_t|\tilde{\mathbf{x}}_t^i)$ (e.g. based on the inverse of the distance between $\mathbf{y}_t$ and $g_t(\mathbf{x}_t^i, w_t)$). Then, the sets $\{\mathbf{x}_t^i : i = 1, \ldots, N_{part}\}$ is created by sampling with replacement N_{part} particles from $\{\tilde{\mathbf{x}}_t^i : i = 1, \ldots, N_{part}\}$ according to the normalised importance weights $\tilde{w}_t^i = w_t^i/(\sum_j w_t^j)$.

The PF is not the sole method to estimate the hidden state of a Markov process via a probabilistic approach. Other classical methods that address this problem are Extended Kalman filter and Gaussian sums (Alspach et al. 1971) but those methods required that $p(\mathbf{x}_t|\mathbf{x}_{t-1})$ and $p(\mathbf{y}_t|\mathbf{x}_t)$ are described by gaussian or sums of gaussian distributions which is not always guarantee [26]. PF has the advantage of not being subjected to such constraints but the price to pay is the high computational cost.

5.3.2 Predictive beam tracking algorithm

Now that the principle of the PF filter has been explained. Let us focus on the integration of the PF in the BT algorithm.

As explained before, the Markov process represents the user motion in which the hidden state corresponds to the angular position and velocity of the user every $\Delta t = 20$ms. The angular position and velocity of the user at time t will be denoted by x_t and $\dot{x}_t$ respectively ($\mathbf{x}_t = [x_t; \dot{x}_t]^T$) and the Markov process considered in this report is the following one:

$$\begin{aligned} x_t &= x_{t-1} + \dot{x}_{t-1}\Delta t \\ \dot{x}_t &= f(\dot{x}_{t-1}; \nu_t) \\ y_t &= g(x_t; w_t) \end{aligned} \tag{5.2}$$

In (5.1), the evolution of the angular position x_t is quite natural since it must depend linearly on the user velocity $\dot{x}_{t-1}$ and the interval time Δt. An additive random variable could also be added to the expression of x_t if one would like to include the fact that the user speed is not necessarily constant between $t-1$ and t.

The evolution of the angular speed $\dot{x}_t$ of the user must consider two different scenarios (see Figure 5.1):

- The user motion at time t follows the one at time $t-1$: $f(\dot{x}_{t-1}; \nu_t) = \dot{x}_{t-1} + \nu_t^1$. In this case, ν_t^1 can be considered as a random gaussian variable expressing the angular acceleration of the user.
- The user motion completely change between time $t-1$ and time t: $f(\dot{x}_{t-1}; \nu_t) = \nu_t^2$. In this case, ν_t^2 can be considered as a random variable taken from a uniform distribution.

For evident reason, the first scenario has a higher probability of occurence than the second one but these two scenarios must be considered by the particles. During the prediction step (see section 5.3.1), the particle set will be split in two with 98% of the particle following scenario 1 and the remaining will follow scenario 2.

Let us investigate deeper the distribution of ν_t^1 and ν_t^2. The choice of their distribution should be motivated by the maximal angular speed of the user. If one consider that the user is moving with an absolute speed inferior to 1.5m/s and is standing constantly at more than 1m from the BS, the maximal angular speed of the user is given by:

$$\dot{x}_{max} = atan(\frac{1.5}{1}) \approx 56°/s. \tag{5.3}$$

Because the angular speed of the user is assumed to be smaller than $\dot{x}_{max}$, ν_t^2 can be considered as a random variable taken from a uniform distribution in the range $[-\dot{x}_{max}; \dot{x}_{max}]$. We note the distribution of ν_t^2 by Ψ_2. Concerning scenario 1, ν_t^1 can

be for example a random variable taken from a zero mean gaussian distribution Ψ_1 of standard deviation $\dot{x}_{max}\Delta t$ meaning that 68% of the particles will accelerate by less than $56°/s^2$ between $t-1$ and t. The choice of the process parameters must be motivated by the physics of the studied process. The better realistic they are, the best will be the final performance of the PF.

A last comment over the Markov process in (5.2) should concern the observation y_t. The observation y_t is used during the update step to select and resample the particles according to some importance weights $w_t^i = p(\mathbf{y}_t|\tilde{\mathbf{x}}_t^i)$. Let us explain how these weights are generated in practice.

The only observation y_t the BS has over x_t is the measured SNR. The function $g(x_t; w_t)$ represents therefore the SNR level of the communication reached when the user is standing in x_t. w_t expresses the fact that the measurement of the SNR level can be noisy. Because of the width of the beams, the BS is not able to precisely measured the user position but it knows that if the SNR level is higher than $SNR_{ref} - SNR_t$ (see Algorithm 2), it means that the user is located in the limits of the beam and inversely.

Let us denote by ϕ_r, the steering direction of the beam before the update step. The update step works as follow. If $SNR < SNR_{ref} - SNR_t$, a BTP is performed (see section 5.2) and ϕ_r is set to the direction of the best beam found in the BTP. If $SNR \geq SNR_{ref} - SNR_t$, ϕ_r is kept unchanged. The importance weights of the particles can after be chosen as follow (ϕ_{wd} represents the beamwidth):

$$w_t^i = \begin{cases} 1 & \text{if } \phi_r - \phi_{wd}/2 < x_t^i < \phi_r + \phi_{wd}/2 \\ 0 & \text{otherwise} \end{cases} \tag{5.4}$$

The particles being inside the beam have therefore an importance weight of one and the particles outside the beam have an importance weight of zero. During the IS operation, the particles will be resampled according to their weights. The IS principle is illustrated in Figure 5.9.

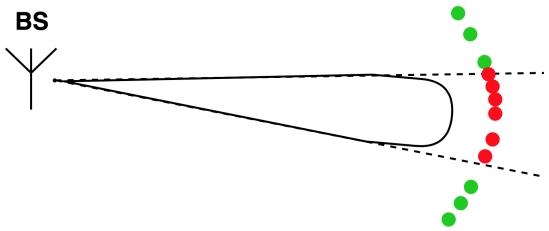

Figure 5.9: Importance sampling (IS) principle illustration. Green particles are standing outside the beam and an importance weight of zero is assigned to them. Inversely, red particles are standing inside the beam and an importance weight of 1 is assigned to them. After the resampling, the red particles will be replicated and the green particles will be discarded so that the total number of particles is conserved.

The final version of the BT algorithm is presented in Algorithm 3. One can note that the initial angular position of the user x_0 should be known in advance to initialise

the particle state. In this our simulation, x_0 is supposed to be perfectly known but in practice, it should be estimated during the SLS and BRP phases (see chapter 3).

Algorithm 3 Predictive BT algorithm

Input: SNR_t, x_0, N_{part}

$SNR_{ref} = 0, t = 1$
$x_0^i = x_0 \quad \forall i = 1, \ldots, N_{part}$ ▷ Initialisation of the particle set
$\dot{x}_0^i \sim \Psi_2 \quad \forall i = 1, \ldots, N_{part}$
while $BTIsOn()$ **do** ▷ Check if BT is activated
  for $i = 1 : N_{part}$ **do** ▷ Prediction step
    $\tilde{x}_t^i = x_{t-1}^i + \dot{x}_{t-1}^i \Delta t$
    $\dot{\tilde{x}}_t^i = f(\dot{x}_{t-1}^i; \nu_t)$
  end for
  $\phi_r = Mean(\{\tilde{x}_t^i : i = 1, \ldots, N_{part}\})$ ▷ User position estimation
  $Adapt\_AWV(\phi_r)$ ▷ Set steering direction to ϕ_r
  $SNR = MeasureSNR()$ ▷ SNR measurement
  if $SNR < SNR_{ref} - SNR_t$ **then**
    $(\phi_r, SNR_{ref}) = BeamTracking()$ ▷ Perform BTP
  else
    $SNR_{ref} = SNR$
  end if
  for $i = 1 : N_{part}$ **do** ▷ Update step
    $w_t^i = ImportanceWeight(\phi_r, x_t^i)$ ▷ Performed (5.4)
    $\tilde{w}_t^i = w_t^i / \sum_j w_t^j$
  end for
  $\{\mathbf{x}_t^i\} = Randsample(\{\tilde{\mathbf{x}}_t^i\}, \{\tilde{w}_t^i\})$ ▷ Importance sampling (IS)
  $t = t + 1$
end while

Figure 5.10 and Figure 5.11 present the performance of the BT algorithm using the PF technique. In Figure 5.10, one can observe that the evolution of the estimated user position (= mean particle position) follows quite well the true user position. Again, the precision of this estimation corresponds to half the beamwidth but is on average better than the one of the BT algorithm presented in section 5.2.

During the simulation, the number of BTPs performed has been dramatically reduced thanks to the PF technique (22 BTPs for the BT algorithm with the PF against 108 for the BT algorithm without the PF). This leads to an important reduction of the training overhead and the number of SNR drops.

The impact of the beamwidth ϕ_{wd} and SNR_t should be discussed. In Figure 5.12 is represented the evolution of the number of BTPs performed with respect to ϕ_{wd} and SNR_t. The evolution of the mean SNR level with respect to ϕ_{wd} and SNR_t is presented in Figure 5.13.

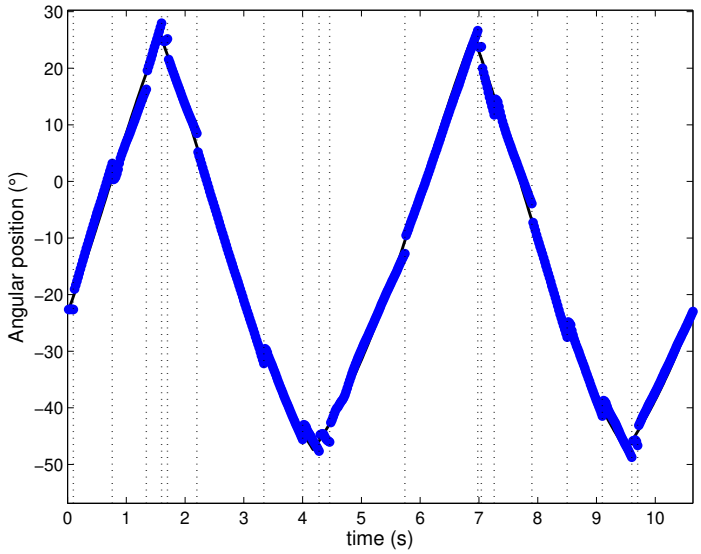

Figure 5.10: Black line: angular position evolution of the UE. Blue line: estimation of the angular position of the UE. The vertical dotted lines represent the time instant for wich a beam tracking algorithm was triggered. For this simulation, $\phi_{wd} = 5°$, $SNR_t = 3$dB and $N_{part} = 1000$.

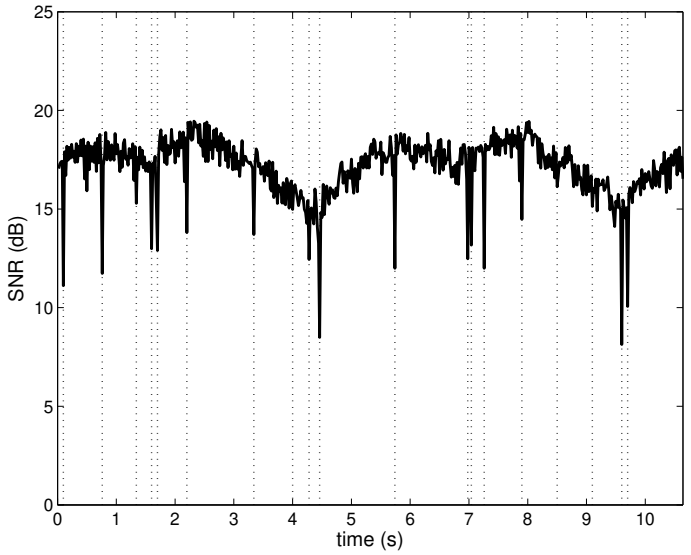

Figure 5.11: SNR evolutions.The vertical dotted lines represent the time instant for which a beam tracking algorithm was triggered. For this simulation, $\phi_{wd} = 5°$, $SNR_t = 3$dB and $N_{part} = 1000$.

Compared to the BT algorithm presented in section 5.2, the used of the PF to estimate the user motion allows a reduction of 85% of the number of BTPs performed for $\phi_{wd} = 2.5°$. This reduction becomes less important when the beamwidth increases (66% of reduction for $\phi_{wd} = 10°$). Because less SNR drops occur thank to user motion

prediction, the mean measured SNR level stays constantly higher when using the PF.

Similar comments applied to the BT algorithm presented in section 5.2 can also be applied on the BT algorithm using the PF. The influence of SNR_t is mostly negligible but must remain superior to the maximal variation of array gain inside the beam and inferior to the minimal difference of array gain inside and outside the beam. Concerning the beamwidth, an increase of ϕ_{wd} leads to a reduction of the number of BTPs performed because the user stays longer inside the beam. However, the lower array gain associated to larger beams reduces the mean measured SNR level.

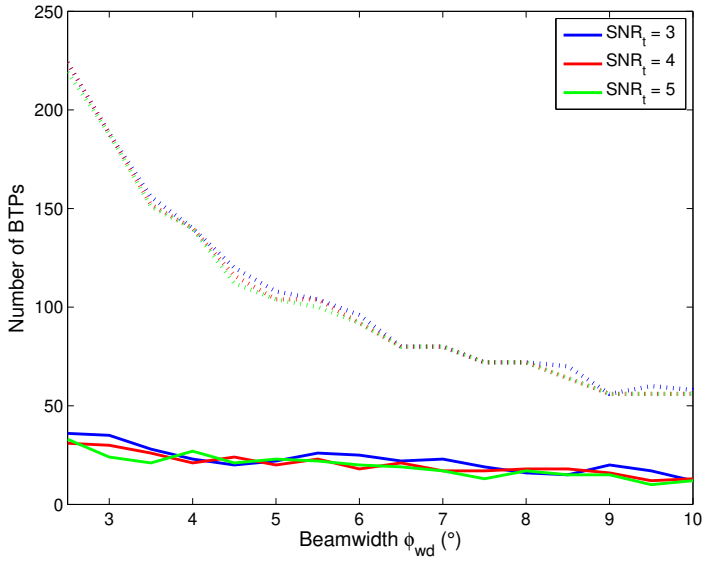

Figure 5.12: Simulated evolution of the number of BTPs with ϕ_{wd} and SNR_t. Dotted lines represent the performance of the BT algorithm without user motion estimation (section 5.2). Normal lines represent the performance of the BT algorithm using the PF technique.

5.4 Conclusion

In this chapter, an indoor scenario considering a stationary base station (BS) and a moving user was investigated. Because of the user motion, the BS must adapt its antenna weight vector (AWV) in order to continuously steer its radiation pattern toward the user position. Two different beam tracking (BT) algorithm was presented.

The first proposed BT algorithm carries out a beam tracking procedure (BTP) every time the measured SNR level becomes lower than a SNR threshold. This procedure shows a good ability to track the user but the number of BTPs performed (and so the BT training overhead) could be dramatically reduced if the BS is able to predict the user motion.

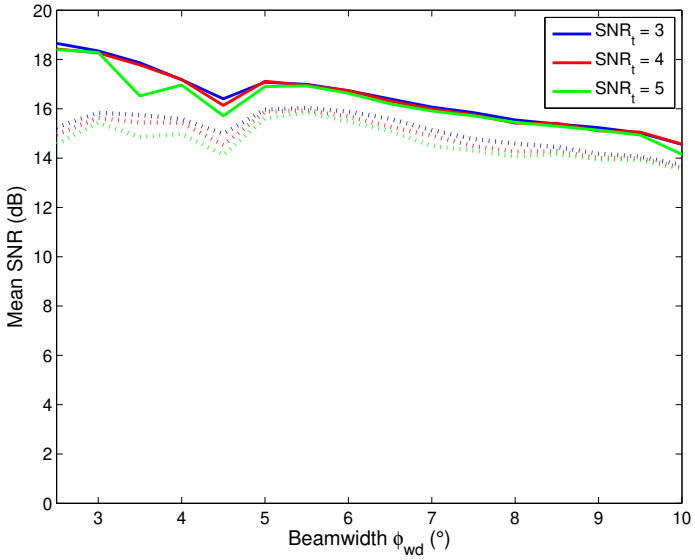

Figure 5.13: Simulated mean evolution of the number of measured SNR with the beamwidth ϕ_{wd} and the SNR threshold SNR_t. Dotted lines represent the performance of the BT algorithm without user motion estimation (section 5.2). Normal lines represent the performance of the BT algorithm using the PF technique.

This prediction was support by the second proposed BT algorithm where a particle filter (PF) was used to estimate the user motion. The BT training overhead was reduced by 66% to 85% and the measured SNR has been improved by 1 to 4dB on average depending on the beamwidth of the AWVs.

Chapter 6

Conclusion

This chapter summarises the main contributions provided by this master thesis and enumerates perspectives for future work.

6.1 Summary

Chapter 2 describes how a multi-antenna system is able to exploit beamforming thanks to the use of phase shifters connected to every antenna element. The study first analyses the emission of a plane wave by a linear and a rectangular antenna arrays. It was described how transmit and receive antenna weight vectors (AWVs) can be designed to maximise the array gain.

In the case of a high number of antennas, it was shown that a relatively small mismatch between the direction of the beam of the radiation pattern and transmitter/receiver direction leads to an important drop of the array gain. To cope with this problem, an algorithm generating antenna weight vectors (AWVs) with larger beam (=radiation pattern) was proposed and validated.

Chapter 3 proposes a description of the beamforming training (BFT) procedures implemented in the ad and ay specifications of the IEEE802.11 standard. These specifications allow Wi-Fi communication in the 60 GHz band with very high data throughput (6.75Gbps for the ad and 20-40Gbps for the ay). The main differences between these two specifications is the introduction of channel bonding and aggregation possibilities in the ay version as well as the introduction of two spatial multiplexing (SM) training procedures (SU-MIMO BFT and MU-MIMO BFT).

The second part of this chapter describes the *Matlab* chain used for the validation of the following chapters.

Chapter 4 presents two different BFT algorithms compatible with the IEEE802.11ad/ay specifications. The first algorithm consists in an exhaustive beam search algorithm in which the space is divided into virtual sectors. Successively, the radiation pattern is steered in each sector via the modification of the AWV. The AWV leading to the higher measured SNR level is then selected for the data transfer. The expected

performance with respect to the beamwidth of the radiation pattern and the number of tested sectors was studied.

The second BFT algorithm is based on the estimation of the one-tap SISO channel via perturbation of the AWV. Two different methods were proposed and are based on the combination of the SNR measurements obtained for each tested AWV. The robustness of those methods with noise on the SNR measurements was analysed and it was shown that an important reduction of performance can be expected in the case of high noise power.

Chapter 5 investigates a beam tracking (BT) algorithm in which a stationary BS adapts continuously its AWV in function of the user motion. The first presented algorithm proposes to adapt the AWV each time the SNR level is significantly reduced.

In the second part of this chapter, an update of this BT algorithm was proposed. The algorithm is taking advantage of a particle filter (PF) to estimate the user motion. It was shown that this update has led to a drastic reduction of the training overhead (80% in the best case) for the studied scenario.

6.2 Perspectives

In this section is proposed a list of different perspectives for future work.

- **Chapter 2:** the efficiency of the beam widening algorithm can be improved. Indeed, the cost function possesses generally a lots of local minima and there is no guarantee that the algorithm will converge toward the global minimum. Furthermore, several state of the art beam widening algorithms already exist in the literature and the presented algorithm could be compared with some of these algorithms.

- **Chapter 3:** in the *Matlab* chain, only first order reflections are taken into account in the model of the channel and no mismatch of polarisation between the antenna array of the BS and the one of the user is considered. Moreover, the evaluation of the SNR level for each antenna configuration is made over the preamble of the data packets. This should be normally be performed over training frames (e.g. SSW packet) or over training fields (TRN fields) according to the BFT procedure defined in the IEEE802.11 standard.

- **Chapter 4:** the performance of the proposed BFT algorithms could be evaluated according to the final bit error rate (BER) obtained. The robustness against noise over SNR measurements has not been investigated for the beam search algorithm and a real comparison with the second algorithm is missing.

- **Chapter 5:** different parameters of the algorithm have not been really optimised in this chapter. Furthermore, a study considering different user motions should be done to highlight to robustness of the algorithm. An experimental validation of this algorithm would be interesting to perform so that a truly realistic scenario (e.g. noise on the SNR measurements, more natural user motion, ...) is considered.

Appendix A

Channel estimation method using Golay sequences

In this appendix, is described how the impulse response of a frequency selective channel can be estimated from noisy received Golay sequences. The first part of this appendix is dedicated the definition of the channel impulse response (CIR). In the second part, the principle of the estimation of the CIR will be investigated.

A.1 Channel impulse response description

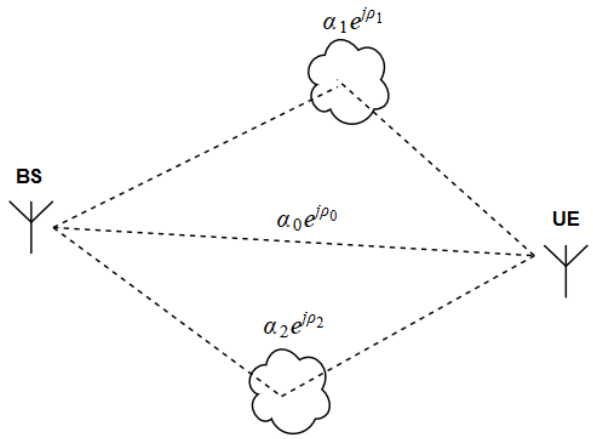

Figure A.1: Example of transmission of a signal between a Base Station (BS) and a User Element (UE) with multiple reflections.

In a multipath transmission as depicted in Figure A.1, the different waves coming from the different paths ($k = 0, ..., N_P - 1$) are suffering from:

- An attenuation α_k effect. This effect is due on one hand to the propagation and reflections in the environments and, on the other hand, to non-isotropic response of the transmit (resp. receive) antenna arrays.
- A phase shift ρ_k effect for the same reasons as for the attenuation effect.

- A delay τ_k due to the distance travelled.

The analog channel impulse response (CIR) associated to path k can be described as:

$$h_k(t) = \alpha_k e^{j\rho_k} \delta(t - \tau_k), \tag{A.1}$$

And the total analog CIR is the summation of all the CIRs:

$$h(t) = \sum_{k=0}^{N_P-1} h_k(t) = \sum_{k=0}^{N_P-1} \alpha_k e^{j\rho_k} \delta(t - \tau_k). \tag{A.2}$$

This model describes the response of the channel to an analog perturbation. In practice, we are more interested in the channel effect on a discrete sequence of symbols transmitted through the channel.

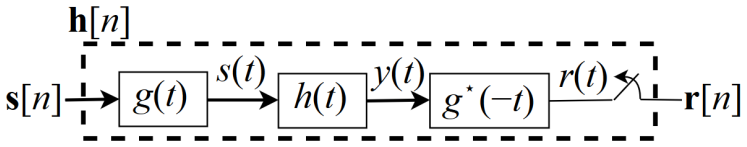

Figure A.2: Transmission chain. The symbols are first converted to an analog signal using a pulse shaping filter with response $g(t)$. Then the signal is transmitted through the channel and goes through a secondary pulse shaping filter at the reception side. The signal is then sampled at a sampling rate $1/T$ and the resulting sequence $\mathbf{r}[n]$ represents a noisy version of the transmitted sequence $\mathbf{s}[n]$.

Let us find out what is the discrete representation of $h(t)$, denoted by $\mathbf{h}[n]$. Figure A.2 represents a typical transmission chain. We consider $\mathbf{s}[n]$, a sequence of symbols that we want to transmit and $\mathbf{r}[n]$, the received sequence. The different signals are given by

$$s(t) = \sum_{n=-\infty}^{\infty} \mathbf{s}[n] g(t - nT), \tag{A.3}$$

$$y(t) = h(t) * s(t) \tag{A.4}$$

$$= \int_{-\infty}^{\infty} h(\tau) s(t - \tau) d\tau \tag{A.5}$$

$$= \int_{-\infty}^{\infty} \sum_{k=0}^{N_P-1} \alpha_k e^{j\rho_k} \delta(\tau - \tau_k) \sum_{n=-\infty}^{\infty} \mathbf{s}[n] g(t - nT - \tau) d\tau \tag{A.6}$$

$$= \sum_{k=0}^{N_P-1} \alpha_k e^{j\rho_k} \sum_{n=-\infty}^{\infty} \mathbf{s}[n] g(t - nT - \tau_k) \underbrace{\int_{-\infty}^{\infty} \delta(\tau - \tau_k) d\tau}_{=1} \tag{A.7}$$

$$= \sum_{k=0}^{N_P-1} \alpha_k e^{j\rho_k} \sum_{n=-\infty}^{\infty} \mathbf{s}[n] g(t - nT - \tau_k), \tag{A.8}$$

$$= \sum_{k=0}^{N_P-1} \alpha_k e^{j\rho_k} \sum_{n=-\infty}^{\infty} \mathbf{s}[n] u(t - nT - \tau_k), \tag{A.9}$$

$$
\begin{aligned}
r(t) &= y(t) * g^{\star}(-t) && \text{(A.10)}\\
&= \int_{-\infty}^{\infty} y(\tau') g^{\star}(-t-\tau') d\tau' && \text{(A.11)}\\
&= \int_{-\infty}^{\infty} \sum_{k=0}^{N_P-1} \alpha_k e^{j\rho_k} \sum_{n=-\infty}^{\infty} \mathbf{s}[n] g(\tau' - nT - \tau_k) g^{\star}(-t-\tau') d\tau' && \text{(A.12)}\\
&= \sum_{k=0}^{N_P-1} \alpha_k e^{j\rho_k} \sum_{n=-\infty}^{\infty} \mathbf{s}[n] \int_{-\infty}^{\infty} g(\tau' - nT - \tau_k) g^{\star}(-t-\tau') d\tau' && \text{(A.13)}\\
&= \sum_{k=0}^{N_P-1} \alpha_k e^{j\rho_k} \sum_{n=-\infty}^{\infty} \mathbf{s}[n] u(t - nT - \tau_k), && \text{(A.14)}
\end{aligned}
$$

where $u(t) = g(t) * g^{\star}(-t)$ is a Nyquist filter (raised-cosine filter for example). The received sequence can be expressed as

$$
\begin{aligned}
\mathbf{r}[n'] &= r(n'T) && \text{(A.15)}\\
&= \sum_{k=0}^{N_P-1} \alpha_k e^{j\rho_k} \sum_{n=-\infty}^{\infty} \mathbf{s}[n] u(n'T - nT - \tau_k) && \text{(A.16)}\\
&= \sum_{n=-\infty}^{\infty} \mathbf{s}[n] \mathbf{h}[n' - n], && \text{(A.17)}\\
&= \mathbf{h}[n'] * \mathbf{s}[n'], && \text{(A.18)}
\end{aligned}
$$

With $\mathbf{h}[n] = \sum_{k=0}^{N_P-1} \alpha_k e^{j\rho_k} u(nT - \tau_k)$ being the CIR that we would like to estimate.

A.2 Channel impulse response estimation

To recover the sequence of true symbols $\mathbf{s}[n]$ from $\mathbf{r}[n]$, a receiver needs to get rid of the effect of $\mathbf{h}[n]$. This operation is named equalization and a good estimation of the CIR is often needed. The estimation of the CIR is a complex operation done by the receiver. This operation can be efficiently performed thanks the transmission of pilot symbols through the channel.

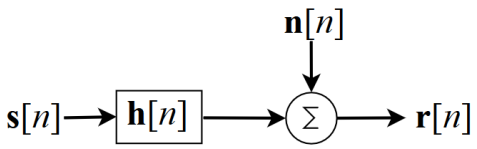

Figure A.3: Transmission chain of pilot symbols with additive white gaussian noise.

In figure A.3 is depicted the transmission chain for the pilot symbols when the transmission is disrupted by an additive white gaussian noise of variance σ_n^2. The pilot sequence symbols $\mathbf{s}[n]$ is known at the receiver and, according to standard IEEE802.11ad, is made of Golay sequences.

A Golay pairs $\mathbf{Ga_N}[n]$ and $\mathbf{Gb_N}[n]$ is a pair of binary sequences of size N such that the sum of their aperiodic correlation is null. Mathematically, this can be written as

$$\mathbf{R_a}[k] + \mathbf{R_b}[k] = 2N\delta[k] \quad \text{with} \quad \mathbf{R_x}[k] = \sum_{i=0}^{N-1-k} \mathbf{Gx_N}[i]\mathbf{Gx_N}[i+k] \tag{A.19}$$

$\mathbf{Ga_4}[k]$	1	1	1	-1	$\mathbf{R_a}[k]$	4	1	0	-1
$\mathbf{Gb_4}[k]$	1	1	-1	1	$\mathbf{R_b}[k]$	4	-1	0	1

Table A.1: Pair of Golay sequences of size $N = 4$. One can note that $\mathbf{R_a}[k]+\mathbf{R_b}[k] = 8\delta[k]$.[27]

Example of Golay sequences of size $N = 4$ is given in Table A.1. From the noisy received Golay sequences, one can estimate the channel $\mathbf{h}[n]$. The procedure is depicted in Figure A.4 and demonstrates below.

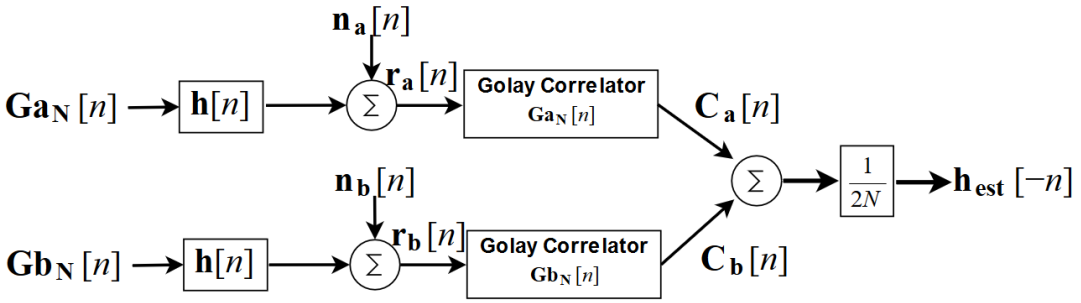

Figure A.4: Procedure for channel estimation using Golay sequences defined in the IEEE802.11ad/ay standard.

The Golay correlator operation is correlating the received sequences $\mathbf{r_a}[n]$ and $\mathbf{r_b}[n]$ with their respective Golay sequence. For the upper branch, we have

$$\mathbf{r_a}[n] = \mathbf{h}[n] * \mathbf{Ga_N}[n] + \mathbf{n_a}[n] \tag{A.20}$$

$$= \sum_{k=-\infty}^{\infty} \mathbf{h}[k]\mathbf{Ga_N}[n-k] + \mathbf{n_a}[n], \tag{A.21}$$

$$\mathbf{C_a}[n] = \sum_{k'=0}^{N-n-1} \mathbf{r_a}[k']\mathbf{Ga_N}[k'+n] \tag{A.22}$$

$$= \sum_{k'=0}^{N-n-1} \sum_{k=-\infty}^{\infty} \mathbf{h}[k]\mathbf{Ga_N}[k'-k]\mathbf{Ga_N}[k'+n] + \sum_{k'=0}^{N-n-1} \mathbf{n_a}[k']\mathbf{Ga_N}[k'+n]. \tag{A.23}$$

Let us denote $k'' = k' - k =$ and $\nu_\mathbf{a}[n] = \sum_{k'=0}^{N-n-1} \mathbf{n_a}[k']\mathbf{Ga_N}[k'+n]$. $\mathbf{C_a}[n]$ becomes

$$\mathbf{C_a}[n] = \sum_{k=-\infty}^{\infty} \mathbf{h}[k] \sum_{k''=-k}^{N-n-1-k} \mathbf{Ga_N}[k'']\mathbf{Ga_N}[k''+k+n] + \nu_\mathbf{a}[n]. \tag{A.24}$$

Because $\mathbf{Ga_N}[k''] = 0$ for $k'' < 0$, one finds that:

$$\mathbf{C_a}[n] = \sum_{k=-\infty}^{\infty} \mathbf{h}[k] \sum_{k''=0}^{N-n-1-k} \mathbf{Ga_N}[k'']\mathbf{Ga_N}[k''+k+n] + \nu_{\mathbf{a}}[n] \tag{A.25}$$

$$= \sum_{k=-\infty}^{\infty} \mathbf{h}[k]\mathbf{R_a}[k+n] + \nu_{\mathbf{a}}[n]. \tag{A.26}$$

Similarly, one finds for the lower branch:

$$\mathbf{C_b}[n] = \sum_{k=-\infty}^{\infty} \mathbf{h}[k]\mathbf{R_b}[k+n] + \nu_{\mathbf{b}}[n], \tag{A.27}$$

with $\nu_{\mathbf{b}}[n] = \sum_{k'=0}^{N-n-1} \mathbf{n_b}[k']\mathbf{Gb_N}[k'+n]$. The estimated channel is therefore

$$\mathbf{h_{est}}[n] = \frac{1}{2N}\Big(\mathbf{C_a}[-n] + \mathbf{C_b}[-n]\Big) \tag{A.28}$$

$$= \frac{1}{2N}\Big(\sum_{k=-\infty}^{\infty} \mathbf{h}[k] \underbrace{\Big(\mathbf{R_a}[k-n] + \mathbf{R_b}[k-n]\Big)}_{=2N\delta[k-n]} + \nu_{\mathbf{a}}[-n] + \nu_{\mathbf{b}}[-n]\Big) \tag{A.29}$$

$$= \mathbf{h}[n] + \frac{1}{2N}\Big(\nu_{\mathbf{a}}[-n] + \nu_{\mathbf{b}}[-n]\Big). \tag{A.30}$$

The estimated channel $\mathbf{h_{est}}[n]$ is therefore equivalent to the true channel $\mathbf{h}[n]$ perturbed by a noisy term. In the IEEE802.11ad/ay standards, the pilot sequences $\mathbf{Ga_N}[n]$ and $\mathbf{Gb_N}[n]$ are sent 4 times in a row with $N = 128$ and an averaging of the estimated channels is performed to reduce the influence of the noisy term.

Bibliography

[1] S. A. Busari, K. M. S. Huq, S. Mumtaz, L. Dai, and J. Rodriguez. Millimeter-wave massive mimo communication for future wireless systems: A survey. *IEEE Communications Surveys Tutorials*, 20(2):836–869, Secondquarter 2018.

[2] Y. Ghasempour, C. R. C. M. da Silva, C. Cordeiro, and E. W. Knightly. Ieee 802.11ay: Next-generation 60 ghz communication for 100 gb/s wi-fi. *IEEE Communications Magazine*, 55(12):186–192, DECEMBER 2017.

[3] A. L. Swindlehurst, E. Ayanoglu, P. Heydari, and F. Capolino. Millimeter-wave massive mimo: the next wireless revolution? *IEEE Communications Magazine*, 52(9):56–62, Sep. 2014.

[4] S. Sun, T. S. Rappaport, R. W. Heath, A. Nix, and S. Rangan. Mimo for millimeter-wave wireless communications: beamforming, spatial multiplexing, or both? *IEEE Communications Magazine*, 52(12):110–121, December 2014.

[5] B. Yang, Z. Yu, J. Lan, R. Zhang, J. Zhou, and W. Hong. Digital beamforming-based massive mimo transceiver for 5g millimeter-wave communications. *IEEE Transactions on Microwave Theory and Techniques*, 66(7):3403–3418, July 2018.

[6] S. Kutty and D. Sen. Beamforming for millimeter wave communications: An inclusive survey. *IEEE Communications Surveys Tutorials*, 18(2):949–973, Secondquarter 2016.

[7] Joan Palacios, Daniel Steinmetzer, Adrian Loch, Matthias Hollick, and Joerg Widmer. Adaptive codebook optimization for beam training on off-the-shelf ieee 802.11ad devices, 10 2018.

[8] L. Zhou and Y. Ohashi. Efficient codebook-based mimo beamforming for millimeter-wave wlans. In *2012 IEEE 23rd International Symposium on Personal, Indoor and Mobile Radio Communications - (PIMRC)*, pages 1885–1889, Sep. 2012.

[9] S. Rajagopal. Beam broadening for phased antenna arrays using multi-beam subarrays. In *2012 IEEE International Conference on Communications (ICC)*, pages 3637–3642, June 2012.

[10] S J Orfanidis. *Electromagnetic Waves and Antennas*. 01 2014.

[11] Wikipedia contributors. Ieee 802.11 — Wikipedia, the free encyclopedia. https://en.wikipedia.org/w/index.php?title=IEEE_802.11&oldid=895450562, 2019. [Online; accessed 8-May-2019].

[12] T. Nitsche, C. Cordeiro, A. B. Flores, E. W. Knightly, E. Perahia, and J. C. Widmer. Ieee 802.11ad: directional 60 ghz communication for multi-gigabit-per-second wi-fi [invited paper]. *IEEE Communications Magazine*, 52(12):132–141, December 2014.

[13] Carlos Cordeiro, Dmitry Akhmetov, and Minyoung Park. Ieee 802.11ad: Introduction and performance evaluation of the first multi-gbps wifi technology. *Wireless Communications and Mobile Computing*, pages 3–8, 09 2010.

[14] E. Perahia, C. Cordeiro, M. Park, and L. L. Yang. Ieee 802.11ad: Defining the next generation multi-gbps wi-fi. In *2010 7th IEEE Consumer Communications and Networking Conference*, pages 1–5, Jan 2010.

[15] Bernhard Schulz. 802.11ad - wlan at 60 ghz a technology introduction: White paper. https://cdn.rohde-schwarz.com/pws/dl_downloads/dl_application/application_notes/1ma220/1MA220_3e_WLAN_11ad_WP.pdf, 2017. [Online; accessed 9-May-2019].

[16] Shivendra Panwar et al. Tcp/ip essentials: Chapter 2 - a single segment network – data link layer. https://slideplayer.com/slide/5178642/.

[17] SaiShankar N et al. Wigig and ieee 802.11ad - for multi-gigabyte-per-second wpan and wlan, NOVEMBER 2012.

[18] Pei Zhou et al. Ieee 802.11ay based mmwave wlans: Design challenges and solutions. *IEEE Communications Magazine*, 20(3), MARCH 2018.

[19] June 2014.

[20] Joan Palacios, Danilo De Donno, and Joerg Widmer. Tracking mm-wave channel dynamics: Fast beam training strategies under mobility. 04 2017.

[21] Jiahui Li, Yin Sun, Limin Xiao, Shidong Zhou, and C Emre Koksal. Analog beam tracking in linear antenna arrays: Convergence, optimality, and performance. pages 1193–1198, 10 2017.

[22] Marco Giordani and Michele Zorzi. Improved user tracking in 5g millimeter wave mobile networks via refinement operations. 06 2017.

[23] Chuang Zhang, Dongning Guo, and Pingyi Fan. Mobile millimeter wave channel acquisition, tracking, and abrupt change detection. 10 2016.

[24] Arnaud Doucet, Nando de Freitas, and Neil Gordon. An introduction to sequential monte carlo methods. *Sequential Monte Carlo Methods in Practice. Springer, Berlin*, 01 2001.

[25] Keith Copsey. Tutorial on particle filters. *NCAF January Meeting, Aston University, Birmingham.*

[26] Arnaud Doucet and Adam Johansen. A tutorial on particle filtering and smoothing: Fifteen years later. *Handbook of Nonlinear Filtering*, 12, 01 2009.

[27] Wikipedia contributors. Complementary sequences — Wikipedia, the free encyclopedia, 2018. [Online; accessed 5-November-2018].

UNIVERSITÉ CATHOLIQUE DE LOUVAIN
École polytechnique de Louvain
Rue Archimède, 1 bte L6.11.01, 1348 Louvain-la-Neuve, Belgique | **www.uclouvain.be/epl**